PRECAST CONCRETE BRIDGE DECK PANELS REINFORCED WITH GLASS FIBER REINFORCED POLYMER BARS

by

Ruifen Liu

A dissertation submitted to the faculty of
The University of Utah
in partial fulfillment of the requirements for the degree of

Doctor of Philosophy

Department of Civil and Environmental Engineering

The University of Utah

December 2011

The University of Utah Graduate School

STATEMENT OF DISSERTATION APPROVAL

The dissertation of **Ruifen Liu**

has been approved by the following supervisory committee members:

Chris P. Pantelides	, Chair	**9/8/2011** Date Approved
Lawrence D. Reaveley	, Member	**9/8/2011** Date Approved
Paul J. Tikalsky	, Member	**9/8/2011** Date Approved
Janice J. Chambers	, Member	**9/8/2011** Date Approved
Daniel O. Adams	, Member	**9/8/2011** Date Approved

and by **Paul J. Tikalsky** , Chair of

the Department of **Civil and Environmental Engineering**

and by Charles A. Wight, Dean of The Graduate School.

ABSTRACT

The present research investigates lightweight and normal weight precast concrete panels for highway bridges. The panels are reinforced with Glass Fiber Reinforced Polymer (GFRP) bars. A benefit of precast concrete panels reinforced with GFRP bars for bridge decks is that they are essentially immune to environments where chloride-induced deterioration is an issue.

Twenty panels constructed using lightweight and normal weight concrete reinforced with GFRP bars for flexure without any shear reinforcement were tested to failure. The variables investigated were concrete compressive strength, deck span, panel thickness and width, and reinforcement ratio. The experimental performance of lightweight precast GFRP reinforced panels versus normal weight precast GFRP reinforced panels was investigated in terms of shear capacity, deck deflections, and moment of inertia.

The experimental results show that lightweight concrete panels performed similar to normal weight concrete panels; however, they experienced larger deflections under the same load and had a lower ultimate shear strength than normal weight concrete panels. An extended database of 97 test results including normal weight and lightweight concrete restricted to members reinforced with GFRP bars for flexure without any shear reinforcement was compiled. The extended database including 77 normal weight concrete members from literature, 8 normal weight concrete panels and 12 lightweight concrete panels tested in the current research; no lightweight concrete members reinforced with GFRP has been found. ACI 440.1R

predicted smaller shear strength conservatism of lightweight concrete panels compared with normal weight concrete panels. A reduction factor has been recommended for the ACI 440.1R shear strength prediction equation when lightweight concrete is used.

Modified Compression Filed Theory (MCFT) was also used for the prediction of ultimate shear strength of GFRP reinforced concrete panels. The comparison of prediction to the experimental results shows that MCFT can predict accurately the shear strength for both lightweight and normal weight concrete panels reinforced with GFRP bars.

All the tested panels both normal weight and lightweight concrete panels designed according to ACI 440.1R satisfy the service load deflection requirements of the AASHTO LRFD Bridge Design Specifications. The experimental results indicate that the moment of inertia for precast panels reinforced with GFRP bars with initial cracks was less than the gross moment of inertia even before the cracking moment is reached. An expression for predicting deflection using a conservative estimate of the moment of inertia for precast concrete panels reinforced with GFRP bars is proposed. Using the proposed equation, a better deflection prediction is obtained for precast concrete panels reinforced with GFRP bars under service load.

TABLE OF CONTENTS

ACKNOWLEDGEMENTS

I wish to express sincere thanks to Dr. Chris Pantelides for making this work possible. I am grateful for his invaluable guidance and teachings, his patience and dedication to help me succeed throughout this research. I appreciate his help with construction, testing, and analyzing collected data.

I would like to express my appreciation for Dr. Larry Reaveley, Dr. Paul Tikalsky, Dr. Janice Chambers, and Dr. Daniel Adams, who gave construction suggestions for the research.

I would like to thank Mark Bryant, Brandon Besser, and Clayton Burningham for help during the experimental portion of the research.

I wish to express my gratitude and sincere appreciation to the Utah DOT and the Expanded Shale Clay and Slate Institute for funding this research. I am grateful for the contribution of Hughes Bros Inc., Utelite Corporation, and Hanson Structural Precast.

I am grateful to my family for their complete support, patience, and cooperation. Their encouragement helped me get through the research and hard times.

1 INTRODUCTION

Corrosion of steel is a major cause of deterioration of reinforced concrete structures. Concrete bridge decks are subjected to severe environmental conditions such as significant use of deicing salts, variations in temperature, and multiple freeze-thaw cycles. As an example, from 1948 until 2000, Salt Lake City had an average of 103 freeze-thaw cycle days per year. The severe environmental conditions reduce the life span of bridge decks. Concrete bridge decks have an average life of 35 to 40 years mainly because of deterioration due to corrosion of steel reinforcement. The expansion of steel reinforcement due to corrosion causes the concrete bridge deck to experience cracking and spalling; this results in major rehabilitation costs and traffic disruption (Yunovich and Thompson 2003). Fiber Reinforced Polymer (FRP) bars are immune to chloride-induced corrosion, and have higher tensile strength compared to steel bars. The noncorrosive FRP bar provides a viable alternative to steel as reinforcement for concrete bridge decks under severe corrosion conditions. In the past two decades, three types of FRP bars have been tested and used, including Glass Fiber Reinforced Polymer (GFRP), Carbon Fiber Reinforced Polymer (CFRP), and Aramid Fiber Reinforced Polymer (AFRP). Compared with CFRP and AFRP, GFRP bars are more economical, and thus are generally used in bridge decks as an alternative to steel or epoxy coated steel reinforcement.

FRP reinforcement has a different mechanical behavior compared to conventional steel reinforcement. One of the major differences is that FRP bars do not yield; they are elastic until failure. The brittle properties of FRP bars compared

with ductile steel rebar cause a lack of ductility in structural concrete members. High tensile strength in the direction of the reinforcing fibers only, which is caused by anisotropic properties of materials, also affects the shear strength and dowel action of FRP bars and the bond performance to concrete. FRP reinforcement has a much smaller modulus of elasticity compared to steel reinforcement, which causes larger deflections in structural components.

1.1 Lightweight Concrete

Sand-lightweight concrete has approximately 75%-85% the density of normal weight concrete. Examination of a number of projects constructed with steel reinforced lightweight concrete bridge decks has demonstrated that they can perform well in service for a range of different environments (Castrodale and Robinson 2008); this includes sites that vary from coastal with salt breezes, to mountainous where salt is applied to deice the deck in winter; in addition, traffic counts varied from very heavy urban interstate travel with a high percentage of trucks to light rural traffic.

The use of lightweight concrete precast bridge decks reinforced with GFRP bars is cost-competitive in environments where chloride-induced deterioration is an issue and the use of GFRP bars could extend the life of the deck. Several benefits could be gained from lightweight concrete precast GFRP reinforced deck panels, especially when they are used in Accelerated Bridge Construction (ABC); in this method of construction, the whole bridge or parts of the bridge are constructed off site and brought to the bridge site using mobile transportation. The reduced weight of decks constructed with lightweight concrete implies that they could be lifted with smaller cranes and could reduce the transportation requirements such as Self

Propelled Modular Transporters (SPMTs). In addition, the reduction in weight is beneficial in the design of the superstructures, substructure, and foundations since the weight of the deck is the main dead load resisted by the girders, substructure, and foundations. Moreover, the reduced weight of GFRP bars compared to steel bars makes them easier to handle during construction. Reduction of weight of concrete and reinforcement is also beneficial when seismic forces are considered.

There are no experimental data known to the author regarding the use of lightweight concrete reinforced with GFRP bars. The Japan Society of Civil Engineers (JSCE) and American Concrete Institute (ACI) 440.1R (2006) Guidelines do not provide guidance for lightweight concrete reinforced with GFRP bars. The American Association of State Highway and Transportation Officials (AASHTO) Load and Resistance Factor Design (LRFD) Bridge Design Guide Specifications for GFRP Reinforced Concrete Bridge Decks and Traffic Railings (2009) do not allow the use of lightweight concrete for decks reinforced with GFRP bars because of the lack of research. The Canadian Design and Construction of Building Components with Fibre-Reinforced Polymers S806 (2002) consider the effect of concrete density on tensile strength through a modification factor. However, it is not clear how this factor is to be obtained.

1.2 Shear Capacity

Extensive research has been carried out to determine the shear capacity of GFRP reinforced beams or slabs without transverse shear reinforcement. Swamy and Aburawi (1997) evaluated the performance of concrete beams reinforced with GFRP bars and suggested that an integrated approach to design based on material and

structural interaction may give engineers the breakthrough to optimum designs with GFRP bars. Deitz et al. (1999) tested several GFRP reinforced deck panels, and proposed two equations for computing the shear capacity of concrete panels reinforced with GFRP bars. Alkhrdaji et al. (2001) found that the contribution of concrete to the internal shear resistance was influenced by the amount of longitudinal GFRP reinforcement. Yost et al. (2001) evaluated the shear strength of intermediate length simply supported concrete beams and found that shear strength was independent of the amount of longitudinal GFRP reinforcement; a simplified empirical equation for predicting the ultimate shear strength of concrete beams reinforced with GFRP bars was endorsed. Tureyen and Frosch (2002) investigated different types of FRP reinforcement and found that the ACI 440 (2001) method was very conservative, whereas the ACI 318 (1999) method resulted in unconservative computations of shear strength. Gross et al. (2003) evaluated the shear strength for normal and high strength concrete beams and found that the longitudinal reinforcement ratio had a small influence on the concrete shear strength; in addition, high strength concrete beams exhibited a slightly lower relative shear strength (experimental shear strength normalized by $\sqrt{f_c'}bd$) than normal strength concrete beams. Ashour (2005) tested concrete beams reinforced with GFRP bars and determined that the theoretical predictions of shear capacity obtained from modifying the ACI 318-99 recommendations were inconsistent and that further research was necessary to establish a rational method for the prediction of shear capacity.

El-Sayed et al. (2005) investigated several full-size slabs and found that the ACI 440.1R-03 (2003) design method for predicting the concrete shear strength of FRP slabs was very conservative; better predictions were obtained by both the

Canadian CAN/CSA-S806-02 Code and the Japan Society of Civil Engineers design recommendations (JSCE 1997). El-Sayed et al. (2006a) investigated the behavior and shear strength of concrete slender beams reinforced with FRP bars and found that ACI 440.1R-03 was very conservative and proposed a modification to the ACI shear prediction. El-Sayed et al. (2006b) reported experimental data on the shear strength of high strength concrete slender beams and found that high strength concrete beams exhibited slightly lower relative shear strength compared to normal strength concrete beams. Alam and Hussein (2009) found that the shear strength of GFRP reinforced concrete beams was a function of the shear span to depth ratio, the effective depth of the beam, and the longitudinal reinforcement ratio. Jang et al. (2009) proposed a shear strength correction factor to evaluate the shear strength of FRP reinforced concrete beams considering the elastic modulus of FRP bar reinforcement, shear span to depth ratio, and flexural reinforcement ratio. Bentz et al. (2010) summarized the results of tests for reinforced concrete beams with GFRP reinforcement and found that members with multiple layers of longitudinal bars appeared to perform better in shear capacity than those with a single layer of longitudinal reinforcing bars; in addition, they found that the fundamental shear behavior of FRP reinforced beams was similar to that of steel-reinforced beams despite the brittle nature of the reinforcement.

1.3 Shear Prediction using Modified Compression Field Theory

Another promising shear prediction method used for GFRP reinforced concrete members is Modified Compression Field Theory (MCFT). It is an analytical model with fifteen equations which produce accurate estimates of shear strength for

steel-reinforced concrete members. Bentz and Collins (2006) reduced the MCFT equations into two, and these equations were found to provide accurate estimates of the shear strength of steel reinforced concrete members (Sherwood et al. 2007). Hoult et al. (2008) found that crack widths are affected by both a size effect and a strain effect regardless of the type of reinforcement used; they also showed that the two MCFT equations proposed by Bentz and Collins (2006) work equally well in predicting the shear capacity of normal weight concrete slabs reinforced with steel or FRP reinforcement. Sherwood et al. (2006) demonstrated that the width of a member does not have a significant influence on the shear stress at failure for steel reinforced concrete members, which indicates that the MCFT could be used for both beams and slabs. Bentz et al. (2010) found that despite the brittle nature of the reinforcement, FRP reinforced large concrete beams have a similar shear behavior as steel reinforced concrete beams.

1.4 Service Load Deflection

GFRP reinforcement has a smaller modulus of elasticity compared to steel reinforcement, and the smaller modulus will induce larger deflections when concrete members are reinforced with GFRP bars. Generally, serviceability requirements control the design of concrete members reinforced with GFRP bars rather than ultimate load conditions. Determination of the moment of inertia is critical in the deflection prediction of concrete member reinforced with GFRP bars. Extensive research has been conducted regarding prediction of the moment of inertia of GFRP reinforced concrete members (Gal et al. 1998, Theriault and Benmokrane 1998, Touganji and Saafi 2000, Yost et al. 2003, Bischoff and Paixao 2004, Bischoff 2005,

2007, Bischoff and Scanlon 2007, Said 2010, and Bischoff and Gross 2010). Efforts have been made for the modification of Branson's (1965) equation to consider the different properties of GFRP and steel bars when they are used as reinforcement and new equations were proposed for the prediction of moment of inertia. All previous research was focused on predicting the moment of inertia after the reinforced concrete member had cracked; it was assumed that the moment of inertia before the cracking moment was equal to the gross moment of inertia. However, precast concrete panels reinforced with GFRP bars can develop initial cracks from shrinkage, lifting, and transportation-induced stresses, which may reduce the value of moment of inertia from the gross moment of inertia value before the cracking moment is reached. Moment deflection diagrams comparing experimental to theoretical results in El-Salakawy and Benmokrane (2004) and Kassen et al. (2011) show that deflections prior to reaching the cracking moment are underestimated; this indicates that the corresponding moment of inertia is lower than the gross moment of inertia before the cracking moment is reached. The accurate prediction of moment of inertia before the cracking moment is just as critical as the accurate prediction of the moment of inertia after the cracking moment. This is justified since the bending moment under service loads can be lower than the value of the cracking moment, especially when high strength concrete is used. In such cases, the design of bridge panels reinforced with GFRP bars may be carried out using the gross moment of inertia and this may lead to unconservative designs.

The present project investigates lightweight and normal weight concrete precast deck panels for highway bridges. The deck panels are reinforced with GFRP bars. The experimental performance of lightweight concrete precast GFRP reinforced

deck panels versus normal weight concrete precast GFRP reinforced deck panels is investigated in terms of flexural performance, panel deflections, and shear capacity. GFRP reinforced concrete panels with different width, thickness, span, and reinforcement ratio were cast with both normal weight and sand-lightweight concrete. The applicability of existing equations in the ACI 440.1R (2006) design guidelines considering the shear capacity of GFRP reinforced concrete members is evaluated, and a reduction factor for consideration of sand-lightweight concrete is proposed. The moment of inertia of high strength normal weight and lightweight concrete precast bridge panels reinforced with GFRP bars is also investigated. Measured deflections at service moment and ultimate moment are compared with predictions using linear elastic analysis. Finally, the experimental shear strength of the precast decks was compared with the shear capacity predicted by the Modified Compression Field Theory (MCFT).

1.5 References

Alam, M. S., and Hussein, A., (2009). "Shear strength of concrete beams reinforced with Glass Fiber Reinforced Polymer (GFRP) bars." FRPRCS-9, Sydney, Australia.

Alkhrdaji, T., Wideman, M., Belarbi, A., and Nanni, A., (2001). "Shear Strength of GFRP RC Beams and Slabs." Proc., Composites in Constructions, J., Figueiras, L., Juvandes, and R. Faria, eds., Balkema, Lisse, the Netherlands, pp. 409-414.

American Association of State Highway and Transportation Officials, (AASHTO), (2009). "AASHTO LRFD Bridge Design Guide Specifications for GFRP Reinforced Concrete Decks and Traffic Railings." 1st edition, AASHTO, Washington, D. C., 68pp.

American Concrete Institute, (ACI 440,1R) (2006). "Guide for the Design and Construction of Structural Concrete Reinforced with FRP Bars." American Concrete Institute, Farmington Hills, Mich., 44pp.

Ashour, A. F., (2005). "Flexural and shear capacities of concrete beams reinforced with GFRP bars." Constru. Build. Mater., 20(10), pp. 1005-1015.

Bentz, E. C., and Collins, M. P., (2006). "Development of the 2004 CSA A23.3 shear provisions for reinforced concrete." Can. J. Civ. Eng., 33(5), 521-534.

Bentz, E. C., Massam, L., and Collins, M. P., (2010). "Shear strength of larger concrete members with FRP reinforcement." J. of Compos. Constr., 14 (6), 637-646.

Bischoff, P. H., and Paixao, R., (2004). "Tension stiffening and cracking of concrete reinforced with glass fiber reinforced polymer (GFRP) bars." Can. J. Civ. Eng., 31, 579-588.

Bischoff, P. H., (2005). "Reevaluation of Deflection prediction for Concrete Beams Reinforced with Steel and Fiber Reinforced Polymer Bars." J. Struct. Eng., 131(5), 752-767.

Bischoff, P. H., (2007). "Deflection Calculation of FRP Reinforced Concrete Beams Based on Modifications to the Existing Branson Equation." J. Compos. Constr., 11(1), 4-14.

Bischoff, P. H., and Gross, S. P., (2011). "Equivalent Moment of Inertia Based on Integration of Curvature." J. Compos. Constru., 15(3), 263-273.

Bischoff, P. H., and Scanlon, A., (2007). "Effective Moment of Inertia for Calculating Deflections of Concrete Members Containing Steel Reinforcement and Fiber-Reinforced Polymer Reinforcement." ACI Struct. Eng., 104(1), 68-75.

Branson, D. E., (1965). "Instantaneous and time-dependent deflections of simple and continuous reinforced concrete beams." HPR Report No. 7, Part 1, Alabama Highway Department, Bureau of Public Roads, Alab. (Dept. of Civil Engineering and Auburn Research Foundation, Auburn Univ., Aug. 1963).

Canadian Standards Association, (CAN/CSA S806) (2002). "Design and Construction of Building Components with Fibre Reinforced Polymers." Canadian Standards Association, Rexdale, Ontario, Canada, 177pp.

Castrodale, R. W., and Robinson, G. M. (2008). "Performance of lightweight concrete bridge decks." Concrete Bridge Conference, May 4-7, St. Louis, MO.

Deitz, D. H., Harik, I. E., and Gesund, H., (1999). "One-way slabs reinforced with Glass Fiber Reinforced Polymer reinforcing bars." Proc., 4th Int. Symp. On Fiber Reinforced Polymer Reinforcement for Reinforced Concrete Structures, Baltimore, pp. 279-286.

El-Salakawy, E. and Benmokrane, B., (2004). "Serviceability of Concrete Bridge Deck Slabs Reinforced with Fiber-Reinforced Polymer Composite Bars." ACI Struct. Eng., 101(5), 727-736.

El-Sayed, A., El-Salakawy, E., and Benmokrane, B., (2005). "Shear strength of one-way concrete slabs reinforced with Fiber-Reinforced Polymer composite bars." J. Composites for Construction, ASCE, V. 9, No. 2, pp. 147-158.

El-Sayed, A. K., El-Salakawy, E. F., and Benmokrane, B., (2006a). "Shear strength of FRP-reinforced concrete beams without transverse reinforcement." ACI Structural J., V. 103, No. 2, pp. 235-243.

El-Sayed, A. K., El-Salakawy, E. F., and Benmokrane, B., (2006b). "Shear capacity of high-strength concrete beams reinforced with FRP bars." ACI Structural J., V. 103, No. 3, pp. 383-389.

Gross, S. P., Yost, J. R., Dinehart, D. W., Svensen, E., (2003). "Shear strength of normal and high strength concrete beams reinforced with GFRP bars." High performance materials in bridges, Proc. Int. Conf., ASCE, Kona, Hawaii, pp. 426-437.

Hoult, N. A., Sherwood, E. G., Bentz, E. C., and Collins, M. P., (2008). "Does the Use of FRP Reinforcement Change the One-Way Shear Behavior of Reinforced Concrete Slabs?" J. Compos. Constr., 12(2), 125-133.

Jang, H., Kim, M., Cho, J., and Kim, C., (2009). "Concrete shear strength of beams reinforced with FRP bars according to flexural reinforcement ratio and shear span to depth ratio." FRPRCS-9, Sydney, Australia.

Japan Society of Civil Engineers (JSCE), (1997). "Recommendation for Design and Construction of Concrete Structures Using Continuous Fiber Reinforcing Materials." Concrete Engineering Series No, 23, 325pp.

Kassem, C., Farghaly, A. S., and Benmokrane, B., (2011). "Evaluation of Flexural Behavior and Serviceability Performance of Concrete Beams Reinforced with FRP Bars." J. Compos. Constru., accepted.

Said, H., (2010). "Deflection Prediction for FRP-Strengthened Concrete Beams." J. Compos. Constr., 14(2), 244-248.

Sherwood, E. G., Lubell, A. S., Bentz, E. C., and Collins, M. P. (2006). "One-way shear strength of thick slabs and wide beams." ACI Struct. J., 103(6), 794-802.

Swamy, N., and Aburawi, M. (1997). "Structural implications of using GFRP bars as concrete reinforcement." Non-Metallic (FRP) Reinforcement for Concrete Structures, Proc. 3rd Int. Symp. Vol. 2, pp. 503-510.

Theriault, M., and Benmokrane, B., (1998). "Effects of FRP Reinforcement Ratio and Concrete Strength on Flexural Behavior of Concrete Beams." J. of Compos. Constr., 2(1), 6-16.

Toutanji, H. A., and Saafi, M., (2000). "Flexural Behavior of Concrete Beams Reinforced with Glass Fiber-Reinforced Polymer (GFRP) Bars." ACI Struct. J., 97(5), 712-719.

Tureyen, A. K., and Frosch, R., (2002). "Shear tests of FRP-reinforced concrete beams without stirrups." ACI Structural J., V. 99, No. 4, pp. 427-434.

Yost, J. R., Gross, S. P., and Dinehart, D. W., (2001). "Shear strength of normal strength concrete beams reinforced with deformed GFRP bars." J. of Composites for Construction, ASCE, V. 5, No. 4, pp. 263-275.

Yost, J. R., Gross, S. P., and Dinehart, D. W., (2003). "Effective Moment of Inertia for Glass Fiber-Reinforced Polymer-Reinforced Concrete Beams." ACI Struct. J., 100(6), 732-739.

Yunovich, M., and Thompson, N. (2003). "Corrosion of highway bridges: Economic impact and control methodologies." ACI Concrete Int., 25(1), 52-57.

2 LIGHTWEIGHT CONCRETE PRECAST BRIDGE DECK PANELS REINFORCED WITH GFRP BARS

Chris P. Pantelides, Ruifen Liu, and Lawrence D. Reaveley

2.1 Abstract

Lightweight concrete results in bridge deck panels that are easier to lift, and its use reduces the bridge deck and substructure weight. Twenty panels constructed using lightweight and normal weight concrete reinforced with GFRP bars for flexure without any shear reinforcement were tested to failure. The variables investigated were concrete compressive strength, deck span, panel thickness and width, and reinforcement ratio. The experimental results show that lightweight concrete panels performed similar to normal weight concrete panels; however, they experienced larger deflections under the same load and had a lower ultimate shear strength than normal weight concrete panels. The ultimate shear strength of lightweight concrete panels reinforced with GFRP bars is predicted using the ACI 440.1R guidelines and the service load deflection is compared to AASHTO requirements. A reduction factor is found to be necessary for predicting shear strength when lightweight concrete is used with GFRP bars.

2.2 Introduction

Deicing salts are used on roadways for the removal of snow and ice. When the concentration of chlorides in bridge decks reaches a critical level, the passivation

layer on the steel reinforcement breaks down over time and active corrosion initiates. Corrosion can also be induced when the structure is near seawater. Corrosion of steel reinforcement leads to significant costs in rehabilitation or replacement and disruption of use. Yeomans[1] found that epoxy coating gave excellent corrosion protection to reinforcing steel provided the coating remained intact. If the coating was damaged severely, corrosion occurred to a similar extent as for black steel in equivalent circumstances. Manning[2] found that the number of defects in the coating is the dominant factor affecting the performance of epoxy coated bars in structures exposed to salt (marine and deicing). According to Manning[2], there is little doubt that coated bars extend the time to corrosion-induced damage in concrete structures. However, in a Canadian Strategic Highway Research Program (C-SHRP), Manning[2] reported that the time to corrosion-induced damage exceeded that of black bar reinforcement in bridges exposed to salt (marine and deicing) by only five to six years. Detection of corrosion in epoxy-coated steel bars has lead to consideration of GFRP bars as an alternative form of reinforcement when life-cycle costs are considered. GFRP bars are noncorrosive, and are becoming cost-competitive for structures that are vulnerable to corrosion. The use of GFRP bars can potentially extend the service life of bridge decks exposed to salt (marine and deicing).

Accelerated Bridge Construction (ABC) is a construction method which reduces on-site construction time and traffic disruption. The use of precast lightweight concrete deck panels reinforced with GFRP bars could benefit ABC. Sand-lightweight concrete commonly used in structures has a density between 90 and 115 lb/ft^3 (1440 to 1840 kg/m^3). Holm and Ries[3] provide details regarding the properties of lightweight concrete and lightweight aggregates. The reduced weight of

lightweight precast concrete bridge deck panels and precast monolithic decks is advantageous for lifting and moving when the ABC method is used. Lightweight concrete is also beneficial for the design of the substructure and foundations since the bridge deck weight is a significant portion of the dead load. Reduction of weight is also beneficial when seismic forces are considered.

Many design provisions and guidelines have been published regarding the performance and design of concrete structures reinforced with GFRP bars, such as the Japan Society of Civil Engineers Design provisions (JSCE) [4], the Canadian Design Provisions (CAN/CSA-S806-02)[5], the American Concrete Institute Guidelines (ACI 440.1R-06)[6], and the American Association of State Highway and Transportation Officials (AASHTO) Load Resistance Factor Design (LRFD) Bridge Design Guide for GFRP-Reinforced Concrete Bridge Decks[7].

Extensive research has been carried out regarding the flexural performance and shear capacity of concrete members reinforced with GFRP bars. Benmokrane et al.[8], Michaluk et al.[9], Masmoudi, et al.[10], Yost and Gross[11], Yost et al.[12], Prachasaree et al.[13], El-Mogy et al.[14], Swamy and Aburawi[15], Deitz et al.[16], Alkhrdaji et al.[17], Yost et al.[18], Tureyen and Frosch[19], Gross et al.[20], Ashour[21], El-Sayed et al.[22-24], Alam and Hussein[25], Jang et al.[26], and Bentz et al.[27], have investigated the flexural performance and shear capacity of normal weight concrete beams or slabs reinforced with GFRP bars without transverse shear reinforcement. The research has shown that flexural performance could be predicted using the plane sections remain plane assumption; however, the shear capacity of members reinforced with GFRP bars could not be predicted as well as flexural capacity.

All research completed to date has investigated normal weight concrete members reinforced with GFRP bars. There are no experimental data regarding the use of lightweight concrete with GFRP bars as reinforcement known to the authors. The JSCE[4] and ACI 440.1R-06[6] guidelines do not provide guidance for lightweight concrete reinforced with GFRP bars. The AASHTO GFRP-Reinforced Deck Specifications[7] do not allow the use of lightweight concrete for decks reinforced with GFRP bars because of the lack of research. The Canadian guidelines CAN/CSA-S806-02[5] consider the effect of concrete density on tensile strength through a modification factor.

This paper presents the test results of twenty panels reinforced with GFRP bars, twelve of which were cast using lightweight and eight using normal weight concrete. The variables studied in this research include concrete compressive strength, reinforcement ratio, slab thickness, deck span, and panel width. The service load deflections of the panels were measured and compared to the AASHTO LRFD Specifications. The ultimate shear strength of lightweight and normal weight concrete specimens was compared, and a reduction factor is found to be necessary when considering the use of lightweight concrete reinforced with GFRP bars.

2.3 Research Significance

Lightweight concrete precast panels are easier to lift and their use results in the reduction of bridge deck and substructure weight. However, there are no data available with respect to the use of lightweight concrete reinforced with GFRP bars known to the authors. The research reported in this paper presents test results that are used to evaluate the performance of lightweight and normal weight concrete panels

reinforced with GFRP bars for flexure without shear reinforcement. The performance of lightweight is evaluated and compared to that of normal weight concrete panels regarding structural behavior, failure modes, service load deflection, and ultimate shear strength.

2.4 Experimental Investigation

2.4.1 Specimen Details

Twenty concrete panels with thickness and reinforcement typical of GFRP reinforced decks were constructed and tested, including twelve lightweight concrete (LW) and eight normal weight concrete (NW) panels. A number of batches were cast for both NW and LW concrete panels at two different time periods. The NW concrete panels were designed using the ACI 440.1R[6] flexural design method; the specimens were designed so that failure was governed by concrete crushing; the panels were checked for service load requirements according to ACI 440.1R[6] (crack width requirement) and AASHTO LRFD guidelines (deflection requirement)[7,28]; additional panels were built using a reinforcement spacing twice that of the flexurally designed panels in the main direction. The flexurally designed panels were designed to fail in a concrete crushing failure mode since the latter gives limited warning of impending failure in the form of extensive cracking and large deflection due to the significant elongation that FRP reinforcement experiences before rupture[6]. In all tests, LW concrete panels were reinforced in an identical manner to NW concrete panels for comparison.

The panels were divided into four series according to their dimensions and reinforcement. Series A and B panels were 2 ft (0.61 m) wide, whereas Series C and

D panels were 6 ft (1.83 m) wide. Tables 2.1-2.4 show relevant dimensions and the reinforcement ratio for all panels. The first letter and the following number is the time of casting of concrete panels, where B1 = first period, B2 = second period; the next two letters stand for concrete type, where NW=normal weight, LW=lightweight; the fifth letter (E) when used stands for the case of reduced reinforcement ratio. Series D panels (Table 2.4) were constructed with 56% of the area of longitudinal reinforcement of Series C panels (Table 2.3). The NW concrete panels in Series A, B, and C were designed according to the ACI 440.1R[6] flexural design method. The NW concrete panels in Series D were built with a reinforcement ratio equal to half that of Series C panels with one additional bar at the two panel edges. The LW concrete panels in each series were reinforced in an identical manner to the NW concrete panels since currently there are no guidelines regarding the design of GFRP panels using LW concrete.

All panels were constructed at a local precast concrete plant and transported to the laboratory. This was done to simulate precast bridge deck construction practice using the Accelerated Bridge Construction (ABC) method. The panels were inspected before testing; initial cracks due to handling and transportation were measured and mapped. The maximum initial crack width of each panel is given in Tables 2.1-2.4. The number and width of the initial cracks are important in estimating the initial stiffness of the panels.

All panels tested had a 2 ft (0.61 m) overhang on each side of the supports (as shown in Figs. 2.1 and 2.2); this overhang increased the length available to develop the full tensile capacity of the GFRP bars. Actual bridge decks are continuous over several spans and can develop full strength in each span. The dimensions,

reinforcement, and transverse section of the panels for Series A and B are shown in Fig. 2.1, and for Series C and D are shown in Fig. 2.2.

The intent of the original flexural design of the panels was to provide a reinforcement ratio (ρ_f) higher than the balanced reinforcement ratio (ρ_b). However, because the concrete as cast had a higher compressive strength than the design strength, the resulting reinforcement ratio ended up being approximately equal to the balanced reinforcement ratio. Series A and B panels shown in Fig. 2.1 were constructed using a width of 2 ft (0.61 m) to simulate the design of bridge decks according to AASHTO Bridge Design Specifications[28]. Series A panels shown in Fig. 2.1(a) had a deck span of 8 ft (2.44 m) typical of GFRP reinforced cast-in-place normal weight concrete bridge decks. Series B panels shown in Fig. 2.1(b) had a deck span of 9 ft-6 in. (2.90 m) which is typical of steel reinforced cast-in-place normal weight concrete bridge decks. Series C panels shown in Fig. 2.2(a) were constructed using a 6 ft (1.83 m) width to simulate the behavior of a recently constructed bridge deck in Utah using 6 ft-10 in. (2.08 m) x 41 ft-5 in. (12.62 m) normal weight precast concrete panels 9 ¼ in. (235 mm) thick, reinforced with GFRP bars. Series D panels shown in Fig. 2.2(b) had the same dimensions as Series C panels with half the reinforcement; the actual reinforcement ratio of Series D panels was 56% the amount of GFRP reinforcement ratio since one extra GFRP bar was added on each side of the panel. This was done to investigate whether the amount of reinforcement and thus the cost of the panels could be reduced, without affecting acceptable performance.

2.4.2 Materials

All concrete panels in this research were reinforced with # 5 (Φ16) GFRP bars. The tensile strength of the specific lot of GFRP bars used in this research was 103,700 psi (655 MPa), and the modulus of elasticity was 6,280,000 psi (40.8 GPa). These properties were determined using ACI 440.3R[29] test procedures for the specific lot of bars used in this research. The compressive strength of NW concrete at the time of testing ranged from 8,500 psi (59 MPa) to 12,600 psi (87 MPa); the compressive strength of LW concrete ranged from 8,100 psi (56 MPa) to 10,900 psi (75 MPa), as shown in Tables 2.1-2.4. The coarse hard rock aggregate for NW concrete had a size of ¾ in. (19 mm); the expanded shale aggregate for LW concrete had a size of ½ in. (12.7 mm). Fine aggregate used for the LW concrete was sand commonly used in NW concrete; thus, the LW concrete used in this research is classified as sand-lightweight concrete. The unit weight of the LW concrete used was 123 lb/ft^3 (1970 kg/m^3). Split cylinder tests were carried out for both types of concrete. The mean tensile splitting strength of LW concrete was 82% that of NW concrete.

2.5 Instrumentation

All specimens were instrumented in a manner similar to that shown in Fig. 2.3. Electrical resistance strain gauges were adhesively bonded to GFRP bars to measure strain in the longitudinal (B10_1 to B10_9) and transverse directions (BL_11 to BL_16) as shown by the solid boxes in Fig. 2.3. Additional electrical resistance strain gauges were bonded to the top surface of the panels to measure strain in the concrete as shown by the dashed boxes in Fig. 2.3 (CSG1 to CSG6). One Linear Variable Differential Transducer (LVDT) was attached to the bottom of the panels at midspan

and two at the quarter span points for the 2 ft (0.61 m) wide panels to measure deflections. One LVDT was attached at midspan and two at the quarter span points for the 6 ft (1.83 m) wide panels; two additional LVDTs were used on each side of the panels at the outer edges at midspan. The dashed lines in Fig. 2.3 are the centerlines of the supporting beams and the rectangle in the middle of the panel is the steel bearing plate used to apply the load.

2.6 Test Setup and Procedure

All panels were tested as shown in Fig. 2.4; the panels were simply supported on two reinforced concrete beams. Elastomeric pads 6 in. (152 mm) wide and 2 in. (51 mm) thick were placed on the two supporting beams so the panels could rotate freely near the support without crushing the panel. This setup is a simplification of actual support conditions for precast concrete panels used in bridge decks. Typically, block-outs in the panels are grouted to connect them to the supporting girders to achieve composite action.

The load was applied using a hydraulic actuator through a 10 in. x 20 in. x 1 in. (254 mm x 508 mm x 25 mm) steel bearing plate, which simulates the area of a double tire truck load on a bridge deck (AASHTO[28]). The load was applied as a series of half-sine downward cycles of increasing amplitude without stress reversals, with a constant loading rate of 0.2 in./min (5.08 mm/min) using displacement control. The loading procedure used for the actuator displacement is shown in Fig. 2.5, where downward displacement is positive. The loading scheme was intended to simulate the repeated truck loading on the panels of a precast concrete bridge deck.

2.7 Experimental Results

2.7.1 Behavior

All panels developed flexural cracks at lower load levels and additional diagonal cracks at higher load levels. Ultimately the panels failed in a diagonal tension failure mode, as shown in Fig. 2.6 for 2 ft (0.61 m) wide panels and Fig. 2.7 for 6 ft (1.83 m) wide panels. The panels were designed so that concrete crushing failure would control; accordingly the reinforcement ratio was intended to be higher than the balanced reinforcement ratio. However, the actual concrete compressive strength was higher than the design strength, which led to a slightly lower reinforcement ratio than the balanced reinforcement ratio; despite this, the panels failed in a concrete crushing failure mode. After formation of the critical diagonal crack near one of the two supports, the concrete was horizontally split along both the top and bottom reinforcing mats and debonding of the top and bottom bars occurred; ultimately, concrete crushed on the compression face of the panels. All panels failed by the same failure mode regardless of concrete type (NW concrete or LW concrete), panel dimensions, or amount of reinforcement. Failure of the panels was sudden; the GFRP bars in the bottom mat did not fracture in any of the tests even though they experienced significant deformation, as shown in Fig. 2.8. The measured maximum load and deflection of all panels tested in this research is provided in Tables 2.1-2.4. A comparison of the ultimate load of NW and LW panels shows that the latter had a lower capacity. This was expected as the tensile strength of LW concrete is lower (75%-100%) compared to NW concrete[3]. On average, LW concrete panels reached 81% of the shear capacity of NW panels. As far as ultimate deflection, on average, LW concrete panels reached 77% of the ultimate deflection of NW panels.

2.7.2 Strain Measurements

Figure 2.9 shows strains measured from strain gauges (SG) in panel #17 B2LW, which is representative of the 6 ft (1.83m) wide LW panels. The strains in a bottom GFRP bar at the mid-width of the panel are shown. The strain gauge numbers correspond to the locations shown in Fig. 2.3. As the load increases, strains also increase during each cycle. After unloading, residual strains remain in the GFRP bars; the residual strains increase as the load increases. Strains are higher in the bar when the strain gauge is located near the load bearing plate as evidenced by comparing strains in SG B10_1, SG B10_2, and SG B10_3. The maximum strain in the GFRP bar occurs near the perimeter of the load bearing plate rather than at midspan; this is shown by comparing SG B10_3 and SG B10_4. Strain Gauge B10_2 reached much higher strains in the last two cycles of loading because the critical diagonal crack formed in its proximity. The strain gauges located symmetrically with respect to midspan show similar strains at the beginning of the test, but have different values in the last few cycles because of the development of the critical diagonal crack near one of the supports.

Figure 2.10 shows the strains in the GFRP bars in the transverse (6 ft (1.83 m)) direction of the panels. The strains in these GFRP bars increase rapidly as the position of the strain gauge approaches the midpoint of the panel. The strains in the transverse direction are much smaller than the strains in the longitudinal direction; in general, the peak strain in the 6 ft (1.83 m) direction was 30% to 60% of the strain in the 12 ft (3.66 m) direction for both NW and LW concrete panels. The strain in the transverse direction is due to the transfer of the applied load across the entire width of

the panel; this shows that the outer edges of the panel are trying to hold up the center section that is directly under the applied load.

2.7.3 Load-Deflection Envelopes

Load-deflection envelopes were constructed by connecting consecutive points of the maximum load for each cycle. Figures 2.11-2.13 show that the load deflection envelopes are generally bilinear. The first line segment is up to the point where the section reached the cracking moment; in this segment, the panels have a higher stiffness; this is the initial stiffness given in Tables 2.1-2.4. Before the section reached the cracking moment, for panels with the same reinforcement ratio, the stiffness was approximately the same for both NW and LW concrete panels within each series. After the section reached the cracking moment, both NW and LW panels had a much smaller stiffness, approximately 13% to 35% of the initial stiffness.

Figures 2.11 and 2.12 show the stiffness of 2 ft (0.61 m) wide panels for two different deck spans. Series B panels had 80% the stiffness of Series A panels before the section reached the cracking moment; after the section reached the cracking moment, Series B panels had 83% the stiffness of Series A panels. The stiffness of the panels with reduced reinforcement ratio (Series D) was 60% of the stiffness of the Series C panels with the higher reinforcement ratio (Series C), for both NW and LW concrete panels. Comparing Tables 2.1 and 2.2, the ultimate load of Series A LW concrete panels is 5% higher than Series B LW panels, while the ultimate load of Series A NW concrete panels is 13% higher than Series B NW panels. By increasing the thickness, Series B panels which had a longer span achieved a similar

performance to Series A panels in terms of stiffness, ultimate load, and ultimate deflection, as shown in Tables 2.1-2.4.

Figure 2.13 shows that after the section reached the cracking moment, the stiffness of the 6 ft (1.83 m) wide panels was influenced by the reinforcement ratio, as evidenced by a comparison of Series C and Series D panels (underlined in Fig. 2.13). Before the section reached the cracking moment, the panel stiffness is related to the number and width of initial cracks but not the reinforcement ratio; this is demonstrated by the fact that the initial stiffness (stiffness before the section reached the cracking moment) of Series D panels reached 94% of the stiffness of Series C panels; after cracking, the stiffness of Series D panels is only 60% of Series C panels. All panels tested had initial cracks 0.002 in. (0.05 mm) wide or wider, as shown in Tables 2.1-2.4. Initial crack widths resulting from specimen handling had no effect on the ultimate load capacity provided they were smaller than 0.01 in. (0.25 mm) wide. It is clear that handling stresses can create cracks, which in turn can reduce local bond and aggregate interlock and thus reduce the shear capacity of the member. Handling of precast concrete panels reinforced with GFRP bars requires extra care. One method for handling such panels would be to lift them with straps placed underneath the panels at multiple points rather than using lifting hoops at the four corners.

Figures 2.11 and 2.13 show the behavior for different panel widths but the same deck span of 8 ft (2.44 m). Before the cracking moment was reached, the stiffness of Series A panels was 50% of the stiffness of Series C panels; after the section reached the cracking moment, Series A panels had a stiffness equal to 39% of the stiffness of Series C panels. Comparing Tables 2.1 and 2.3, the ultimate load

capacity of Series C panels was on average 2.7 times that of Series A panels for both NW and LW concrete. This demonstrates that panel capacity is not linearly proportional to panel width. This is due to the manner in which the panels were loaded (steel plate in the middle section of the panel) and the elastomeric support conditions (the middle sections of the elastomeric supports deflected more than the outer sections).

Comparing Tables 2.3 and 2.4, the ultimate load capacity of NW panels with reduced reinforcement ratio (Series D) was on average 77% of the NW panels with nominal reinforcement (Series C); similarly, the capacity of the LW Series D panels was on average 80% of the LW Series C panels. This is true even though the ratio of reduced to nominal reinforcement was 56%. The explanation for this is that the GFRP bar strains for the Series D panels were on average 10% to 16% higher than the Series C panels, thus contributing to higher flexural capacity; the increase in GFRP bar strain was limited because of the shear failure mode observed in all tests.

2.8 Service Load Deflection Comparison with AASHTO LRFD Specifications

Service load deflections typically control the design of GFRP reinforced concrete bridge decks. The deflections of GFRP reinforced precast concrete panels were recorded continuously during the tests. The recorded service load deflections of the panels were compared to the deflection requirements of the AASHTO LRFD Bridge Design Specifications[28]. Table 2.5 shows the deflection of the panels at service load and the ratio of the measured deflection to the allowable. The allowable deflection at service load in AASHTO[28] is $L/800$, where L is the span length; thus

the deflection requirement at service load is 0.12 in. (3.0 mm) and 0.14 in. (3.6 mm) for the 8 ft (2.44 m) span and 9 ft-6 in. (2.90 m) span panels, respectively. Comparing the experimental deflection measured at service load, it is found that all panels satisfy the service load deflection requirement of AASHTO[28], except for the two lightweight concrete panels with reduced reinforcement ratio of Series D. On average, the deflection of all lightweight concrete panels is 1.4 times that of all normal weight concrete panels at service load.

2.9 Ultimate Load and Ultimate Moment Comparisons with AASHTO LRFD Specifications

In AASHTO LRFD Bridge Design Specifications[28], an HL-93 live load is used for design. The HL-93 live load consists of a design truck or tandem, combined with a design lane load. For 2 ft (0.61 m) wide panels, an HS truck causes the maximum shear load; for 6 ft (1.83 m) wide panels, tandem causes the maximum shear load. Table 2.6 shows the ratio of the achieved ultimate load to the AASHTO load on average. The minimum load ratio is 1.5 for NW concrete and 1.3 for LW concrete panels. This comparison shows that all panels exceeded the load capacity required by AASHTO Specifications, with the wider panels having more conservative results. This conservatism becomes more pronounced when one considers that for HS trucks, the distance between wheel axles is 14 ft (4.27 m). AASHTO bridge decks are designed using ultimate moment capacity. Table 2.6 shows the ratio of ultimate moment achieved to the AASHTO design moment. The minimum moment ratio is 3.9 for NW panels and 3.3 for LW panels. The comparison shows that all panels exceeded the moment capacity required by AASHTO Specifications.

2.10 Shear Strength Comparison with ACI 440.1R Guidelines

To predict the shear capacity of flexural members using GFRP bars as the main reinforcement, ACI 440.1R[6] uses the following equations:

$$V_c = \frac{2}{5}\sqrt{f_c'}\,b_w c \qquad 2.1(a)$$

$$c = kd \qquad 2.1(b)$$

$$k = \sqrt{2\rho_f n_f + (\rho_f n_f)^2} - \rho_f n_f \qquad 2.1(c)$$

$$E_c = 0.043 w_c^{1.5}\sqrt{f_c'} \qquad 2.1(d)$$

$$E_c = \left[3.32\sqrt{f_c'} + 6895\right]\left(\frac{w_c}{2320}\right)^{1.5} \qquad 2.1(e)$$

where f_c' = specified compressive strength of concrete (MPa); b_w = web width (mm); c = cracked transformed section neutral axis depth (mm); d = distance from extreme compression fiber to centroid of tension reinforcement (mm); n_f = ratio of modulus of elasticity of FRP bars to modulus of elasticity of concrete; ρ_f = FRP reinforcement ratio; k = ratio of depth of neutral axis to reinforcement depth; E_c = modulus of elasticity of concrete (MPa), where Eq. (2.1d) applies to normal strength concrete for f_c' less than 41 MPa and Eq. (2.1e) for high strength concrete for f_c' greater than 41 MPa; and w_c =density of concrete.

Figure 2.14 shows a comparison of experimental ultimate shear to the ACI 440.1R predicted shear strength using Eq. (2.1) for the present study; the experimental shear strength is larger than the predicted shear strength. In addition, the shear strength of lightweight concrete panels had a smaller reserve strength compared to normal weight concrete panels. Figure 2.15 shows the comparison of experimental ultimate shear to the ACI 440.1R predicted shear strength using an extended database. The extended database includes beam or slab tests from the literature (Swamy and Aburawi[15], Deitz et al.[16], Alkhrdaji et al.[17], Yost et al.[18], Tureyen and Frosch[19], Gross et al.[20], Ashour[21], El-Sayed et al.[22-24], Alam and Hussein[25], Jang et al.[26], and Bentz et al.[27]), in which the normal weight concrete specimens were reinforced with GFRP bars without any transverse reinforcement and failed in one-way shear. Figure 2.15 shows the same trend as Fig. 2.14. Comparing the experimental shear of normal weight to lightweight concrete members, it is found that the ACI 440.1R equation must use a reduction factor for lightweight concrete, if lightweight concrete members reinforced with GFRP bars are to have the same conservatism as normal weight concrete members.

2.11 Conclusions

The performance of precast lightweight concrete panels reinforced with GFRP bars was investigated and compared to that of normal weight concrete panels reinforced in an identical manner. The main findings of this research are summarized as follows:

1. Satisfactory performance of panels with different spans was achieved following the ACI 440.1R guidelines. Panels were tested for two different

deck spans, 8 ft (2.44 m) and 9 ft-6 in. (2.90 m), with the same reinforcement spacing. By increasing the thickness of the panels to 10 ¾ in. (273 mm), panels with a 9 ft-6 in. (2.90 m) span achieved a similar performance in terms of stiffness, service load deflection, and ultimate load compared to 8 ft (2.44 m) span panels with a 9 ¼ in. (235 mm) thickness.

2. All panels designed and reinforced according to ACI 440.1R satisfied the service load deflection limit of the AASHTO LRFD Specifications. Lightweight concrete panels with only 56% the reinforcement ratio of the panels designed according to ACI 440.1R did not satisfy the service load deflection limit of the AASHTO LRFD Specifications, even though normal weight concrete panels with reduced reinforcement ratio satisfied the deflection requirement. On average, the service load deflection of lightweight concrete panels was 1.4 times that of normal weight concrete panels.
3. The number and width of initial cracks controlled panel stiffness before the section reached the cracking moment. Initial crack widths resulting from handling of the specimens had no effect on the ultimate load capacity provided they were smaller than 0.01 in. (0.25 mm) wide. After the panels reached the cracking moment, both normal weight and lightweight concrete panels had a reduced stiffness ranging from 13% to 35% of the initial stiffness. Handling of precast panels reinforced with GFRP bars requires extra care; one suggested method is to lift the panels with straps placed underneath the panels at multiple points rather than using lifting hoops at the four corners of the panel.
4. The shear strength of lightweight concrete panels reinforced with GFRP bars was on average 81% that of normal weight concrete panels reinforced with

GFRP bars. This is due to the lower tensile strength of lightweight concrete compared to normal weight concrete, and the resulting reduction of the splitting resistance.

5. The ultimate shear strength of panels with a reduced reinforcement ratio (56% of flexurally designed panels) was 77% and 80% of the panels designed according to ACI 440.1R for normal weight and lightweight concrete, respectively. The reason for this is that GFRP bars in panels with the reduced amount of reinforcement developed higher strains (10%-16%) than the flexurally designed panels; however, this increase in strain was limited due to the shear failure mode of the panels.
6. The ultimate load performance of both normal weight and lightweight concrete panels is acceptable when compared to the standard design truck load. The 2 ft (0.61 m) wide panels with the load configuration tested in this research achieved a capacity of 1.3 to 1.7 times the load, and 4.4 to 6.1 times the moment requirement of the AASHTO LRFD Specifications. The 6 ft (1.83 m) wide panels achieved a capacity of 1.8 to 2.7 times the load, and 3.1 to 5.5 times the moment requirement of the AASHTO LRFD Specifications.
7. The ACI 440.1R shear strength equations are conservative in predicting the ultimate shear strength of GFRP reinforced members. Lightweight concrete had a smaller shear strength reserve compared to normal weight concrete for panels tested in this research and for panels from an extended database, which included normal weight concrete from the literature. This research has shown that a reduction factor is required for predicting the shear strength of lightweight concrete when GFRP bars are used as reinforcement.

2.12 Notation

b_w =web width;

c = cracked transformed section neutral axis depth;

d = distance from extreme compression fiber to centroid of tension reinforcement;

E_c = modulus of elasticity of concrete;

$f_c^{'}$ =concrete compressive strength;

h =overall height of flexural member;

k = ratio of depth of neutral axis to reinforcement depth;

LW=lightweight concrete;

n_f = ratio of modulus of elasticity of FRP bars to modulus of elasticity of concrete;

NW=normal weight concrete;

$p_{\max}$ =maximum load recorded from actuator;

S =deck span;

w_c =density of concrete;

ρ_f =FRP reinforcement ratio;

ρ_{fb} =FRP reinforcement ratio producing balanced strain conditions

2.13 Acknowledgments

The research reported in this paper was supported by the Utah DOT and the Expanded Shale Clay and Slate Institute. The authors acknowledge the contribution of Hughes Bros Inc., Utelite Corporation, and Hanson Structural Precast. The authors

acknowledge the assistance of Mark Bryant, Brandon T. Besser, and Clayton A. Burningham of the University of Utah in the experimental portion of the research.

2.14 References

1. Yeomans, S.R., "Performance of Black, Galvanized, and Epoxy-Coated Reinforcing Steels in Chloride-Contaminated Concrete." Corrosion, Jan. 1994, pp. 72-81.

2. Manning, D.G., "Corrosion performance of epoxy-coated reinforcing steel: North American experience." Construction and Building Materials, V. 10, No.5. 1996, pp. 349-365.

3. Holm, T.A., and Ries, J.P. "Lightweight concrete and aggregates." ASTM 169D, Chapter 46, 2006, pp. 548-560.

4. Japan Society of Civil Engineers (JSCE). "Recommendation for Design and Construction of Concrete Structures Using Continuous Fiber Reinforcing Materials". Concrete Engineering Series No. 23, 1997, 325pp.

5. Canadian Standards Association (CAN/CSA S806—02). "Design and Construction of Building Components with Fibre Reinforced Polymers," Canadian Standards Association, Rexdale, Ontario, Canada, 2002, 177pp.

6. American Concrete Institute (ACI 440.1R-06). "Guide for the Design and Construction of Structural Concrete Reinforced with FRP Bars". American Concrete Institute, Farmington Hills, Mich., 2006, 44 pp.

7. American Association of State Highway and Transportation Officials (AASHTO). "AASHTO LRFD Bridge Design Guide Specifications for GFRP Reinforced Concrete Decks and Traffic Railings." 1st edition, AASHTO, Washington, D.C., 2009, 68 pp.

8. Benmokrane, B., Chaallal, O., and Masmoudi, R., "Flexural Response of Concrete Beams Reinforced with FRP Reinforcing Bars," ACI Structural Jouranl, V. 91, No. 2, 1995, pp. 46-55.

9. Michaluk, C. R., Rizkalla, S. H., Tadros, G., and Benmokrane, B., "Flexural Behavior of One-Way Concrete Slabs Reinforced by Fiber Reinforced Plastic Reinforcements," ACI Structural Journal, V. 95, No. 3, 1998, pp. 353-365.

10. Masmoudi, R., Theriault M. and Benmokrane, B., "Flexural Behavior of Concrete Beams Reinforced with Deformed Fiber Reinforced Plastic Reinforcing Rods," ACI Structural Journal, V. 95, No. 6, 1998, pp. 665-676.

11. Yost, J. R., and Gross, S. P., "Flexural Design Methodology for Concrete Beams Reinforced with Fiber-Reinforced Polymers," ACI Structural Journal, V. 99, No. 3, 2002, pp. 308-316.

12. Yost, J. R., Goodspeed, C. H., and Schmeckpeper, E. R., "Flexural Performance of Concrete Beams Reinforced with FRP Grids," Journal of Composites for Construction, V. 5, No. 1, 2001, pp. 18-25.

13. Prachasaree, W., Gangarao H. V. S., and Shekar V., "Performance Evaluation of FRP Bridge Deck under Shear Loads," Journal of Composite Materials, V. 43, No. 4, 2009, pp. 377-395.

14. El-Mogy, M., El-Ragaby, A., and El-Salakawy, E., "Flexural Behavior of Continuous FRP-Reinforced Concrete Beams," Journal of Composites for Construction, V. 14, No. 6, 2010, pp. 669-680.

15. Swamy, N., and Aburawi, M., "Structural implications of using GFRP bars as concrete reinforcement," Non-Metallic (FRP) Reinforcement for Concrete Structures, Proc. 3rd Int. Symp., Vol. 2, 1997, pp. 503-510.

16. Deitz, D.H., Harik, I.E., and Gesund, H., "One-way slabs reinforced with Glass Fiber Reinforced Polymer reinforcing bars," Proc., 4th Int. Symp. on Fiber Reinforced Polymer Reinforcement for Reinforced Concrete Structures, Baltimore, 1999, pp. 279-286.

17. Alkhrdaji, T., Wideman, M., Belarbi, A., and Nanni, A., "Shear Strength of GFRP RC Beams and Slabs," Proceedings, Composites in Constructions, J. Figueiras, L. Juvandes, and R. Faria, eds., Balkema, Lisse, the Netherlands, 2001, pp. 409-414.

18. Yost, J.R., Gross, S.P., and Dinehart, D.W. "Shear strength of normal strength concrete beams reinforced with deformed GFRP bars," Journal of Composites for Construction, V. 5, No. 4, Oct. 2001, pp. 263-275.

19. Tureyen, A.K., and Frosch, R., "Shear tests of FRP-reinforced concrete beams without stirrups," ACI Structural Journal, V. 99, No. 4, July 2002, pp. 427-434.

20. Gross, S.P., Yost, J.R., Dinehart, D.W., Svensen, E., "Shear strength of normal and high strength concrete beams reinforced with GFRP bars," High performance materials in bridges, Proceedings of the International Conference, 2003, pp. 426-437.

21. Ashour, A.F., "Flexural and shear capacities of concrete beams reinforced with GFRP bars," Construction and Building Materials, V. 20, No. 10, Dec. 2005, pp. 1005-1015.

22. El-Sayed, A., El-Salakawy, E., and Benmokrane, B., "Shear strength of one-way concrete slabs reinforced with Fiber-Reinforced Polymer composite bars," Journal of Composites for Construction, V. 9, No. 2, April 2005, pp. 147-157.

23. El-Sayed, A.K., El-Salakawy, E.F. and Benmokrane, B., "Shear strength of FRP-reinforced concrete beams without transverse reinforcement," ACI Structural Journal, V. 103, No. 2, March 2006, pp. 235-243.

24. El-Sayed, A.K., El-Salakawy, E.F. and Benmokrane, B., "Shear capacity of high-strength concrete beams reinforced with FRP bars," ACI Structural Journal, V. 103, No. 3, May 2006, pp. 383-389.

25. Alam, M.S., Hussein, A., "Shear strength of concrete beams reinforced with Glass Fiber Reinforced Polymer (GFRP) bars," Proceedings of the 9th International Symposium of the Fiber-Reinforced Polymer Reinforcement for Reinforced Concrete Structures, Sydney, Australia, 2009.

26. Jang, H., Kim, M., Cho, J., Kim, C., "Concrete shear strength of beams reinforced with FRP bars according to flexural reinforcement ratio and shear span to depth ratio," Proceedings of the 9th International Symposium of the Fiber-Reinforced Polymer Reinforcement for Reinforced Cocnrete Structures, Sydney, Australia, 2009.

27. Bentz, E.C, Massam, L., and Collins, M.P., "Shear Strength of Large Concrete Members with FRP Reinforcement," Journal of Composites for Construction, V. 14, No. 6, Dec. 2010, pp. 637-646.

28. American Association of State Highway and Transportation Officials (AASHTO). "AASHTO LRFD Bridge Design Specifications", 4th Edition, AASHTO, Washington, D.C., 2007, 1526pp.

29. American Concrete Institute (ACI 440.3R-04). "Guide Test Methods for Fiber-Reinforced Polymers (FRPs) for Reinforcing or Strengthening Concrete Structures". American Concrete Institute, Farmington Hills, Mich., 2004, 40 pp.

Table 2.1 Series A panels: 2 ft (0.61 m) wide x 9 ¼ in. (235 mm) thick with 8 ft (2.44 m) span

Specimen Number	f_c' psi (MPa)	ρ_f %	ρ_b %	Initial crack width in. (mm)	Initial stiffness kip/in. (kN/mm)	V_{exp} kips (kN)	P_{max} kips (kN)	$\Delta_{ult.}$ in. (mm)
#1 B1NW	10,370 (71.50)	0.94	0.95	0.002 (0.051)	87.79 (15.37)	30.62 (136.2)	59.37 (264.1)	2.09 (53.1)
#2 B2NW	12,650 (87.22)	0.94	1.16	0.002 (0.051)	175.30 (34.20)	30.26 (134.6)	58.56 (260.5)	1.77 (45.0)
#3 B2NW	8,760 (60.40)	0.94	0.80	0.002 (0.051)	160.36 (28.08)	27.62 (122.9)	53.38 (237.4)	1.70 (43.2)
#4 B1LW	9,090 (62.67)	0.94	0.83	0.007 (0.178)	-	24.26 (112.4)	48.66 (216.5)	1.52 (38.6)
#5 B1LW	10,930 (75.36)	0.94	1.00	0.002 (0.051)	102.35 (17.92)	23.09 (102.7)	44.32 (197.1)	1.06 (26.9)
#6 B2LW	8,700 (59.98)	0.94	0.80	0.005 (0.127)	-	23.18 (103.1)	44.50 (197.9)	1.61 (40.9)
#7 B1LW*	8,730 (60.19)	0.94	0.91	0.002 (0.051)	-	27.46 (122.2)	53.20 (236.6)	0.69 (17.6)

*span was 6.66 ft (2.03 m)

Table 2.2 Series B panels: 2 ft (0.61 m) wide x 10 ¾ in. (273 mm) thick with 9 ft-6 in. (2.82 m) span

Specimen Number	f_c' psi (MPa)	ρ_f %	ρ_b %	Initial crack width in. (mm)	Initial stiffness kip/in. (kN/mm)	V_{exp} kips (kN)	P_{max} kips (kN)	$\Delta_{ult.}$ in. (mm)
#8 B1NW	11,420 (78.74)	0.79	1.05	0.016 (0.406)	80.35 (14.07)	24.01 (106.8)	45.45 (202.2)	2.73 (69.3)
#9 B2NW	8,840 (60.95)	0.79	0.81	0.002 (0.051)	122.80 (21.51)	27.95 (124.3)	53.32 (237.2)	1.81 (46.0)
#10 B1LW	9,080 (62.60)	0.79	0.83	0.004 (0.102)	93.93 (16.45)	22.44 (99.8)	42.30 (188.2)	1.79 (45.5)
#11 B2LW	8700 (59.98)	0.79	0.80	0.003 (0.076)	119.84 (20.99)	23.69 (105.4)	44.80 (199.3)	1.88 (47.8)

Table 2.3 Series C panels: 6 ft (1.83 m) wide x 9 ¼ in. (235 mm) thick with 8 ft (2.44 m) span

Specimen Number	f_c' psi (MPa)	ρ_f %	ρ_b %	Initial crack width in. (mm)	Initial stiffness kip/in. (kN/mm)	V_{exp} kips (kN)	P_{max} kips (kN)	$\Delta_{ult.}$ in. (mm)
#12 B1NW	12,130 (83.63)	0.96	1.11	0.007 (0.178)	269.62 (47.22)	87.63 (389.8)	169.82 (755.4)	3.31 (84.1)
#13 B2NW	8,510 (58.67)	0.96	0.78	0.002 (0.051)	270.60 (47.39)	72.74 (323.6)	140.05 (623.0)	2.64 (67.1)
#14 B1LW	9,080 (62.60)	0.96	0.83	0.003 (0.076)	296.11 (51.86)	61.76 (274.7)	118.09 (525.3)	1.83 (46.5)
#15 B1LW	9,080 (62.60)	0.96	0.83	0.007 (0.178)	201.59 (35.30)	65.23 (290.2)	125.02 (556.1)	3.32 (84.3)
#16 B2LW	8,250 (56.88)	0.96	0.76	0.002 (0.051)	245.85 (43.06)	67.21 (299.0)	128.99 (573.8)	2.63 (66.8)
#17 B2LW	8,060 (55.57)	0.96	0.74	0.005 (0.127)	283.61 (49.67)	68.01 (302.5)	130.58 (580.8)	1.65 (41.9)

Table 2.4 Series D panels: 6 ft (1.83 m) wide x 9 ¼ in. (235 mm) thick with 8 ft (2.44 m) span

Specimen Number	f_c' psi (MPa)	ρ_f %	ρ_b %	Initial crack width in. (mm)	Initial stiffness kip/in. (kN/mm)	V_{exp} kips (kN)	P_{max} kips (kN)	$\Delta_{ult.}$ in. (mm)
#18 B1NWE	12,130 (83.63)	0.54	1.11	0.005 (0.127)	334.24 (58.53)	62.09 (276.2)	118.75 (528.2)	2.96 (75.2)
#19 B1LWE	9,080 (62.60)	0.54	0.83	0.009 (0.229)	213.27 (37.35)	56.03 (249.2)	106.62 (474.3)	2.35 (59.7)
#20 B2LWE	8,060 (55.57)	0.54	0.74	0.005 (0.127)	189.19 (33.13)	49.71 (221.1)	93.99 (418.1)	1.99 (50.5)

Table 2.5 Service load deflection of panels and comparison with AASHTO LRFD Specifications

Series	Specimen	Service load deflection	Service/AASHTO
		$\Delta_{service}$ (mm)	$\Delta_{service}/\Delta_{all}$
A	#1 B1NW	2.01	66%
	#2 B2NW	1.02	33%
	#3 B2NW	1.22	40%
	#4 B1LW	1.70	56%
	#5 B1LW	1.68	55%
B	#8 B1NW	3.05	84%
	#9 B2NW	1.45	40%
	#10 B1LW	1.88	52%
	#11 B2LW	1.73	48%
C	#12 B1NW	1.80	59%
	#13 B2NW	1.88	62%
	#14 B1LW	1.75	57%
	#15 B1LW	2.74	90%
	#16 B2LW	2.79	92%
	#17 B2LW	1.83	60%
D	#18 B1NWE	1.60	52%
	#19 B1LWE	3.63	120%
	#20 B2LWE	3.71	122%

Table 2.6 Ultimate load and ultimate moment comparisons with AASHTO LRFD Specifications

Series	Specimens	Ultimate load/AASHTO	Ultimate Moment/AASHTO
A	NW	1.7	5.5
	LW	1.4	4.6
B	NW	1.5	5.7
	LW	1.3	5.1
C	NW	2.7	5.0
	LW	2.2	4.1
D	NW	2.1	3.9
	LW	1.8	3.3

NW=normal weight concrete; LW=lightweight concrete

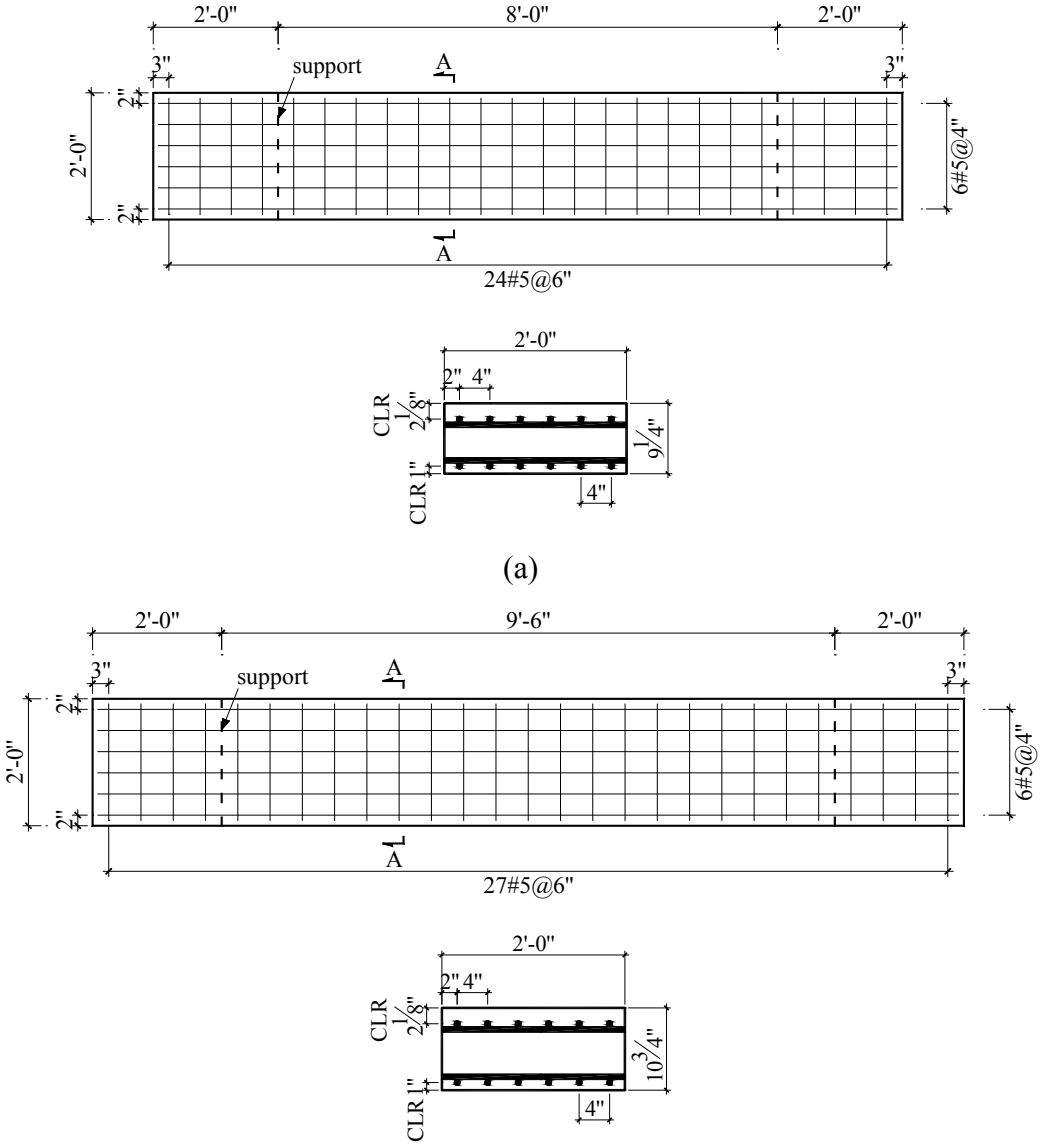

Fig. 2.1 Dimensions and details of top and bottom GFRP reinforcement mat: (a) Series A panels; (b) Series B panels (1 in. =25.4 mm)

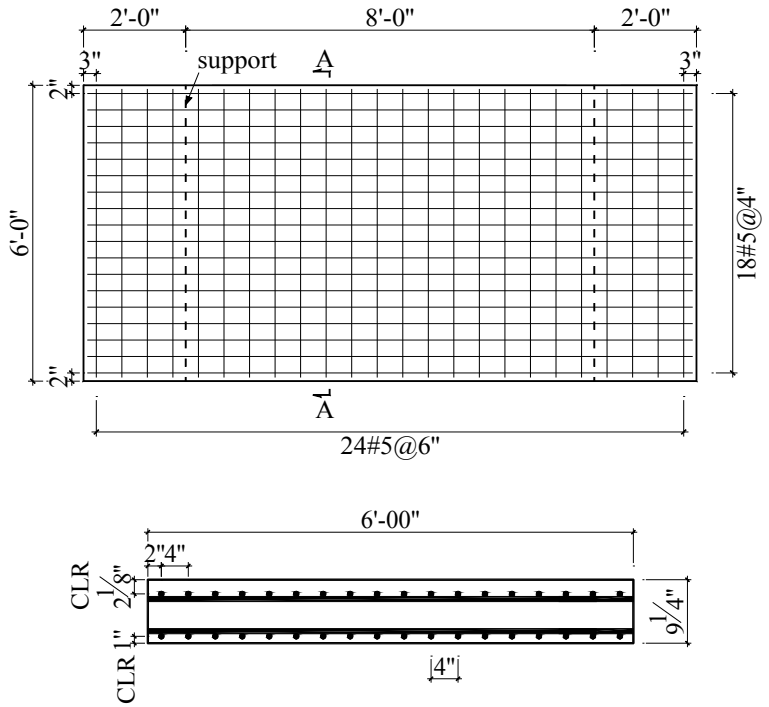

Section A-A

(a)

Fig. 2.2 Dimensions and details of the top and bottom GFRP reinforcement mat: (a) Series C panels; (b) Series D panels (1 in. =25.4 mm)

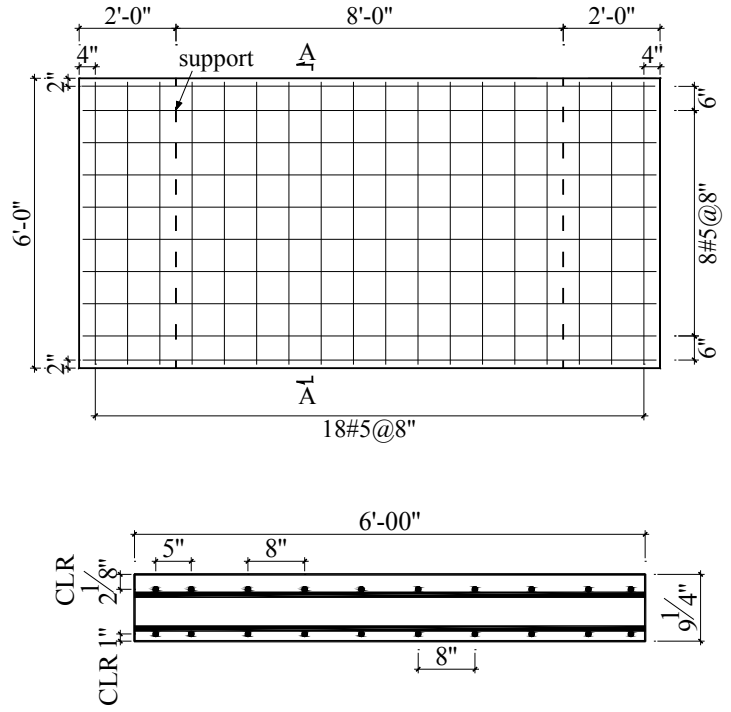

Section A-A

(b)

Fig. 2.2 (continued)

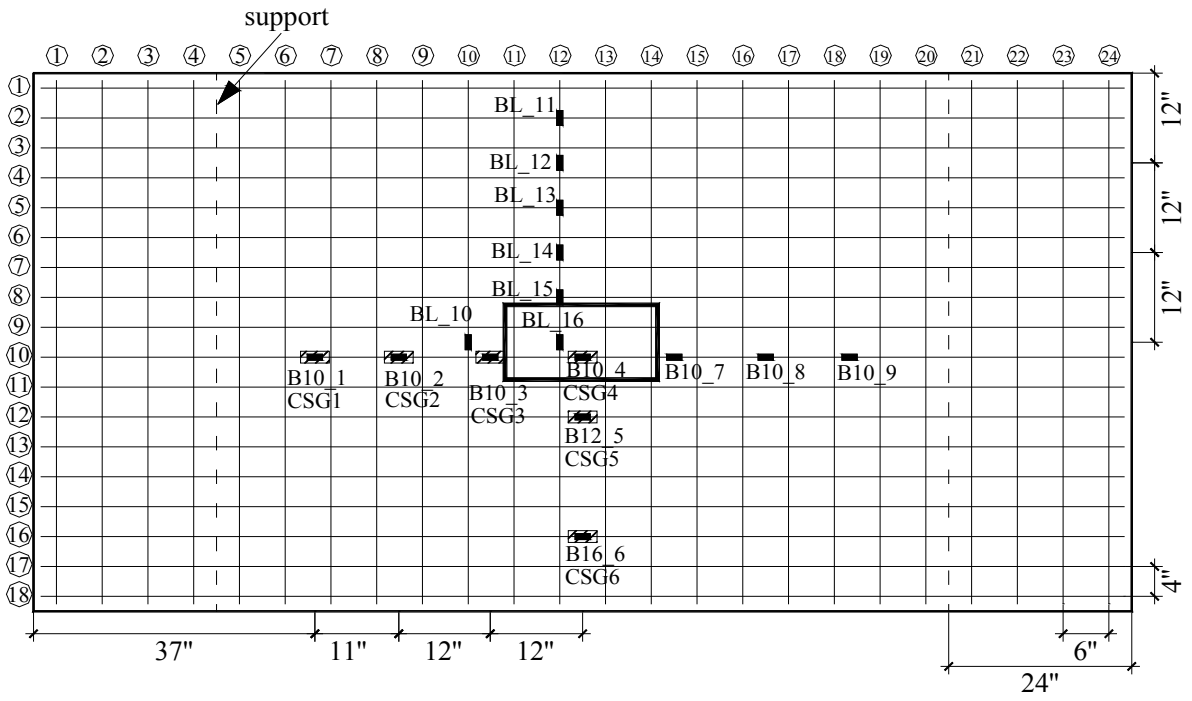

Fig. 2.3 Strain gauges for 6 ft (1.83 m) wide GFRP reinforced panels (flexurally designed)

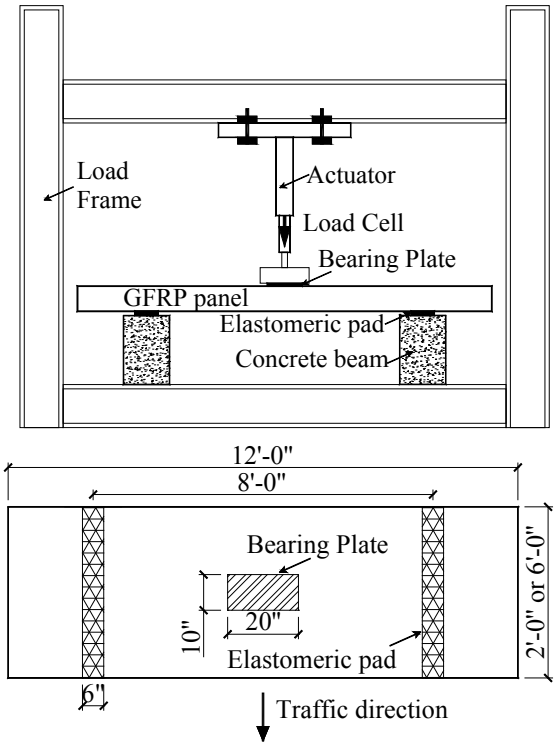

Fig. 2.4 Test setup: (a) elevation; (b) plan (1 in. =25.4 mm, 1 ft = 0.305 m)

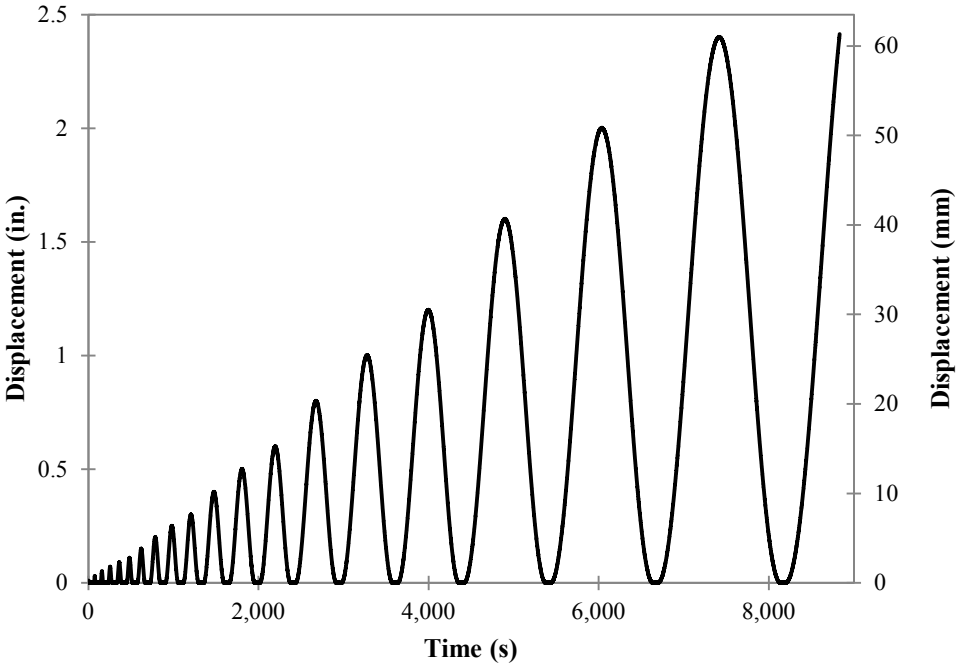

Fig. 2.5 Loading procedure for actuator displacement

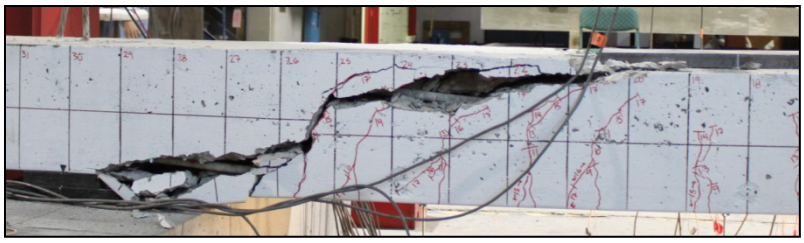

(a)

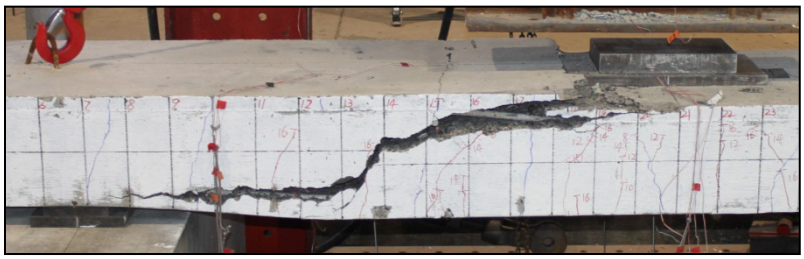

(b)

Fig. 2.6 Diagonal tension failure of 2 ft (0.61 m) wide panels: (a) NW panel; (b) LW panel

(a)

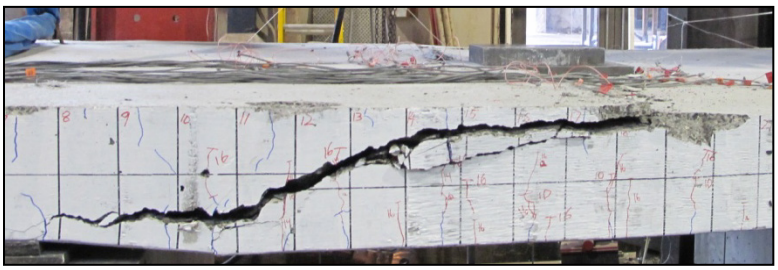

(b)

Fig. 2.7 Diagonal tension failure of 6 ft (1.83 m) wide panels: (a) NW panel; (b) LW panel

Fig. 2.8 Deformation of GFRP bars at bottom of panels after shear failure

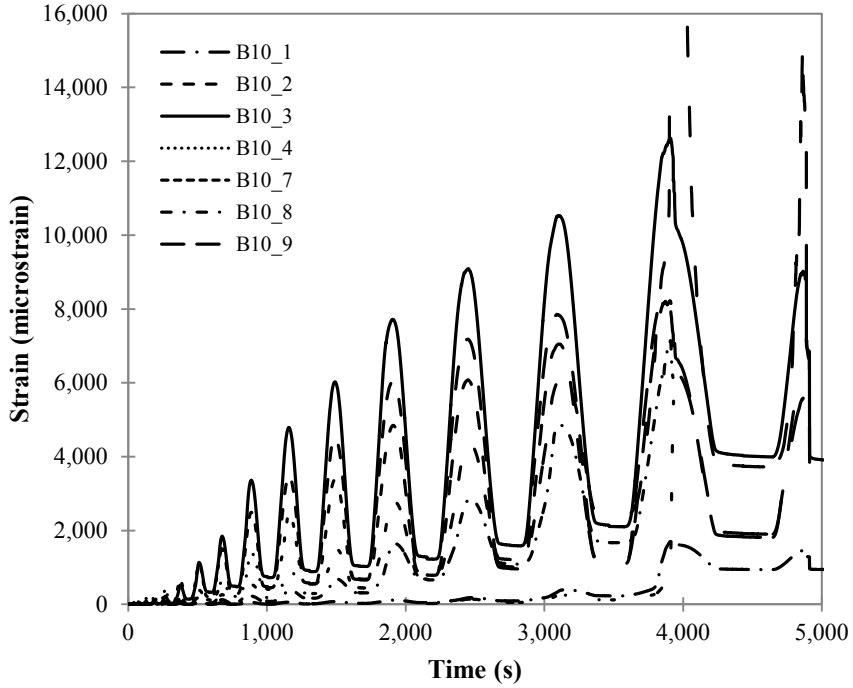

Fig. 2.9 Strains in GFRP bar along 12 ft (3.66 m) dimension of lightweight concrete panel #17 B2LW

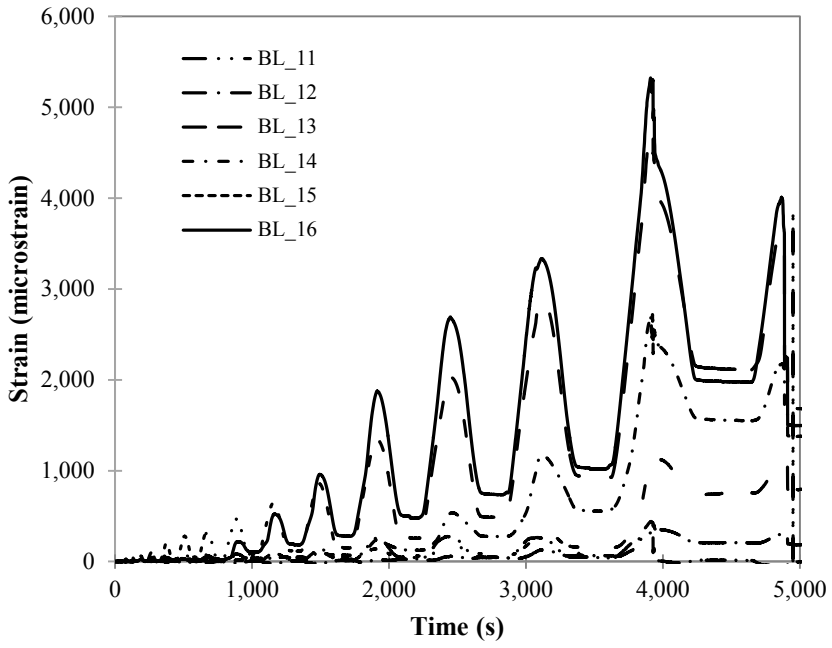

Fig. 2.10 Strains in GFRP bar along 6 ft (1.83 m) dimension of lightweight concrete panel #17 B2LW

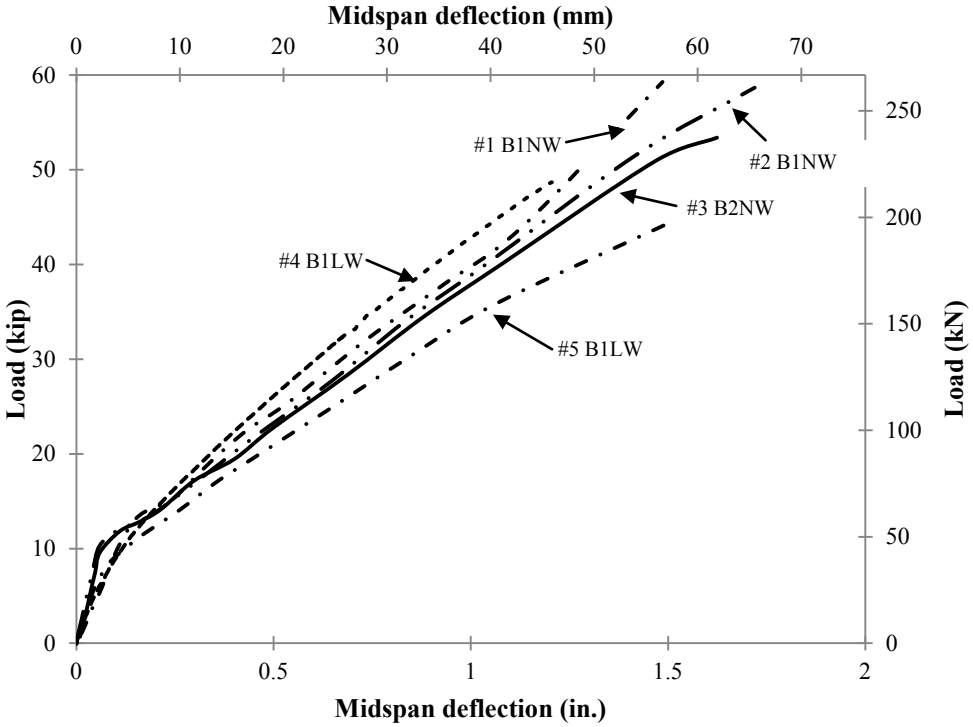

Fig. 2.11 Load-deflection diagrams for 2 ft (0.61 m) wide Series A panels

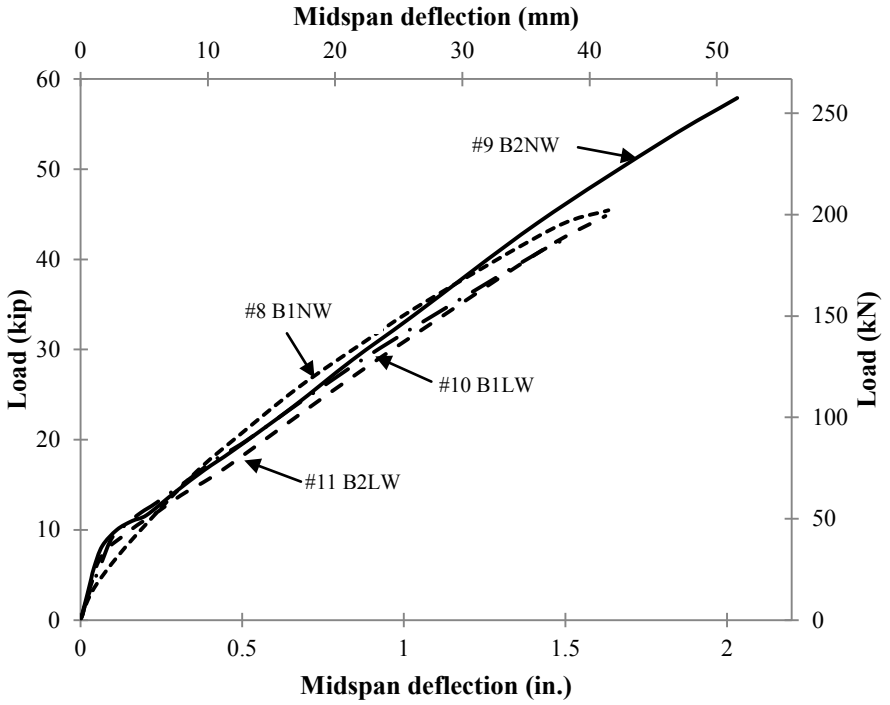

Fig. 2.12 Load-deflection diagrams for 2 ft (0.61 m) wide Series B panels

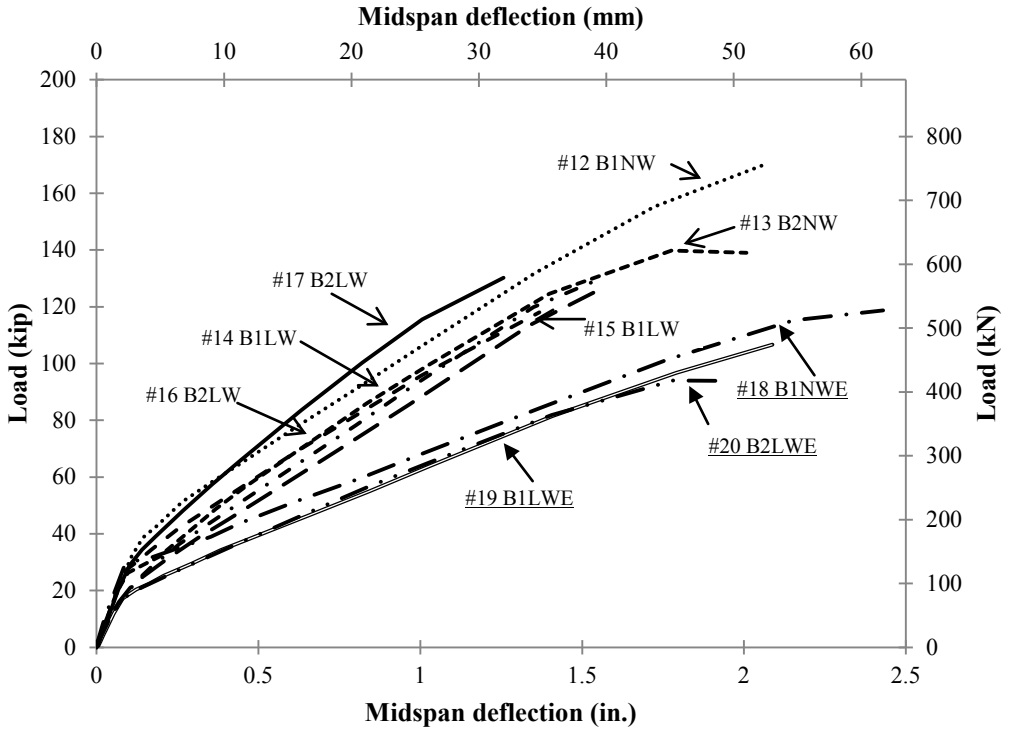

Fig. 2.13 Load-deflection diagrams for 6 ft (1.83 m) wide Series C and Series D panels (underlined)

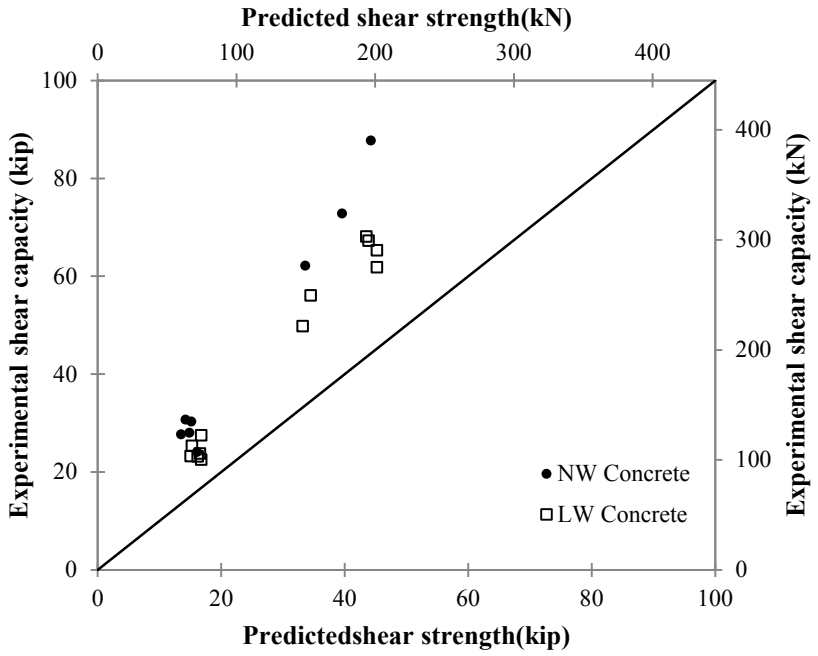

Fig. 2.14 Comparison of predicted and experimental shear strength (current research)

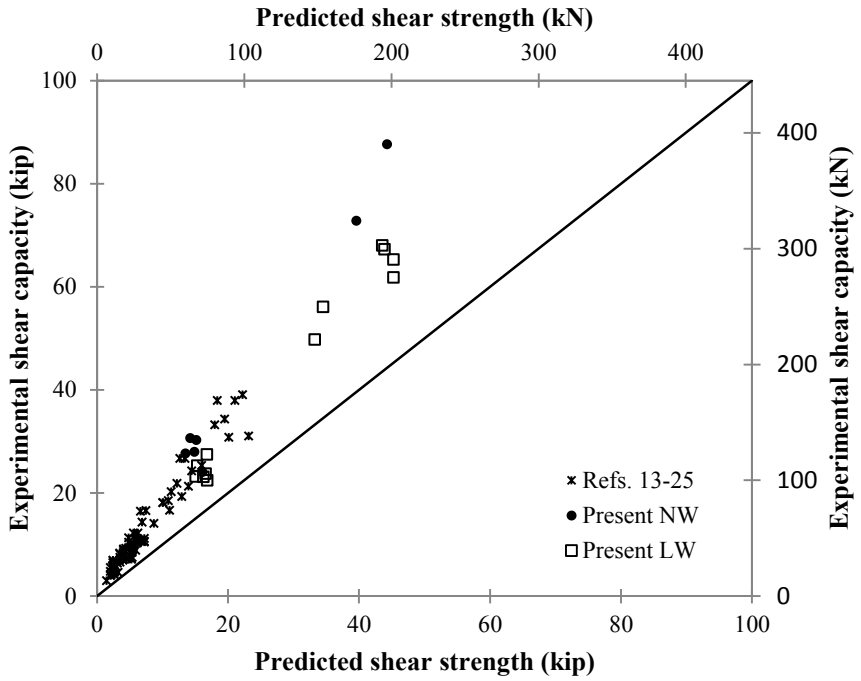

Fig. 2.15 Comparison of predicted and experimental shear strength (extended database)

3 SHEAR STRENGTH OF PRECAST GFRP REINFORCED LIGHTWEIGHT CONCRETE PANELS

Ruifen Liu, Chris P. Pantelides

3.1 Abstract

The capacity of lightweight concrete panels reinforced with GFRP bars is investigated in terms of shear strength. An extended database of 97 test results including normal weight and lightweight concrete restricted to members reinforced with GFRP bars for flexure without any shear reinforcement was compiled. The shear strength of lightweight concrete panels was compared to that of normal weight concrete beams and panels tested in this research and the extended database. Analysis of the data has resulted in a proposed reduction factor for sand-lightweight concrete panels reinforced with GFRP bars for possible use in the current ACI 440.1R-06 guidelines. The shear predictions using Canadian (CAN/CSA-S806-02) and Japanese (JSCE) recommendations are also compared to the extended database; each of these two provisions predicts the shear strength of lightweight and normal weight concrete panels reinforced with GFRP bars with a similar degree of conservatism.

3.2 Introduction

Fiber Reinforced Polymer (FRP) composites have gained acceptance as structural reinforcement for concrete members because of concern for chloride induced corrosion of steel. Several guidelines have been published for the design of

fiber reinforced polymer bars in concrete members. For flexural design, the provisions of the available guidelines follow a rational theory similar to that used for flexural members reinforced with conventional steel. The flexural strengths predicted by the developed guidelines are unlikely to vary by more than 10% (El-Sayed and Benmokrane, 2008).

Many design provisions and guidelines have been published regarding the shear capacity of concrete beams or slabs reinforced with GFRP bars, such as the Japan Society of Civil Engineers Design Provisions (JSCE, 1997), the Canadian Design Provisions (CAN/CSA-S806, 2002), the American Concrete Institute Guidelines (ACI 440.1R, 2006), and the American Association of State Highway and Transportation Officials Load Resistance Factor Design Guide Specifications for GFRP Reinforced Decks and Traffic Railings (AASHTO, 2009). The shear capacity of GFRP reinforced members has been investigated extensively in the literature. Swamy and Aburawi (1997), Deitz et al. (1999), Alkhrdaji et al. (2001), Yost et al. (2001), Tureyen and Frosch (2002), Gross et al. (2003), Ashour (2005), El-Sayed et al. (2003, 2006a, 2006b), Alam and Hussein (2009), Jang et al. (2009), and Bentz et al. (2010) have investigated the shear capacity of normal weight concrete beams or slabs reinforced with GFRP bars without transverse shear reinforcement. In the aforementioned studies, normal weight concrete was used with either normal or high strength; in addition, all members tested failed in one-way shear.

There is a paucity of research regarding the use of lightweight concrete with GFRP bars as reinforcement. ACI 440.1R (2006) does not provide specific guidance for lightweight concrete reinforced with GFRP bars; AASHTO (2009) does not allow the use of lightweight concrete for decks reinforced with GFRP bars. The Canadian

guidelines CAN/CSA-S806 (2002) consider the effect of concrete density on tensile strength through a modification factor.

A research program has been carried out to investigate the shear capacity of GFRP reinforced lightweight concrete panels. This paper presents the quantification of the shear strength of concrete panels reinforced with GFRP bars, twelve of which were lightweight concrete and eight normal weight concrete. The variables included concrete compressive strength, reinforcement ratio, slab thickness, deck span, and panel width. Available test data for normal weight concrete reinforced with GFRP bars in flexure were collected and compared to tests in the present research. A reduction factor is proposed for the shear capacity of lightweight concrete members reinforced with GFRP bars for possible use in the ACI 440 guidelines.

3.3 Current Recommendations for One-way Shear Strength of GFRP Reinforced Concrete Members

3.3.1 American Concrete Institute Guidelines (ACI 440.1R 2006)

The concrete shear capacity V_c of flexural members using GFRP bars as the main reinforcement is given as:

$$V_c = \frac{2}{5}\sqrt{f_c'}\,b_w c \tag{3.1a}$$

$$c = kd \tag{3.1b}$$

$$k = \sqrt{2\rho_f n_f + \left(\rho_f n_f\right)^2} - \rho_f n_f \tag{3.1c}$$

$$E_c = 0.043 w_c^{1.5}\sqrt{f_c'} \tag{3.1d}$$

$$E_c = \left[3.32\sqrt{f_c'} + 6895\right]\left(\frac{w_c}{2320}\right)^{1.5} \tag{3.1e}$$

where f_c' = specified compressive strength of concrete (MPa); b_w = web width (mm); c = cracked transformed section neutral axis depth (mm); d = distance from extreme compression fiber to centroid of tension reinforcement (mm); n_f = ratio of modulus of elasticity of FRP bars to modulus of elasticity of concrete; ρ_f = FRP reinforcement ratio; k = ratio of depth of neutral axis to reinforcement depth; E_c = modulus of elasticity of concrete (MPa), where Eq. (3.1d) applies to normal strength concrete for f_c' less than 41 MPa and Eq. (3.1e) for high strength concrete for f_c' greater than 41 MPa; w_c =density of concrete.

3.3.2 Canadian Design Provisions (CAN/CSA-S806 2002)

The concrete contribution to shear strength is calculated using the following equations:

$$V_c = 0.035\lambda_d\phi_c\left(f_c'\rho_f E_f\frac{V_f}{M_f}d\right)^{1/3} b_w d \tag{3.2a}$$

$$0.1\lambda_d\phi_c\sqrt{f_c'}b_w d \le V_c \le 0.2\lambda_d\phi_c\sqrt{f_c'}b_w d \tag{3.2b}$$

$$\frac{V_f}{M_f}d \le 1.0 \tag{3.2c}$$

where λ_d = factor for the concrete density effect; ϕ_c = resistance factor for concrete; E_f = modulus of elasticity of GFRP bars (MPa); V_f = shear at section of interest (kN); M_f = moment at section of interest (kN x m). The Canadian Code specifies that λ_d = 0.85 for sand-lightweight concrete (semi-low-density) in which all the fine aggregate is natural sand, and λ_d = 0.75 for all lightweight (low-density) concrete in which none of the fine aggregate is natural sand. These values of λ_d are the same values used in the ACI 318-08 Building Code Requirements[19] for steel reinforcement.

For sections with an effective depth greater than 300 mm without transverse shear reinforcement or less transverse reinforcement than the minimum required by code, the value of V_c is calculated using the following equation:

$$V_c = \left(\frac{130}{1000 + d}\right)\lambda_d \phi_c \sqrt{f_c'} b_w d \geq 0.08 \lambda_d \phi_c \sqrt{f_c'} b_w d \tag{3.2d}$$

3.3.3 Japan Society of Civil Engineer Design Provisions (JSCE 1997)

The Japan Society of Civil Engineers has published design provisions for shear design; the shear capacity is given as:

$$V_c = \beta_d \beta_p \beta_n f_{vcd} b_w d / \gamma_b \tag{3.3a}$$

$$f_{vcd} = 0.2\left(f_c'\right)^{1/3} \leq 0.72 \, {}^{N}\!/_{mm^2} \tag{3.3b}$$

$$\beta_d = \left(1000/d\right)^{1/4} \leq 1.5 \tag{3.3c}$$

$$\beta_p = \left(100\rho_f E_f / E_s\right)^{1/3} \leq 1.5 \tag{3.3d}$$

$$\beta_n = 1 + M_O/M_d \leq 2 \text{ for } N_d^{'} \geq 0 \tag{3.3e}$$

$$\beta_n = 1 + 2M_O/M_d \geq 0 \text{ for } N_d^{'} < 0 \tag{3.3f}$$

where γ_b = member safety factor (γ_b=1.3); E_s = modulus of elasticity of steel (MPa); M_O = decompression moment (kN x m); M_d = design bending moment (kN x m); $N_d^{'}$ = design axial compressive force (kN).

3.3.4 Proposal by El-Sayed et al. (2006a)

A proposal for the shear capacity based on research by El-Sayed et al. (2006a) is given as:

$$V_c = \left(\frac{\rho_f E_f}{90\beta f_c^{'}}\right)^{1/3}\left(\frac{\sqrt{f_c^{'}}}{6} b_w d\right) \leq \frac{\sqrt{f_c^{'}}}{6} b_w d \tag{3.4}$$

where β = factor taken as 0.85 for concrete compressive strength up to and including 28 MPa. For compressive strength above 28 MPa, this factor is reduced continuously at a rate of 0.05 per each 9 MPa of compressive strength in excess of 28 MPa, but is not taken less than 0.65.

3.4 Experimental Behavior

The geometry and properties of all the materials used in the present experiments are described in Table 3.1, which includes the compressive strength of each specimen at the time of testing. Twelve panels were cast using lightweight concrete and eight using normal weight concrete. Two panel widths (2 ft and 6 ft) and two spans (8 ft and 9 ft-6 in.) were tested. Typical dimensions are shown in Fig. 3.1(a) and the test setup is shown in Fig. 3.1(b). The panels were divided into four series according to their dimensions and reinforcement. Series A panels were 2 ft wide x 12 ft long (0.61 m x 3.66 m), with a thickness of 9 ¼ in. (235 mm); Series B panels were 2 ft wide x 13 ½ ft long (0.61 m x 4.12 m), with a thickness of 10 ¾ in. (273 mm), and the same reinforcement details as Series A panels. Series C and D deck panels were 6 ft wide x 12 ft long (1.83 m x 3.66 m), with a thickness of 9 ¼ in. (235 mm); Series D panels had 56% the reinforcement ratio of Series C panels and are denoted by the letter E in the specimen designation in Table 3.1. Series A, C, and D had a span of 8 ft (2.44 m) and Series B panels had a span of 9 ½ ft (2.90 m). Series A, B, and C were designed according to the ACI 440.1R (2006) guidelines. The design was governed by service load deflection and crack width. Series D panels did not meet ACI 440.1R (2006) guidelines because of the reduced reinforcement ratio.

All panels tested in this research had a diagonal tension failure mode. During testing, all panels initially developed flexural cracks at midspan at lower load levels; as the load level was increased, shear cracks developed on each side of the panels. The panels failed with the formation of a critical diagonal crack near one of the two supports. After formation of the critical diagonal crack, the concrete was horizontally split along both the top and bottom mats of the longitudinal reinforcement and

concrete crushed on the compression face. At the end of the loading procedure, concrete at the bottom of the panels near the support spalled off but none of the bottom GFRP bars which were in tension ruptured, and the panels were able to hold a significant percentage of the ultimate load after the peak load was reached. Figure 3.2 shows the diagonal tension failure of normal weight and lightweight concrete panels for 2 ft (0.61 m) x 12 ft (3.66 m) specimens. Figure 3.3 shows the diagonal tension failure of normal weight and lightweight concrete panels for 6 ft (1.83 m) x 12 ft (3.66 m) specimens. The panels failed in shear due to formation of a critical diagonal crack for both 2 ft (0.61 m) and 6 ft (1.83 m) wide specimens. Series A, B, and C panels satisfied the service load deflection limit of the AASHTO LRFD Specifications (2009) of span/800. Regarding Series D panels, normal weight panel #18 B1NWE also satisfied the deflection limit but lightweight concrete panels #19 B1LWE and #20 B2LWE did not. More details of the experimental program are presented in Pantelides et al. (2011).

The results for all tests carried out in the present study are shown in Table 3.2. A summary of the average shear strength obtained from the tests in this study is shown in Table 3.3 for both lightweight and normal weight concrete specimens. It is clear from Table 3.3 that the lightweight concrete panels have a shear strength that ranges from 82% to 89% of the normal weight concrete panels for the specimens designed with a reinforcement ratio according to ACI 440 recommendations, and 85% for the specimens with a reduced reinforcement ratio (Series D).

3.5 Comparison of Design Provisions and Test Results

The shear strength of twelve lightweight concrete panels and eight normal weight concrete panels tested in this research, reinforced with GFRP bars, was compared with the shear design provisions of the ACI 440.1R (2006) design guidelines. The ratio of experimental shear strength to predicted shear strength according to Eq. (3.1) is shown in Fig. 3.4; it is clear that the ratio of experimental to ACI 440.1R (2006) predicted shear capacity of lightweight concrete panels reinforced with GFRP bars is considerably lower than that of normal weight concrete panels.

To investigate further the trend observed in Fig. 3.4, the shear strength of panels in the extended database reinforced with GFRP bars was compared with the shear design provisions of the ACI 440.1R (2006) design guidelines, the CAN/CSA-S806 (2002) code, the JSCE (1997) design manual, and an equation proposed by El-Sayed et al. (2006a). In the CAN/CSA-S806 (2002) recommendations, a coefficient λ_d is used to consider the concrete density effect; however, to investigate the applicability of this coefficient, a value of $\lambda_d = 1.0$ was used in this research so that comparisons could be made to the experimental results and other provisions or equations. The ratio of experimental shear strength to predicted shear strength according to each design equation is shown in Figs. 3.5-3.8. Figures 3.5-3.8 include results from experiments carried out in this research, and an extended database using data collected from additional research carried out by other investigators (Swamy and Aburawi (1997), Deitz et al. (1999), Alkhrdaji et al. (2001), Yost et al. (2001), Tureyen and Frosch (2002), Gross et al. (2003), Ashour (2005), El-Sayed et al. (2003,

2006a, 2006b), Alam and Hussein (2009), Jang et al. (2009), and Bentz et al. (2010)). These experiments were selected from the available literature to create a database that includes slabs or beams reinforced with GFRP bars in flexure but without any shear reinforcement of any kind (steel or GFRP). All specimens in the database failed in shear, either in diagonal tension failure or shear compression failure. The relevant geometrical properties of the members in the database and their original sources are given in Appendix 3.A.

The comparison of predicted to experimental shear capacities using the four methods (ACI 440.1R (2006), CAN/CSA-S806 (2002), JSCE (1997), and El-Sayed et al. (2006a)) for the present experiments and the database is given in Table 3.2 and Appendix 3.B. The mean values of all ratios of experimental to predicted shear capacity are shown in Table 3.4. ACI 440.1R is the only one which is safe for all tests in the database, as shown in Fig. 3.5; however, it is also the most conservative compared to the other three predictions. Figures 3.6-3.8 show that the CAN/CSA (2002), JSCE (1997) and the El-Sayed et al. (2006a) predictions have a better agreement with the experimental results but in a few cases, they slightly overpredict the shear capacity. The ACI 440.1R (2006) predictions are more scattered for normal weight concrete GFRP reinforced panels compared to lightweight concrete, as is evident from Table 3.4. The coefficient of variation for the ACI 440.1R (2006) prediction is 18%, which is similar to the other three predictions (18%, 16%, and 14% for the El-Sayed et al. (2006a), the JSCE (1997), and CAN/CSA (2002) requirements, respectively). Figure 3.5 shows that regardless of concrete type (normal weight or lightweight) and compressive strength, the value of the minimum ratio of experimental to ACI 440.1R (2006) predicted shear strength is 1.3.

Table 3.4 shows that ACI 440.1R (2006) predicts that the ratio of experimental to predicted shear capacity of lightweight concrete panels reinforced with GFRP bars is considerably lower than that of normal weight concrete panels. On the other hand, the JSCE (1997), the CAN/CSA (2002) guidelines, and to some degree the El-Sayed et al. (2006a) equation predict similar ratios of experimental to predicted shear strength for both normal weight and lightweight concrete panels; this is the case even though in the CAN/CSA (2002) code the coefficient λ_d for lightweight concrete was assumed to be equal to 1.0. Table 3.4 and Figs. 3.6 and 3.7 demonstrate that the CAN/CSA (2002) and JSCE (1997) provisions predict the shear strength of lightweight and normal weight concrete panels reinforced with GFRP bars with a similar degree of conservatism; this is attributed to the indirect manner of including the concrete tensile strength in these two guidelines. The mean value of the El-Sayed et al. (2006a) prediction for lightweight concrete panels shown in Fig. 3.8 is 90% of the normal weight concrete panels, so a correction factor for lightweight concrete panels seems appropriate in this case. In all shear predictions for lightweight concrete, the coefficient of variation was lower than the coefficient of variation for normal weight concrete; this is expected since the database for lightweight concrete specimens is smaller and the tests were carried out only in the present research; in addition, the range of lightweight concrete compressive strength and reinforcement ratios were narrow while the normal weight concrete specimens had a wider range of concrete compressive strengths and reinforcement ratios.

Figure 3.9 shows the correlation of experimental to predicted shear strength versus reinforcement ratio. Figure 3.9 shows that the minimum ratio of experimental to predicted shear strength is relatively independent of the reinforcement ratio. The

minimum ratio of experimental shear strength to that of predicted shear strength by ACI 440.1R (2006) regardless of reinforcement ratio, type of concrete (normal weight or lightweight concrete), or concrete compressive strength is 1.3.

3.6 Proposed Modification to ACI 440.1R-06

Shear Equation for Lightweight Concrete

Figures 3.4, 3.5, 3.9, and Tables 3.3 and 3.4 clearly show that the type of concrete (normal weight or lightweight concrete) should be considered in the shear capacity prediction using ACI 440.1R (2006). However, the ACI 440.1R recommendations do not include provisions for evaluating the shear capacity of lightweight concrete structural members reinforced with GFRP bars. A reduction factor for one-way shear capacity is presented herein by the same procedure used in the ACI Building Code Requirements for Structural Concrete ACI 318 (2008), to include the effect of lightweight concrete and introduce the same level of conservatism as for normal weight concrete. The reduction factor is defined as λ in the ACI 318 Building Code Requirements for steel reinforced lightweight concrete members; the value of λ for steel reinforced sand-lightweight concrete is given as $\lambda = 0.85$. Equation (3.1a) from the ACI 440.1R recommendations is modified for the shear capacity prediction of lightweight concrete panels reinforced with GFRP bars as follows:

$$V_{MOD} = \frac{2}{5}\lambda_f \sqrt{f_c'} b_w c \tag{3.5}$$

The tests carried out in this research and the extended database established in Table 3.1 and Appendix 3.A for 97 beams and one-way slabs reinforced with GFRP bars for flexure without any shear reinforcement are used to investigate the applicability of Eq. (3.5) and to determine an appropriate value of the reduction factor λ_f for lightweight concrete panels reinforced with GFRP bars. The experimental results in Table 3.3 suggest that a lower bound reduction value of λ_f equal to 0.80 is appropriate. Figure 3.10 shows the correlation of experimental-to-predicted shear strength versus compressive concrete strength for a value of λ_f equal to 0.80 for the specimens tested in this research. Comparing Figs. 3.4 and 3.10, it is clear that the modified equation yields predictions which are more rational for evaluating shear strength capacity of lightweight concrete panels reinforced with GFRP bars.

A reduction factor value of λ_f equal to 0.80 for sand-lightweight concrete reinforced with GFRP bars was determined to be adequate from the extended database as well. The correlation of experimental-to-predicted shear strength versus compressive concrete strength is given in Fig. 3.11 using the reduction factor λ_f = 0.80 for lightweight concrete and the modified Eq. (3.5). This reduction factor is smaller than the reduction factor in the ACI 318 Building Code Requirements (2008) for sand-lightweight concrete reinforced with steel bars. The fact that the reduction factor λ_f = 0.80 for sand-lightweight concrete reinforced with GFRP bars is smaller than λ = 0.85 for sand-lightweight concrete reinforced with steel bars is justified for the following reasons: (a) the bond mechanism of GFRP bars to concrete is different than that of steel bars, (b) the modulus of elasticity of GFRP bars is lower than that of steel bars, and under the same situation, GFRP reinforced members will have larger

deflection; the neutral axis is closer to the compression concrete fiber and the compression area of concrete is smaller, which will reduce the ultimate shear strength, and (c) GFRP reinforced concrete members have larger cracks compared with steel reinforced concrete members, which reduces the aggregate interlock, which will also reduce the ultimate shear strength. The mean value and coefficient of variation for the ratio of experimental to predicted shear strength using $\lambda_f = 0.80$ is given in Table 3.5 for the panels tested in this research, and in Table 3.6 for the panels in the extended database.

Figure 3.12 shows the correlation of experimental to predicted shear strength versus reinforcement ratio using the modified Eq. (3.5). Comparing Figs. 3.9 and 3.12, it is clear that the proposed modification yields a similar conservatism for normal weight and lightweight concrete panels reinforced with GFRP bars. Table 3.6 and Figs. 3.11 and 3.12 show that the modified equation (Eq. 3.5) yields predictions that are more rational for evaluating the shear strength of sand-lightweight concrete panels reinforced with GFRP bars without shear reinforcement. All four methods (CAN/CSA (2002), JSCE (1997), El-Sayed et al. (2006a), and the modified equation (Eq. 3.5)) estimate the ratio of experimental to predicted shear strength for lightweight concrete to be within 10% of the ratio for normal weight concrete.

3.7 Conclusions

The behavior and shear capacity of precast lightweight concrete panels reinforced with GFRP bars and its comparison to normal weight concrete panels reinforced with GFRP bars have been analyzed. The main findings of this research can be summarized as follows:

1. The current ACI 440.1R (2006) design guidelines provide a lower bound for the shear capacity of panels reinforced with GFRP bars for flexure without any shear reinforcement, for both lightweight concrete and normal weight concrete panels; moreover, all panels in the database achieved 1.3 times the ACI 440.1R predicted shear capacity.
2. The predictions using the Canadian CAN/CSA (2002) guidelines, the Japanese JSCE (1997) guidelines, and an equation proposed by El-Sayed et al. (2006a) had a smaller conservatism compared to the ACI 440.1R guidelines for both normal weight and lightweight concrete panels reinforced with GFRP bars. However, in a few cases, the last three predictions (CAN/CSA, JSCE, El-Sayed et al.) were slightly unconservative.
3. This research has shown that precast concrete panels can be designed using either normal weight or lightweight concrete provided that an appropriate reduction factor is used for lightweight concrete. The Canadian CAN/CSA and Japanese JSCE guidelines predict the shear strength of lightweight concrete panels reinforced with GFRP bars for flexure, without any shear reinforcement, with the same degree of conservatism as normal weight concrete panels.
4. A reduction factor is introduced to modify the shear prediction equation in ACI 440.1R for lightweight concrete members reinforced with GFRP bars for flexure without any shear reinforcement. A value of the reduction factor of λ_f = 0.80 was determined comparing a database of 97 members reinforced with GFRP bars without stirrups, 85 of which were normal

weight concrete beams or panels and 12 were lightweight concrete panels. Using the modified equation proposed herein and a reduction factor λ_f = 0.80, the lightweight concrete panels achieved a similar conservatism as the normal weight concrete panels in the database.

5. The fact that the reduction factor for sand-lightweight concrete reinforced with GFRP bars (λ_f =0.80) is lower than the corresponding factor for steel bars (λ =0.85) is justified because of the different failure mode, bond mechanism, modulus of elasticity, maximum stress, and stress distribution for the two reinforcing bar types.

3.8 Acknowledgments

The research reported in this paper was supported by the Utah DOT and the Expanded Shale Clay and Slate Institute. The authors acknowledge the contribution of Hughes Bros Inc., Utelite Corporation, and Hanson Structural Precast. The authors acknowledge the assistance of Professor Lawrence D. Reaveley, Mark Bryant, Brandon T. Besser, and Clayton A. Burningham of the University of Utah in the experimental portion of the research.

3.9 Notation

a =shear span of the flexural member;

b_w =width of the web;

c =cracked transformed section neutral axis depth;

d =distance from extreme compression fiber to neutral axis at balanced strain condition;

E_c =modulus of elasticity of concrete;

E_s =modulus of elasticity of steel;

E_f =modulus of elasticity of FRP;

$f_c^{'}$ =design compressive strength of concrete;

f_u =tensile strength of GFRP bars;

h =overall height of flexural member;

k =ratio of depth of neutral axis to reinforcement depth;

M_d =design bending moment;

M_f =moment at section of interest;

M_O =decompression moment;

n_f =ratio of modulus of elasticity of FRP bars to modulus of elasticity of concrete;

$N_d^{'}$ =design axial compressive force;

V_{ACI} = shear strength predicted using ACI code;

V_c =nominal shear strength provided by concrete;

$V_{CAN/CSA}$ =shear strength predicted using CAN/CSA code;

V_{JSCE} =shear strength predicted using JSCE code;

V_{MOD} =shear strength predicted using modified equations;

$V_{\exp}$ =experimental shear strength;

V_f =shear at section of interest;

w_c =density of concrete;

β =factor taken as 0.85 for concrete strength $f_c^{'}$ up to and including 28 MPa. For strength above 28 MPa, this factor is reduced continuously at a rate of 0.05 per each 9 MPa of strength in excess of 28 MPa, but is not taken less than 0.65;

ρ_f =FRP reinforcement ratio;

ρ_{fb} =FRP reinforcement ratio producing balanced strain conditions;

λ =reduction factor for steel bars used in lightweight concrete;

λ_d =factor reflecting concrete density effect;

λ_f =reduction factor for GFRP bars used in lightweight concrete;

ϕ_c =resistance factor for concrete;

γ_b =member safety factor (γ_b =1.3).

3.10 References

ACI Committee 318, (2008). "Building Code Requirements for Structural Concrete (ACI 318-08) and Commentary (318 R-08)." American Concrete Institute, Farmington Hills, Mich.

Alam, M.S., Hussein, A., (2009). "Shear strength of concrete beams reinforced with Glass Fiber Reinforced Polymer (GFRP) bars." Proc., 9th Int. Symp. on Fiber Reinforced Polymer Reinforcement for Reinforced Concrete Structures, Sydney, Australia.

Alkhrdaji, T., Wideman, M., Belarbi, A., and Nanni, A., (2001). "Shear Strength of GFRP RC Beams and Slabs." Proc., Compos. Constr., Porto, Portugal, 409-414.

American Association of State Highway and Transportation Officials, (AASHTO), (2009). "AASHTO LRFD Bridge Design Guide Specifications for GFRP Reinforced Concrete Decks and Traffic Railings." 1st edition, AASHTO, Washington, D.C., 68 pp.

American Concrete Institute, (ACI 440.1R-06), (2006). "Guide for the Design and Construction of Structural Concrete Reinforced with FRP Bars." American Concrete Institute, Farmington Hills, Mich., 44 pp.

Ashour, A.F., (2005). "Flexural and shear capacities of concrete beams reinforced with GFRP bars". Constr. Build. Mater., 20(10), 1005-1015.

Bentz, E.C, Massam, L., and Collins, M.P., (2010). "Shear strength of large concrete members with FRP reinforcement." J. of Compos. Constr., 14(6), 637-646.

Canadian Standards Association, (CAN/CSA S806-02), (2002). "Design and Construction of Building Components with Fibre Reinforced Polymers." Canadian Standards Association, Rexdale, Ontario, Canada.

Deitz, D.H., Harik, I.E., and Gesund, H., (1999). "One-way slabs reinforced with Glass Fiber Reinforced Polymer reinforcing bars." Proc., 4th Int. Symp. on Fiber Reinforced Polymer Reinforcement for Reinforced Concrete Structures, Baltimore, MD.

El-Sayed, A., and Benmokrane, B., (2008). "Evaluation of the new Canadian highway bridge design code shear provisions for concrete beams with fiber-reinforced polymer reinforcement." Can. J. Civ. Eng., 35(6), 609-623.

El-Sayed, A., El-Salakawy, E., and Benmokrane, B., (2005). "Shear strength of one-way concrete slabs reinforced with Fiber-Reinforced Polymer composite bars." J. Compos. Constr., 9(2), 147-157.

El-Sayed, A.K., El-Salakawy, E.F. and Benmokrane, B., (2006a). "Shear strength of FRP-reinforced concrete beams without transverse reinforcement." ACI Struct. J., 103(2), 235-243.

El-Sayed, A.K., El-Salakawy, E.F. and Benmokrane, B., (2006b). "Shear capacity of high-strength concrete beams reinforced with FRP bars." ACI Struct. J., 103(3), 383-389.

Gross, S.P., Yost, J.R., Dinehart, D.W., Svensen, E., (2003). "Shear strength of normal and high strength concrete beams reinforced with GFRP bars." High performance materials in bridges, Proc. Int. Conf., ASCE, Kona, Hawaii, 426-437.

Jang, H., Kim, M., Cho, J., Kim, C., (2009). "Concrete shear strength of beams reinforced with FRP bars according to flexural reinforcement ratio and shear span to depth ratio." Proc., 9th Int. Symp. on Fiber Reinforced Polymer Reinforcement for Reinforced Concrete Structures, Sydney, Australia.

Japan Society of Civil Engineers (JSCE), (1997). "Recommendation for Design and Construction of Concrete Structures Using Continuous Fiber Reinforcing

Materials." Research Committee on Continuous Fiber Reinforcing Materials, Japan Society of Civil Engineers, Tokyo, Japan.

Pantelides, C.P., Liu, R., and Reaveley, L.D. (2011). "Experimental study of precast GFRP reinforced lightweight concrete panels." under review, ACI Struct. J.

Swamy, N., and Aburawi, M., (1997). "Structural implications of using GFRP bars as concrete reinforcement." Proc., 3rd Int. Symp. on Non-Metallic (FRP) Reinforcement for Concrete Structures, Sapporo, Japan.

Tureyen, A.K., and Frosch, R., (2002). "Shear tests of FRP-reinforced concrete beams without stirrups." ACI Struct. J., 99(4), 427-434.

Yost, J.R., Gross, S.P., and Dinehart, D.W., (2001). "Shear strength of normal strength concrete beams reinforced with deformed GFRP bars". J. of Compos. Constr., 5(4), 263-275.

Table 3.1 Properties and dimensions of precast panels tested in present study

Specimen	f_c'	E_c	f_u	E_f	b_w	h	d	Span	ρ_f	ρ_f/ρ_{fb}
	MPa	GPa	MPa	GPa	mm	mm	mm	m		
#1 B1NW	72	35.0	715	43.3	635	235	202	2.44	0.0094	0.99
#2 B2NW	87	37.9	715	43.3	635	235	202	2.44	0.0094	0.81
#3 B2NW	60	32.7	715	43.3	635	235	202	2.44	0.0094	1.17
#4 B1LW	63	25.9	715	43.3	635	235	202	2.44	0.0094	1.13
#5 B1LW	75	27.9	715	43.3	635	235	202	2.44	0.0094	0.94
#6 B2LW	60	25.52	715	43.3	635	235	202	2.44	0.0094	1.18
#7 B1LW	68	26.8	715	43.3	635	260	227.	2.03	0.0083	0.92
#8 B1NW	79	36.4	715	43.3	635	273	240	2.90	0.0079	0.75
#9 B2NW	61	32.8	715	43.3	635	273	240	2.90	0.0079	0.97
#10 B1LW	63	25.9	715	43.3	635	273	240	2.90	0.0079	0.95
#11 B2LW	60	25.5	715	43.3	635	273	240	2.90	0.0079	0.99
#12 B1NW	84	37.3	715	43.3	1854	235	202	2.44	0.0096	0.87
#13 B2NW	59	32.3	715	43.3	1854	235	202	2.44	0.0096	1.24
#14 B1LW	63	25.9	715	43.3	1854	235	202	2.44	0.0096	1.16
#15 B1LW	63	25.9	715	43.3	1854	235	202	2.44	0.0096	1.16
#16 B2LW	57	25.0	715	43.3	1854	235	202	2.44	0.0096	1.27
#17 B2LW	56	24.7	715	43.3	1854	235	202	2.44	0.0096	1.30
#18 B1NWE	84	37.3	715	43.3	1854	235	202	2.44	0.0054	0.48
#19 B1LWE	63	25.9	715	43.3	1854	235	202	2.44	0.0054	0.64
#20 B2LWE	56	24.7	715	43.3	1854	235	202	2.44	0.0054	0.72

NW=normal weight; LW=lightweight; E=reduced reinforcement ratio

Table 3.2 Comparison of different shear prediction methods for precast panels tested in present study

Specimen	V_{exp}	V_{exp}/V_{ACI}	$V_{exp}/V_{CAN/CSA}$	V_{exp}/V_{JSCE}	$V_{exp}/V_{El\text{-}Sayed}$	V_{exp}/V_{MOD}
	kN					
#1 B1NW	136.19	2.21	1.84	1.72	1.68	2.21
#2 B2NW	134.59	2.05	1.70	1.70	1.61	2.05
#3 B2NW	122.87	2.10	1.75	1.55	1.56	2.10
#4 B1LW	112.37	1.69	1.58	1.42	1.42	1.99
#5 B1LW	102.72	1.46	1.36	1.30	1.26	1.72
#6 B2LW	103.12	1.58	1.48	1.30	1.31	1.85
#7 B1LW	122.15	1.68	1.40	1.47	1.40	1.98
#8 B1NW	106.80	1.53	1.24	1.25	1.16	1.53
#9 B2NW	124.31	1.93	1.58	1.46	1.40	1.93
#10 B1LW	99.80	1.37	1.25	1.17	1.12	1.61
#11 B2LW	105.36	1.47	1.34	1.24	1.19	1.73
#12 B1NW	389.80	2.03	1.69	1.67	1.59	2.03
#13 B2NW	323.58	1.89	1.58	1.39	1.40	1.89
#14 B1LW	274.74	1.40	1.32	1.18	1.18	1.65
#15 B1LW	290.16	1.48	1.39	1.24	1.24	1.74
#16 B2LW	298.99	1.57	1.48	1.28	1.30	1.85
#17 B2LW	302.52	1.60	1.51	1.30	1.32	1.89
#18 B1NWE	276.21	1.90	1.46	1.44	1.37	2.23
#19 B1LWE	249.23	1.67	1.45	1.30	1.30	1.96
#20 B2LWE	221.14	1.54	1.34	1.15	1.18	1.81

NW=normal weight; LW=lightweight; E=reduced reinforcement ratio

Table 3.3 Ratio of lightweight (LW) to normal weight (NW) concrete GFRP panel shear strength from current research

Series	NW GFRP panel average shear strength kips (kN)	LW GFRP panel average shear strength kips (kN)	(LW/NW) GFRP panel shear strength ratio
A	29.5 (131.2)	24.5 (109.0)	0.83
B	26.0 (115.6)	23.1 (102.6)	0.89
C	80.2 (356.7)	65.6 (291.6)	0.82
D	62.1 (276.2)	52.9 (235.2)	0.85

Table 3.4 Comparison of experimental to predicted shear strength ratio of three design codes and other research

	ACI 440.1R (2006)	CAN/CSA (2002)	JSCE (1997)	El-Sayed et al. (2006a)
NW mean	1.91	1.33	1.27	1.35
NW Coefficient of variation%	18	18	16	14
LW mean	1.50	1.38	1.25	1.24
LW Coefficient of variation %	7	6	7	7
$(LW_m)/(NW_m)$ %	78	104	98	92

NW=normal weight concrete; LW=lightweight concrete;
(xx_m) =mean value

Table 3.5 Comparison of experimental to predicted shear strength ratio of specimens tested in this research using ACI 440.1R (2006) equation and modified equation

Method	NW mean	NW Coefficient of variation %	LW mean	LW Coefficient of variation %	$(LW_m)/(NW_m)$ %
ACI 440.1R (Eq. 1)	1.90	10	1.50	7	79
Modified (Eq. 5)	1.90	10	1.88	7	99

NW=normal weight concrete; LW=lightweight concrete;
(xx_m) =mean value;

Table 3.6 Comparison of experimental to predicted shear strength ratio using ACI 440.1R (2006) equation and modified equation for extended database

Method	NW mean	NW Coefficient of variation %	LW mean	LW Coefficient of variation %	$(LW_m)/(NW_m)$ %
ACI 440.1R (Eq. 1)	1.91	18	1.50	7	78
Modified (Eq. 5)	1.91	18	1.88	7	98

NW=normal weight concrete; LW=lightweight concrete;
(xx_m) =mean value

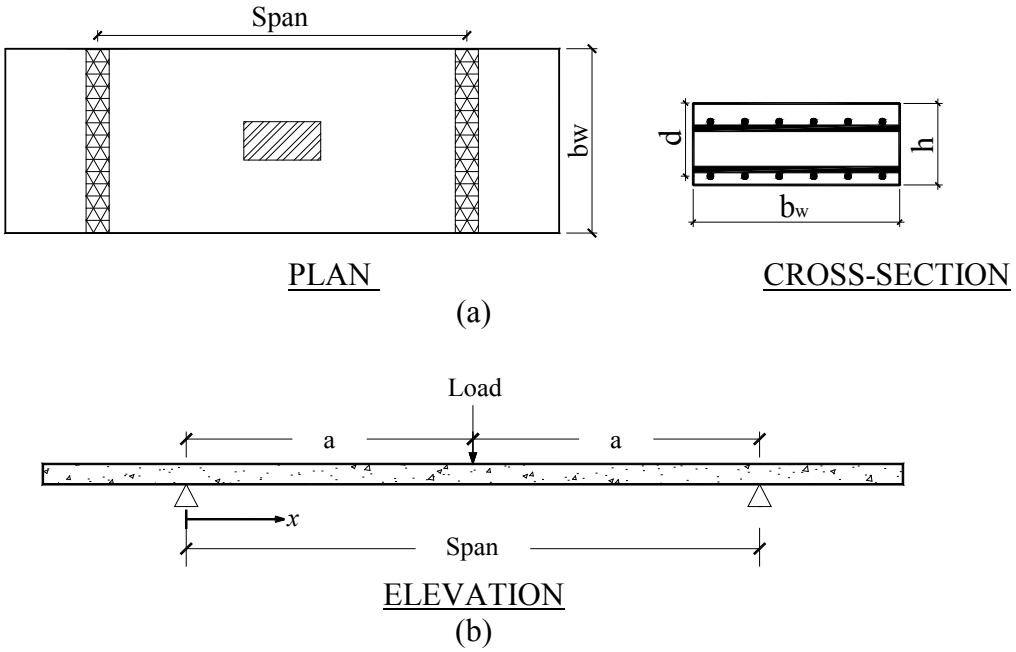

Fig. 3.1 Dimension details and loading setup of the panels (a) details of Series A-D; (b) load setup

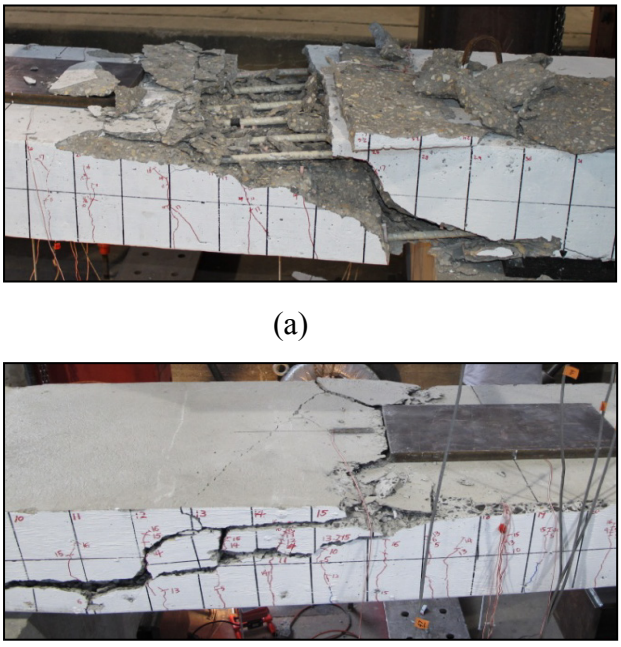

(a)

(b)

Fig. 3.2 Diagonal tension failure of 2 ft (0.61 m) x 12 ft (3.66 m) GFRP reinforced panels: (a) normal weight concrete (b) lightweight concrete

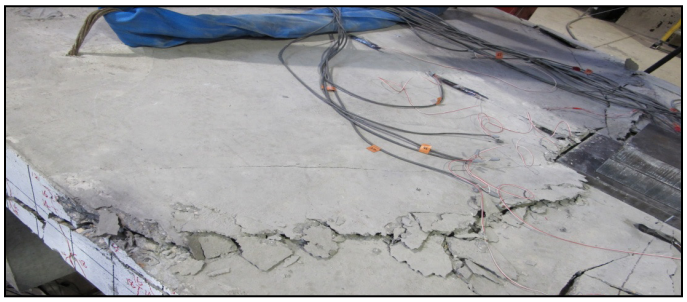

(a)

(b)

Fig. 3.3 Diagonal tension failure of 6 ft (1.83 m) x 12 ft (3.66 m) GFRP reinforced panels: (a) normal weight concrete (b) lightweight concrete

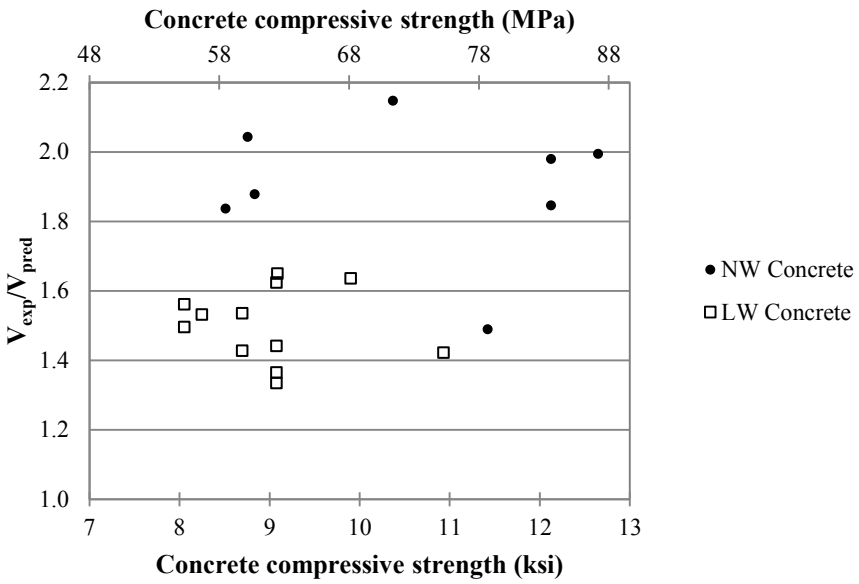

Fig. 3.4 Comparison of experimental shear strength of specimens tested in this research with predicted shear strength from ACI 440.1R (2006)

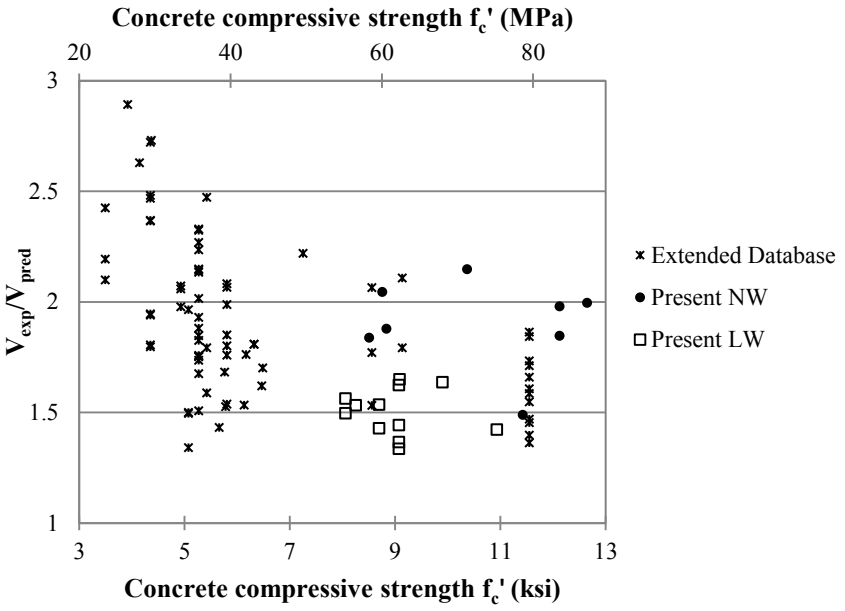

Fig. 3.5 Correlation of experimental to predicted shear strength from ACI 440.1R (2006) for extended database

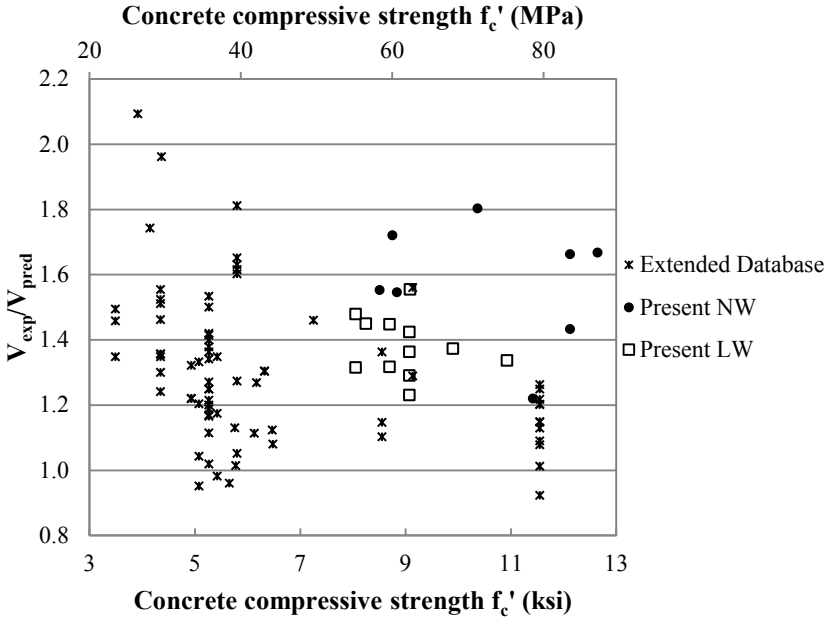

Fig. 3.6 Correlation of experimental to predicted shear strength from CAN/CSA-S806 (2002) for extended database

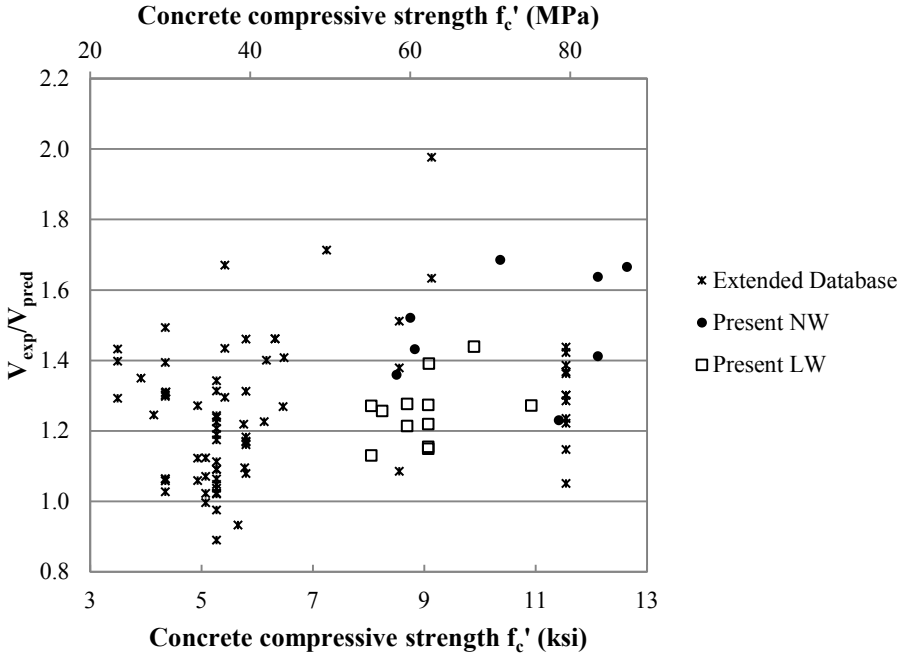

Fig. 3.7 Correlation of experimental to predicted shear strength from JSCE (1997) for extended database

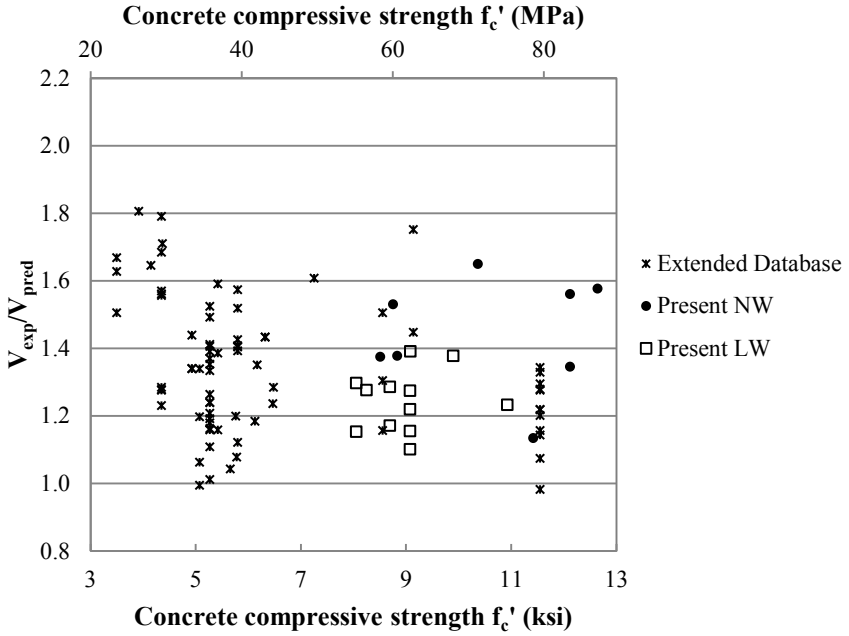

Fig. 3.8 Correlation of experimental to predicted shear strength from El Sayed et al. (2006a) for extended database

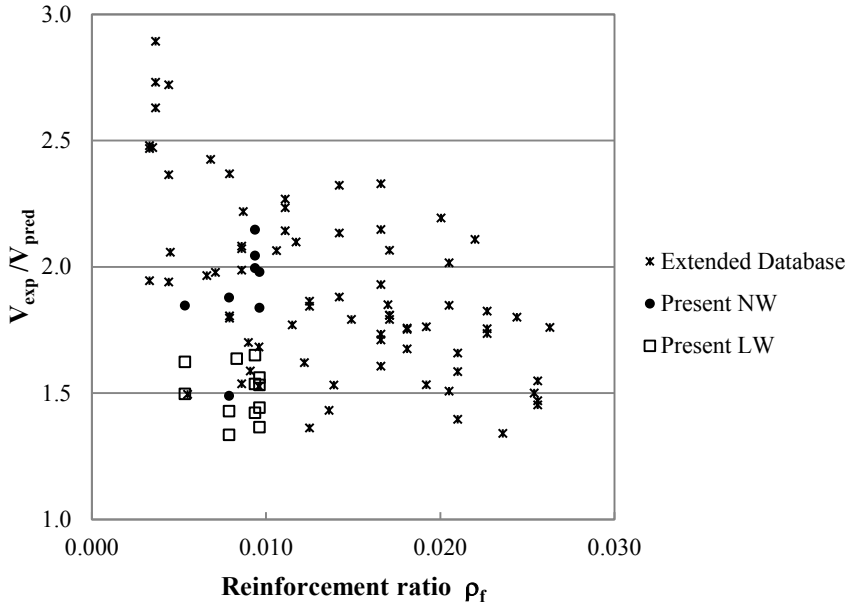

Fig. 3.9 Correlation of experimental to predicted shear strength versus reinforcement ratio from ACI 440.1R (2006) for extended database

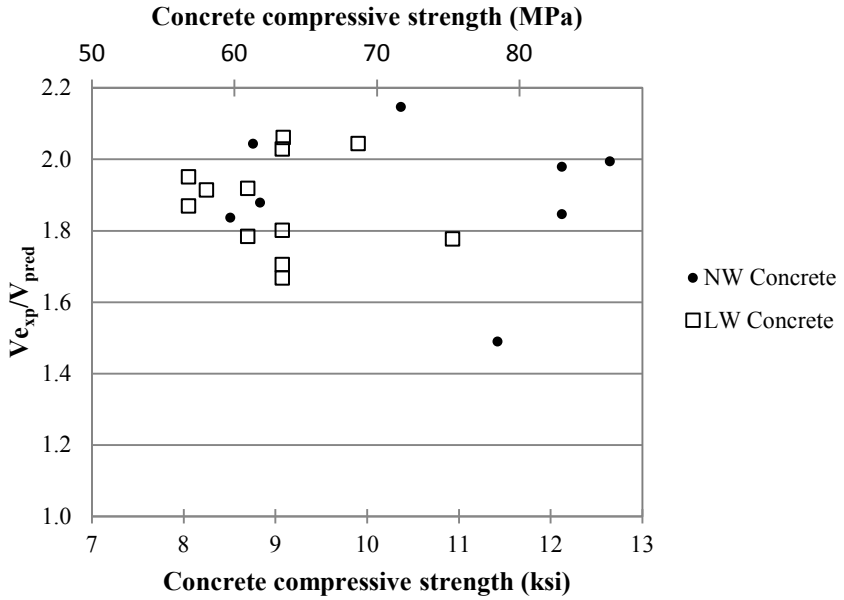

Fig. 3.10 Comparison of experimental shear strength of specimens tested in this research with predicted shear strength from modified Eq. (3.5)

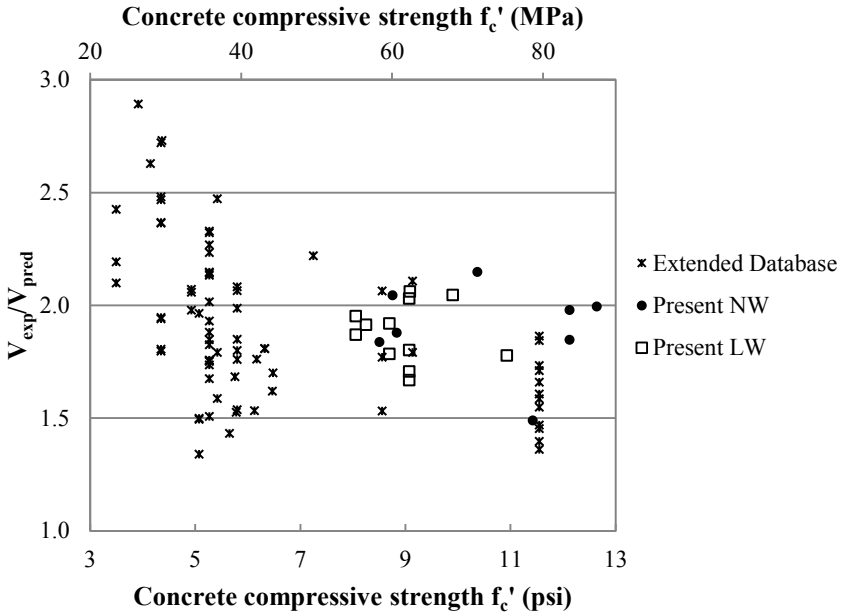

Fig. 3.11 Correlation of experimental to predicted shear strength using modified Eq. (3.5) for extended database

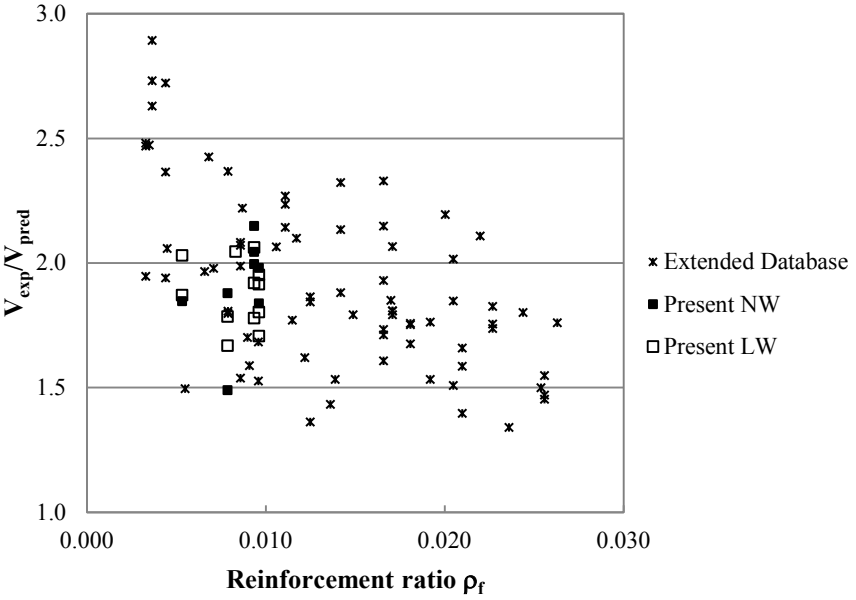

Fig. 3.12 Correlation of experimental to predicted shear strength versus reinforcement ratio using modified Eq. (3.5) for extended database

Appendix 3.A Properties of beams and one-way slabs used for determination of λ_f

Author	Specimen	f_c'	E_c	f_u	E_f	b_w	h	d	Span	ρ_f	ρ_f/ρ_{fb}
		MPa	GPa	MPa	GPa	mm	mm	mm	m		
Swamy and Aburawi (1997)	F-3-GF	39	29.6	586	34	154	254	220.7	2.10	0.0136	2.12
Deitz, et al. (1999)	GFRP1	29	25.3	612	40	305	190	157.5	2.74	0.0037	0.67
	GFRP2	30	26.0	612	40	305	190	157.5	2.74	0.0037	0.64
	GFRP3	27	24.6	612	40	305	190	157.5	2.74	0.0037	0.70
Alkhrdaji, et al. (2001)	BM7	24.1	23.2	717	40	178	330	296.7	1.50	0.0201	5.76
	BM8	24.1	23.2	717	40	178	330	296.7	1.50	0.0068	1.96
	BM9	24.1	23.2	717	40	178	330	296.7	1.50	0.0117	3.37
Yost, et al (2001)	1FRP, a	36.3	39.9	690	40	229	286	225	2.13	0.0111	2.10
	1FRP, b	36.3	39.9	690	40	229	286	225	2.13	0.0111	2.10
	1FRP, c	36.3	39.9	690	40	229	286	225	2.13	0.0111	2.10
	2FRP, a	36.3	39.9	690	40	178	286	225	2.13	0.0142	2.71
	2FRP, b	36.3	39.9	690	40	178	286	225	2.13	0.0142	2.71
	2FRP, c	36.3	39.9	690	40	178	286	225	2.13	0.0142	2.71
	3FRP, a	36.3	39.9	690	40	229	286	225	2.13	0.0166	3.15
	3FRP,b	36.3	39.9	690	40	229	286	225	2.13	0.0166	3.15
	3FRP,c	36.3	39.9	690	40	229	286	225	2.13	0.0166	3.15
	4FRP,a	36.3	39.9	690	40	279	286	225	2.13	0.0181	3.44
	4FRP,b	36.3	39.9	690	40	279	286	225	2.13	0.0181	3.44
	4FRP,c	36.3	39.9	690	40	279	286	225	2.13	0.0181	3.44
	5FRP,a	36.3	39.9	690	40	254	286	224	2.13	0.0205	3.89
	5FRP,b	36.3	39.9	690	40	254	286	224	2.13	0.0205	3.89
	5FRP,c	36.3	39.9	690	40	254	286	224	2.13	0.0205	3.89
	6FRP,a	36.3	39.9	690	40	229	286	224	2.13	0.0227	4.32
	6FRP,b	36.3	39.9	690	40	229	286	224	2.13	0.0227	4.32
	6FRP,c	36.3	39.9	690	40	229	286	224	2.13	0.0227	4.32
Tureyen and Frosch (2002)	V-G1-1	39.7	29.8	607	41	457	406	360	2.44	0.0096	5.05
	V-G2-1	39.9	29.9	593	38	457	406	360	2.44	0.0096	5.33
	V-G1-2	42.3	30.8	607	41	457	427	360	2.44	0.0192	4.92
	V-G2-2	42.5	30.9	593	38	457	427	360	2.44	0.0192	5.33
Gross, et al. (2003)	FRP-1a-26-HS	79.6	46.1	689	40	203	286	226	2.13	0.0125	1.31
	FRP-1b-26-HS	79.6	46.1	689	40	203	286	226	2.13	0.0125	1.31
	FRP-1c-26-HS	79.6	46.1	689	40	203	286	226	2.13	0.0125	1.31
	FRP-2a-26-HS	79.6	46.1	689	40	152	286	226	2.13	0.0166	1.74
	FRP-2b-26-HS	79.6	46.1	689	40	152	286	226	2.13	0.0166	1.74
	FRP-2c-26-HS	79.6	46.1	689	40	152	286	226	2.13	0.0166	1.74
	FRP-3a-26-HS	79.6	46.1	689	40	165	286	224	2.13	0.0210	2.20
	FRP-3b-26-HS	79.6	46.1	689	40	165	286	224	2.13	0.0210	2.20
	FRP-3c-26-HS	79.6	46.1	689	40	165	286	224	2.13	0.0210	2.20
	FRP-4a-26-HS	79.6	46.1	689	40	203	286	224	2.13	0.0256	2.69
	FRP-4b-26-HS	79.6	46.1	689	40	203	286	224	2.13	0.0256	2.69
	FRP-4c-26-HS	79.6	46.1	689	40	203	286	224	2.13	0.0256	2.69

Appendix 3.A (continued)

Author	Specimen	f_c'	E_c	f_u	E_f	b_w	h	d	Span	ρ_f	ρ_f/ρ_{fb}
		MPa	GPa	MPa	GPa	mm	mm	mm	m		
Ashour, A. F. (2005)	Beam 1	34	27.6	650	38	150	200	168	2.00	0.0045	0.80
	Beam 3	34	27.6	705	32	150	250	212	2.00	0.0071	1.71
	Beam 5	34	27.6	705	32	150	300	263	2.00	0.0086	2.07
	Beam 7	59	32.4	705	32	150	200	163	2.00	0.0139	2.51
	Beam 9	59	32.4	705	32	150	250	213	2.00	0.0106	1.91
	Beam 11	59	32.4	705	32	150	300	262	2.00	0.0115	2.08
El-Sayed, et al. (2005)	S-G1	40	30.0	597	40	1000	200	162	2.50	0.0086	1.00
	S-G2	40	30.0	540	40	1000	200	159	2.50	0.0170	2.00
	S-G2B	40	30.0	597	40	1000	200	162	2.50	0.0171	2.00
	S-G3	40	30.0	540	40	1000	200	159	2.50	0.0244	3.00
	S-G3B	40	30.0	597	40	1000	200	162	2.50	0.0263	3.10
El-Sayed, et al. (2006a)	GN-1	50	30.4	608	39	250	400	326	2.75	0.0087	1.18
	GN-2	45	29.1	754	42	250	400	326	2.75	0.0122	2.50
	GN-3	44	28.8	754	42	250	400	326	2.75	0.0171	3.50
El-Sayed, et al. (2006b)	GN-1.7	44	28.8	754	42	250	400	326	2.75	0.0171	3.50
	GH-1.7	63	33.3	754	42	250	400	326	2.75	0.0171	2.61
	GH-2.2	63	33.3	754	42	250	400	326	2.75	0.0220	3.36
Alam and Hussein (2009)	G-2.5	40	29.9	751	48	250	350	305	2.84	0.0086	1.34
	G-3.5	40	29.9	751	48	250	350	305	3.54	0.0086	1.34
	G-500	45	29.1	751	48	250	500	440	3.54	0.0090	1.27
	G-650	37	28.9	751	48	300	650	584	4.04	0.0091	1.49
	G-0.5-500	37	28.9	751	48	250	500	455	3.54	0.0035	0.57
	G-2.5-500	37	28.9	751	48	250	500	429	3.54	0.0149	2.44
Jang, et al. (2009)	G-2.5-R1-1,2	30	25.9	980	48	200	250	221	2.20	0.0033	1.19
	G-2.5-R2-1,2	30	25.9	980	48	150	250	221	2.20	0.0044	1.59
	G-2.5-R3-1,2	30	25.9	941	49	150	250	214	2.20	0.0079	2.60
	G-3.5-R1-1,2	30	25.9	980	48	200	250	221	2.20	0.0033	1.19
	G-3.5-R2-1,2	30	25.9	980	48	150	250	221	2.20	0.0044	1.59
	G-3.5-R3-1,2	30	25.9	941	49	150	250	214	2.20	0.0079	2.60
	G-4.5-R1-1,2	30	25.9	980	48	200	250	221	2.20	0.0033	1.19
	G-4.5-R2-1,2	30	25.9	980	48	150	250	221	2.20	0.0044	1.59
	G-4.5-R3-1,2	30	25.9	941	49	150	250	214	2.20	0.0079	2.60
Bentz, et al. (2010)	M05-0	35	28.0	397	41	450	500	438	3.05	0.0055	0.39
	S05-0	35	28.0	474	41	450	250	194	1.52	0.0066	0.64
	M20-0	35	28.0	397	41	450	500	405	3.05	0.0236	1.67
	S20-0	35	28.0	397	41	450	250	188	1.52	0.0254	1.80

Appendix 3.B Comparison and verification of different shear prediction methods

Author	Specimen	V_{exp}	V_{exp}/V_{ACI}	$V_{exp}/V_{CAN/CSA}$	V_{exp}/V_{JSCE}	$V_{exp}/V_{El\text{-}Sayed}$	V_{exp}/V_{MOD}
		kN					
Swamy and Aburawi (1997)	F-3-GF	20.44	1.43	0.96	0.93	1.04	1.43
Deitz, et al. (1999)	GFRP1	28.59	2.63	1.74	1.24	1.65	2.63
	GFRP2	30.10	2.73	1.96	1.31	1.71	2.73
	GFRP3	30.99	2.89	2.09	1.35	1.81	2.89
Alkhrdaji, et al. (2001)	BM7	54.40	2.19	1.49	1.43	1.67	2.19
	BM8	37.05	2.42	1.46	1.40	1.63	2.42
	BM9	41.05	2.10	1.35	1.29	1.50	2.10
Yost, et al (2001)	1FRP, a	40.64	2.27	1.42	1.24	1.41	2.27
	1FRP, b	40.04	2.23	1.40	1.22	1.39	2.23
	1FRP, c	38.39	2.14	1.34	1.17	1.33	2.14
	2FRP, a	29.34	1.88	1.21	1.06	1.21	1.88
	2FRP, b	36.24	2.32	1.50	1.31	1.49	2.32
	2FRP, c	33.29	2.13	1.38	1.21	1.37	2.13
	3FRP, a	41.59	1.93	1.27	1.11	1.26	1.93
	3FRP,b	50.19	2.33	1.53	1.34	1.52	2.33
	3FRP,c	46.29	2.15	1.41	1.24	1.41	2.15
	4FRP,a	45.74	1.67	1.11	0.98	1.11	1.67
	4FRP,b	47.84	1.75	1.17	1.02	1.16	1.75
	4FRP,c	47.99	1.76	1.17	1.02	1.16	1.76
	5FRP,a	39.47	1.51	1.02	0.89	1.01	1.51
	5FRP,b	52.77	2.01	1.36	1.19	1.35	2.01
	5FRP,c	48.37	1.85	1.25	1.09	1.24	1.85
	6FRP,a	45.09	1.82	1.25	1.09	1.24	1.82
	6FRP,b	43.34	1.75	1.20	1.05	1.19	1.75
	6FRP,c	42.89	1.74	1.19	1.04	1.18	1.74
Tureyen and Frosch (2002)	V-G1-1	108.09	1.68	1.13	1.22	1.20	1.68
	V-G2-1	94.75	1.53	1.01	1.10	1.08	1.53
	V-G1-2	137.01	1.53	1.11	1.23	1.18	1.53
	V-G2-2	152.57	1.76	1.27	1.40	1.35	1.76
Gross, et al. (2003)	FRP-1a-26-HS	43.00	1.84	1.25	1.42	1.33	1.84
	FRP-1b-26-HS	31.77	1.36	0.92	1.05	0.98	1.36
	FRP-1c-26-HS	43.47	1.86	1.26	1.44	1.34	1.86
	FRP-2a-26-HS	32.04	1.61	1.13	1.28	1.20	1.61
	FRP-2b-26-HS	34.11	1.71	1.20	1.37	1.28	1.71
	FRP-2c-26-HS	34.55	1.73	1.22	1.39	1.29	1.73
	FRP-3a-26-HS	39.56	1.66	1.20	1.36	1.28	1.66
	FRP-3b-26-HS	33.31	1.40	1.01	1.15	1.07	1.40
	FRP-3c-26-HS	37.80	1.58	1.15	1.30	1.22	1.58
	FRP-4a-26-HS	49.67	1.55	1.15	1.30	1.22	1.55
	FRP-4b-26-HS	47.14	1.47	1.09	1.23	1.16	1.47
	FRP-4c-26-HS	46.63	1.45	1.08	1.22	1.14	1.45

Appendix 3.B (continued)

Author	Specimen	V_{exp}	V_{exp}/V_{ACI}	$V_{exp}/V_{CAN/CSA}$	V_{exp}/V_{JSCE}	$V_{exp}/V_{El\text{-}Sayed}$	V_{exp}/V_{MOD}
		kN					
Ashour, A. F. (2005)	Beam 1	13.18	2.06	1.32	1.06	1.34	2.06
	Beam 3	18.35	1.98	1.22	1.12	1.34	1.98
	Beam 5	26.03	2.07	1.22	1.27	1.44	2.07
	Beam 7	18.18	1.53	1.15	1.08	1.16	1.53
	Beam 9	28.35	2.06	1.36	1.51	1.50	2.06
	Beam 11	31.03	1.77	1.10	1.38	1.30	1.77
El-Sayed, et al. (2005)	S-G1	118.69	1.99	1.60	1.16	1.39	1.99
	S-G2	147.69	1.85	1.63	1.17	1.41	1.85
	S-G2B	168.69	2.07	1.81	1.31	1.57	2.07
	S-G3	168.69	1.80	1.65	1.18	1.43	1.80
	S-G3B	173.69	1.76	1.61	1.17	1.40	1.76
El-Sayed, et al. (2006a)	GN-1	73.63	2.22	1.46	1.71	1.61	2.22
	GN-2	62.56	1.62	1.12	1.27	1.24	1.62
	GN-3	80.63	1.81	1.30	1.46	1.43	1.81
El-Sayed, et al. (2006b)	GN-1.7	80.63	1.81	1.30	1.46	1.43	1.81
	GH-1.7	90.13	1.79	1.29	1.63	1.45	1.79
	GH-2.2	118.63	2.11	1.56	1.98	1.75	2.11
Alam and Hussein (2009)	G-2.5	63.83	2.08	1.27	1.46	1.52	2.08
	G-3.5	47.13	1.54	1.05	1.08	1.12	1.54
	G-500	82.24	1.70	1.08	1.41	1.28	1.70
	G-650	112.67	1.59	0.98	1.29	1.16	1.59
	G-0.5-500	73.04	2.47	1.35	1.67	1.59	2.47
	G-2.5-500	97.24	1.79	1.17	1.43	1.39	1.79
Jang, et al. (2009)	G-2.5-R1-1,2	25.97	2.47	1.36	1.30	1.56	2.47
	G-2.5-R2-1,2	24.58	2.72	1.55	1.49	1.79	2.72
	G-2.5-R3-1,2	27.37	2.37	1.46	1.39	1.68	2.37
	G-3.5-R1-1,2	26.10	2.48	1.52	1.31	1.57	2.48
	G-3.5-R2-1,2	21.36	2.36	1.51	1.30	1.56	2.36
	G-3.5-R3-1,2	20.77	1.80	1.24	1.06	1.28	1.80
	G-4.5-R1-1,2	20.47	1.95	1.30	1.03	1.23	1.95
	G-4.5-R2-1,2	17.52	1.94	1.35	1.06	1.28	1.94
	G-4.5-R3-1,2	20.87	1.81	1.36	1.06	1.28	1.81
Bentz, et al. (2010)	M05-0	86.00	1.49	0.95	1.02	0.99	1.49
	S05-0	54.50	1.96	1.33	1.12	1.34	1.96
	M20-0	138.00	1.34	1.04	1.07	1.06	1.34
	S20-0	74.00	1.50	1.20	1.00	1.20	1.50

4 DEFLECTION PERFORMANCE OF INITIALLY CRACKED PRECAST CONCRETE PANELS REINFORCED WITH GFRP BARS

Ruifen Liu, and Chris P. Pantelides

4.1 Abstract

Initial cracks in precast concrete panels reinforced with GFRP bars can develop from shrinkage, handling, lifting, and transportation-induced stresses. Seventeen lightweight and normal weight precast concrete panels reinforced with GFRP bars with initial cracks were tested to investigate their deflection performance at service load and ultimate conditions. The test results show that both normal weight and lightweight concrete panels designed according to ACI 440.1R satisfy the service load deflection requirements of the AASHTO LRFD Bridge Design Specifications. The test results indicate that the moment of inertia for precast panels reinforced with GFRP bars with initial cracks was less than the gross moment of inertia even before the cracking moment is reached. An expression for predicting deflection using a conservative estimate of the moment of inertia for precast concrete panels reinforced with GFRP bars is proposed. Using the proposed equation, a better deflection prediction is obtained for precast concrete panels reinforced with GFRP bars under service load; this is critical in the design of such panels, since service load deflection generally controls the design.

4.2 Introduction

Fiber Reinforced Polymer bars are corrosion resistant, they have high tensile strength and light weight, and are easy to install. However, concrete panels reinforced with Glass Fiber Reinforced Polymer (GFRP) bars develop larger deflections and cracks than concrete panels reinforced with steel bars having the same reinforcement ratio. This is primarily due to the lower modulus of elasticity of GFRP bars compared to steel bars. Consequently, the design of GFRP reinforced concrete panels is typically governed by serviceability requirements instead of ultimate limit states.

Determination of the effective moment of inertia of the member is critical in the deflection prediction of concrete reinforced with GFRP bars. Extensive research has been conducted regarding prediction of the moment of inertia of GFRP reinforced concrete members (Theriault and Benmokrane 1998, Toutanji and Saafi 2000, Yost et al. 2003, Bischoff and Paixao 2004, Bischoff 2005, Bischoff 2007, Bischoff and Scanlon 2007, Said 2010, and Bischoff and Gross 2010). Efforts have been made for the modification of Branson's (1965) equation and new equations were proposed to consider the use of GFRP bars as reinforcement for the prediction of the effective moment of inertia. All previous research was focused on predicting the moment of inertia after the reinforced concrete member reached the cracking moment; it was assumed that the moment of inertia before the cracking moment is reached was equal to the gross moment of inertia. However, precast concrete panels reinforced with GFRP bars can develop initial hairline cracks from shrinkage, handling, lifting, and transportation-induced stresses, which may reduce the moment of inertia even before the cracking moment is reached. The moment deflection diagrams in El-Salakawy and Benmokrane (2004) and in Kassem et al. (2011) show that deflections prior to the

cracking moment are underestimated; this indicates that the corresponding moment of inertia is lower than the gross moment of inertia before the cracking moment is reached. It should be noted that in Kassem et al. (2011), the beams tested were initially uncracked.

The value of the moment of inertia before the cracking moment is critical in predicting deflections under service loads for precast concrete members reinforced with GFRP bars. This is the case since the bending moment under service loads may be lower than the cracking moment, especially when high strength concrete is used. In such cases, the design of precast concrete panels reinforced with GFRP bars is typically carried out using the gross moment of inertia, which may lead to unconservative designs.

The objective of this paper is to investigate the moment of inertia of high strength normal weight and lightweight concrete precast panels reinforced with GFRP bars that have cracks of varying spacing and width. These initial cracks were not intentionally inflicted but resulted from shrinkage, handling, lifting, and transportation-induced stresses. Measured deflections at service and ultimate moment are compared with predictions using linear elastic analysis. From the experimental results, the moment of inertia before and after the cracking moment is compared with the moment of inertia predicted by the ACI 440.1R (2006) guidelines, as well as from research studies available in the literature.

4.3 Experimental Program

4.3.1 Specimen Details

Seventeen precast concrete panels reinforced with GFRP bars were tested; ten of the panels were cast using normal weight (NW) concrete and seven using lightweight (LW) concrete. The panel variables included concrete compressive strength, span, panel thickness, and reinforcement ratio. The NW concrete panels were designed according to the ACI 440.1R (2006) flexural design method and satisfied the deflection requirements of the AASHTO LRFD guidelines (2007). Fourteen panels were designed using a reinforcement ratio larger than the balanced reinforcement ratio as recommended by ACI 440.1R (2006), and three panels were built using a reinforcement ratio equal to approximately one half that of the other panels. The LW concrete panels were reinforced in an identical manner to the NW concrete panels.

The precast concrete panels are divided into four series according to their dimensions and reinforcement ratio, as shown in Tables 4.1-4.4 and Fig. 4.1. Series A panels had a dimension of 3.66 m x 0.61 m x 0.235 m with a deck span of 2.44 m, and Series B panels had a dimension of 4.12 m x 0.61 m x 0.273 m with a deck span of 2.90 m. Series C panels were constructed with a dimension of 3.66 m x 1.83 m x 0.235 m. The panels had a 0.61 m overhang on each side of the supports, as shown in Fig. 4.1, which increased the length available to develop the full strength of the GFRP bars. Series A and B panels were 0.61 m wide to simulate the strip design method of bridge decks according to AASHTO Bridge Design Specifications (2007), whereas Series C and D panels were 1.83 m wide to simulate the behavior of a recently constructed bridge deck in Utah with 12.62 m x 2.08 m x 0.235 m normal weight

precast concrete panels reinforced with GFRP bars. Series A panels (Table 4.1), Series C panels (Table 4.3), and Series D panels (Table 4.4) were constructed with a span of 2.44 m; Series B panels (Table 4.2) were constructed with a span of 2.90 m. Series D panels were constructed with the same geometry as Series C panels but with 56% of the area of longitudinal reinforcement, and are identified by symbol E in the specimen number. A number of batches were cast for both NW and LW precast concrete panels at two different time periods.

All panels were reinforced with ϕ16 diameter Aslan 100 GFRP bars. For Series A, B, and C panels, the reinforcement in the span direction was ϕ16 @ 102 mm; the reinforcement in the short direction was ϕ16 @ 152 mm. For Series D panels, the reinforcement along both directions was ϕ16 @ 203 mm.

The panels were constructed at a Precast/Prestressed Concrete Institute certified plant following the same construction procedure as steel reinforced concrete members, and then transported to the laboratory, which simulates precast bridge deck construction. Embedded lifting hoops at the four corners were used for lifting the panels. The panels were inspected before testing; initial cracks due to shrinkage, handling, lifting, and transportation-induced stresses were measured and mapped. For each panel, the measured concrete compressive strength at the time of testing, reinforcement ratio, balanced reinforcement ratio, experimental cracking moment, and service moment per AASHTO LRFD Bridge Design Specifications (2007) are given in Tables 4.1-4.4. The experimental cracking moment is defined as the point of change in slope of the bilinear load-deflection diagram. The maximum initial crack width of each panel is shown in Table 4.5. The initial crack widths ranged from 0.051 mm to 0.406 mm. It is clear that handling of precast concrete panels reinforced with

GFRP bars requires extra care. One method for handling theses panels is to lift them with straps placed underneath the panels at multiple points rather than using lifting hoops at the four corners, as was done in this case.

4.3.2 Materials

The tensile strength of the specific lot of GFRP bars used in this research was 655 MPa, and the modulus of elasticity 40.8 GPa. The compressive strength of both NW and LW concrete at the time of testing was higher than 55 MPa, as shown in Tables 4.1-4.4; thus, both types of concrete are classified as high strength concrete. The coarse hard rock aggregate for NW concrete had a size of 19 mm; the expanded shale aggregate for LW concrete had a size of 12.7 mm. Fine aggregate used for the LW concrete was sand commonly used in NW concrete; thus, the LW concrete used in this research is classified as sand-lightweight concrete.

4.3.3 Instrumentation

Three Linear Variable Differential Transducers (LVDTs) were used to measure the deflection of the 0.61 m wide panels: one was attached at midspan and two at the quarter span points. Five LVDTs were used to measure the deflection of the 1.83 m wide panels: one was attached at midspan, two at the quarter span, and one on each side of the panels at the outer edges at midspan.

4.3.4 Test Setup and Procedure

The panels were tested using a hydraulic actuator as shown in Fig. 4.1; the panels were supported on two reinforced concrete beams. Elastomeric pads 152 mm wide and 51 mm thick were placed on the two supporting beams so the panels could

rotate freely at the supports. The load was applied through a 254 mm x 508 mm x 25 mm steel bearing plate to simulate the area of a double tire truck load on a bridge deck (AASHTO 2007). The load was applied as a series of half-sine downward cycles of increasing amplitude. The number of half cycles to crack the panels ranged from six to nine, and the number of half cycles to ultimate load from seventeen to twenty. The load application was displacement controlled, with a loading rate of 5 mm/min.

4.4 Deflection Comparison of Theoretical to Experimental Results

Deflection is important in the design of GFRP reinforced concrete members, as serviceability requirements usually control the design of concrete bridge decks reinforced with GFRP bars. Figure 4.2 shows the deflection of a typical panel during testing, and typical crack spacing, which was mostly uniform along the span. The ACI 440.1R (2006) design guide and the AASHTO LRFD Bridge Design Guide Specifications for GFRP Reinforced Concrete Decks and Traffic Railings (2009) require the use of a direct method of deflection control. When the applied bending moment is smaller than the cracking moment, the gross moment of inertia I_g is used to calculate panel deflection; in the range from cracking moment to ultimate moment, the effective moment of inertia should be used to calculate the panel deflection. To account for the lower modulus of elasticity of GFRP bars and the different bond behavior of GFRP bars to concrete, ACI 440.1R (2003) recommended the following equation for finding the effective moment of inertia after the cracking moment:

$$I_e = \left(\frac{M_{cr}}{M_a}\right)^3 \beta_d I_g + \left[1 - \left(\frac{M_{cr}}{M_a}\right)^3\right] I_{cr} \leq I_g \tag{4.1a}$$

$$\beta_d = \alpha_b \left(\frac{E_f}{E_s} + 1\right) \tag{4.1b}$$

where I_e = effective moment of inertia; I_{cr} = moment of inertia of transformed cracked section; I_g = gross moment of inertia; β_d = reduction coefficient used in calculating deflection;

M_{cr} = cracking moment; M_a = maximum moment in the member when deflection is computed; α_b = bond dependent coefficient taken as 0.5; E_f = modulus of elasticity of GFRP bars; E_s = modulus of elasticity of steel bars.

Toutanji and Saafi (2000), and Yost et al. (2003) found that the degree of tension stiffening is affected by the amount and stiffness of the flexural reinforcement and by the relative reinforcement ratio. The reduction coefficient related to the reduced tension stiffening β_d was modified from Eq. (4.1b) in ACI 440.1R (2006) to the following expression:

$$\beta_d = \frac{1}{5}\left(\frac{\rho_f}{\rho_{fb}}\right) \tag{4.2}$$

where, ρ_f = GFRP reinforcement ratio; ρ_{fb} = GFRP reinforcement ratio at balanced strain conditions. Bischoff and Scanlon (2007) proposed an alternative expression for

the effective moment of inertia after the cracking moment, without empirical correction factors, as:

$$I_e = \frac{I_{cr}}{1-\eta\left(\frac{M_{cr}}{M_a}\right)^2} \le I_g \tag{4.3}$$

where, $\eta = 1 - I_{cr}/I_g$.

The moment of inertia equations presented previously only address the moment of inertia after the cracking moment; it is generally assumed that the moment of inertia before the cracking moment is the gross moment of inertia. However, for precast concrete panels reinforced with GFRP bars, the presence of initial cracks may reduce the gross moment of inertia before the cracking moment is reached. The focus of this investigation is the effect of initial cracks, which may be present in precast concrete panels reinforced with GFRP bars due to shrinkage, handling, lifting, and transportation-induced stresses, on the moment of inertia before the section reaches the cracking moment. The member deflection in this study was predicted using linear elastic analysis, based on a simplified model of the panels, as shown in Fig. 4.3. The panels were supported on two concrete beams; the distributed load on the steel bearing plate is equal to $q = P/B$, where P = load recorded from the actuator, and B = steel bearing plate length, as shown in Fig. 4.1. The following equations based on linear elastic analysis are used to calculate the deflection and compare it with the measured deflection at midspan:

$$M(x) = \frac{P}{2}x \qquad 0 \le x \le \frac{L-B}{2} \tag{4.4a}$$

$$M(x) = \frac{P}{2}x - \frac{q\left(x - \frac{L-B}{2}\right)^2}{2} \qquad \frac{L-B}{2} \le x \le \frac{L}{2} \tag{4.4b}$$

$$m(x) = \frac{1}{2}x \qquad 0 \le x \le \frac{L}{2} \tag{4.4c}$$

$$\Delta = \int_0^L \frac{M(x)m(x)}{E_c I_{ave}}\,dx \tag{4.4d}$$

$$I_{ave} = \frac{1}{\Delta E_c}\left(\int_0^L M(x)m(x)\,dx\right) \tag{4.4e}$$

where, $M(x)$ = bending moment due to applied load; $m(x)$ = moment due to unit load; Δ = measured deflection at midspan; I_{ave} = average moment of inertia for the panel span; E_c = concrete modulus of elasticity. Equation (4.4e) is valid since the initial crack widths observed were mostly uniform throughout the panel span, as shown in Figs. 4.2 and 4.4.

Measured midspan deflection at service and ultimate load conditions, and the deflection predicted using the moment of inertia given in the ACI 440.1R (2006) guidelines (Eqs. (4.1a), (4.2) and Eq. (4.4d)) are given in Table 4.5. In general, the deflections predicted by ACI 440.1R (2006) at ultimate load are close to those of the NW and LW precast GFRP reinforced concrete panels tested in this study; however, the deflections at service load conditions are underestimated.

At service load, the deflection predicted using Eqs. (4.1a), (4.2), and (4.4d) is much smaller than the experimentally observed deflection; the ratio of experimentally

observed to predicted deflection at service load ranged from 2.7 to 7.5 for NW precast panels and 3.0 to 6.8 for LW precast panels. The panels with larger initial crack widths generally had a higher ratio of experimentally observed to predicted deflection at service load (panels #8 B1NW, #19 B1LWE, #12 B1NW, #15 B1LW, and #20 B2LWE); it should be stressed that these five panels had significantly wide initial cracks, which may not be typical. However, the remaining panels also show significantly large ratios of observed to predicted deflection at service load. The deflection predicted using Eqs. (4.1a), (4.2), and Eq. (4.4d) at ultimate load is close to the experimentally measured deflection; the ratio of experimentally observed to predicted deflection at ultimate load ranges from 0.8 to 1.4 for NW precast concrete panels and 0.9 to 2.4 for LW precast concrete panels.

In Table 4.5, the under-prediction of deflection for service loads indicates that the ACI 440.1R (2006) guidelines suggest a much higher moment of inertia for precast concrete panels for both NW and LW concrete reinforced with GFRP bars than that implied from the experimentally observed deflections. A similar trend exhibited by the specimens in this research for the initial loading prior to the cracking moment was observed in the moment versus deflection diagrams of some of the slabs tested by El-Salakawy and Benmokrane (2004) and beams tested by Kassem et al. (2011). Comparing these three research studies, it is clear that the lower moment of inertia prior to the cracking moment is not caused by the loading procedure (monotonic loading or cyclic loading), the concrete type (normal weight or lightweight), or the member depth (slab or beam).

4.5 Proposed Modification of Equation for Moment of Inertia of Precast GFRP Reinforced Concrete Panels

Comparing the experimentally observed to predicted midspan deflections at service moment, it has been shown that ACI 440.1R (2006) over-predicts the moment of inertia up to the cracking moment for the precast high strength concrete panels reinforced with GFRP bars with initial cracks tested in this study.

To investigate the moment of inertia before and after the cracking moment, Figs. 4.5(a) and 4.5(b) show the normalized moment of inertia calculated from Eq. (4.4e) for the 0.61 m and 1.83 m wide precast panels, respectively. The cracking moment M_{cr} used in Figs. 4.5(a) and 4.5(b) is the actual cracking moment determined as the point of change in slope of the bilinear load deflection diagram. The bending moment M_a was calculated based on the load recorded by the actuator and the midspan deflection was measured by the LVDTs. Beyond very small deflections (0.1 mm) for which there is disturbance due to instrument inaccuracies, Figs. 4.5(a) and 4.5(b) show that the normalized moment of inertia is generally constant up to the cracking moment. Figure 4.5(a) shows that when $M_a/M_{cr} < 1$, the normalized moment of inertia is in the range of 20% to 40% of the gross moment of inertia for the 0.61 m wide precast panels. Figure 4.5(b) shows that when $M_a/M_{cr} < 1$, the normalized moment of inertia is in the range of 20% to 32% of the gross moment of inertia for the 1.83 m wide precast panels, including the panels with a reduced reinforcement ratio. When $M_a/M_{cr} \geq 1$, the moment of inertia drops significantly, and the values of I_{ave}/I_g for different panels are close to each other, and within ±5% of the median value.

Figures 4.5(a) and 4.5(b) show that even though the initial crack widths caused by shrinkage, handling, lifting, and transportation of the panels ranged from 0.051 mm to 0.406 mm, the moment of inertia is 20% to 40% of the gross moment of inertia before the cracking moment; moreover, this value is relatively constant regardless of the M_a/M_{cr} ratio when $M_a/M_{cr}<1$. In addition, the width and concrete compressive strength of the panel do not seem to affect significantly the value of the moment of inertia before the cracking moment is reached. Beyond the cracking moment, ACI 440.1R (2006) predicts the effective moment of inertia accurately as compared to the experimental moment of inertia. Based on these observations, the moment of inertia of precast concrete panels reinforced with GFRP bars before the cracking moment is reached should be modified. Due to the lower modulus of elasticity of GFRP bars and the resulting cracks caused by shrinkage, handling, lifting, and transportation of precast concrete panels, the moment of inertia could be predicted adequately as follows:

$$M_a < M_{cr} \quad : \quad I_e = \max\left(0.2I_g, \beta_d I_g\right) \le I_g \tag{4.5a}$$

$$M_a \ge M_{cr} \quad ; \quad I_e = \left(\frac{M_{cr}}{M_a}\right)^3 \beta_d I_g + \left[1-\left(\frac{M_{cr}}{M_a}\right)^3\right] I_{cr} \le I_g \tag{4.5b}$$

$$\beta_d = \frac{1}{5}\frac{\rho_f}{\rho_{fb}} \tag{4.5c}$$

The moment of inertia calculated from the experiments using Eq. (4.4e), ACI 440.1R-06 (2006) (Eqs. (4.1a) and (4.2b)), the Bischoff and Scanlon (2007) equation (Eq. (4.3)), and the proposed expression Eq. (4.5) are compared in Figs. 4.6 and 4.7 for the 0.61 m wide and 1.83 m wide precast concrete panels, respectively. The cracking moment used in Figs. 4.6 and 4.7 is the experimental cracking moment, and the vertical line in the figures is located where the applied moment is equal to the service moment; in many cases, the service moment is less than the cracking moment which indicates that Eq. (4.5a) should be used in the design of GFRP reinforced precast concrete panels rather than the gross moment of inertia.

Figures 4.6 and 4.7 show that Eq. (4.5) can predict the moment of inertia in a satisfactory manner for panels with two different spans and two different widths, before the cracking moment is reached. Both the ACI 440.1R (2006) equation and the Bischoff and Scanlon (2007) equation use the gross moment of inertia before the cracking moment is reached. However, this does not reflect what occurred in the present tests of initially cracked precast concrete panels reinforced with GFRP bars. The panels tested but not shown in this paper displayed a similar trend to the results shown in Figs. 4.6 and 4.7.

The load deflection diagram from the experiments and that calculated using the moment of inertia based on ACI 440.1R (2006), Bischoff and Scanlon (2007), and Eq. (4.5) are shown in Figs. 4.8 - 4.10. Figures 4.8 and 4.9 show the load deflection diagram before and shortly after the cracking moment. Figure 4.10 shows the load deflection diagram up to the ultimate load. The first line segment of the bilinear load

deflection diagram corresponds to the applied moment being less than the cracking moment; the second line segment corresponds to the applied moment after the cracking moment. When the load is less than or equal to that corresponding to the cracking moment, the deflections are predicted in a satisfactory manner using the proposed expression; however, the deflections are underestimated by both the ACI 440.1R (2006) and the Bischoff and Scanlon (2007) methods. On the other hand, when the applied moment exceeds the cracking moment, predictions of deflection are acceptable and conservative up to the ultimate moment; in this region, the Bischoff and Scanlon (2007) equation predicts the deflection slightly better than Eq. (4.5b), which is identical to the ACI 440.1R (2006) equation.

4.6 Deflection Requirements of the AASHTO LRFD Bridge Design Specifications

The GFRP reinforced precast concrete panels were checked for deflection at the service moment according to the AASHTO LRFD Bridge Design Specifications (2007); all panels except the lightweight concrete panels with reduced reinforcement ratio satisfied the deflection requirement. The AASHTO Specifications use an HL-93 live load for the service and ultimate load design of bridge decks. According to AASHTO, the HL-93 live load consists of either a design truck or tandem, combined with a design lane load. In the present case, the service moments were calculated based on the following assumptions: for the 0.61 m wide specimens, only one set of wheels from a truck could be placed on the panel with a load equal to 71.2 kN; for the 1.83 m wide specimens, two sets of wheels from the tandem could be placed on the panel with a total load equal to 111.2 kN; the design lane load is a uniform load of

9.34 kN/m. To simplify the calculation, the service moments from Section 4 in Table A4-1 of the AASHTO LRFD Bridge Specifications were used, which is similar to the calculated service moments based on the HL-93 live load. Figure 4.11 shows the moment-deflection diagram with the service moment (including both HL-93 live load and dead load of the panels) and the service load deflection limits; the solid line represents normal weight concrete panel, while the dashed line represents lightweight concrete panel. Figure 4.11(a) shows the moment-deflection diagram and the allowable deflection at the service moment for Series A panels; Figure 4.11(b) shows the same comparison for Series B panels; Figures 4.11(c) and 4.11(d) show the moment-deflection comparison for Series C and D panels, respectively. Figure 4.11 shows that all panels satisfy the deflection requirement under the service moment, including panels with increased span and deck thickness, except for two panels. The lightweight concrete panels with reduced reinforcement ratio did not satisfy the deflection requirement at service moment, as shown in Fig. 4.11(d); the experimental deflection was within 25% of the deflection requirement at the service moment.

4.7 Conclusions

The midspan deflection at service and ultimate moment and the corresponding values of the moment of inertia for seventeen GFRP reinforced precast concrete panels constructed using normal weight and lightweight concrete are presented. The precast panels had initial crack widths ranging from 0.051 mm to 0.406 mm. Based on the experimental results, the following conclusions can be drawn:

1. For precast concrete panels with initial cracks, the experimental moment of inertia is much smaller than the ACI 440.1R (2006) guidelines when the

applied bending moment is less than the cracking moment. The effective moment of inertia predicted by the ACI 440.1R (2006) guidelines from the cracking moment to ultimate moment is close to that observed in this research.

2. For precast concrete panels reinforced with GFRP bars with initial cracks, the moment of inertia should not be taken as the gross moment of inertia when the service moment is less than the cracking moment. The present tests show that before reaching the cracking moment, the moment of inertia was 20% to 40% of the gross moment of inertia for 0.61 m wide panels. The moment of inertia was 20% to 32% of the gross moment of inertia for 1.83 m wide panels.
3. High strength concrete increases the design cracking moment; in this case, the service moment can be smaller than the cracking moment. Since precast concrete panels reinforced with GFRP bars can develop initial cracks due to shrinkage, handling, lifting, and transportation-induced stresses, use of the gross moment of inertia is unconservative. The type of concrete, i.e. normal weight concrete or lightweight concrete, does not affect the moment of inertia significantly before the cracking moment is reached.
4. For initially cracked precast concrete panels reinforced with GFRP bars, an expression is proposed to evaluate the moment of inertia when the design service moment is less than the cracking moment; in the range of applied bending moments, the equation predicts deflections more accurately compared to the ACI 440.1R (2006) prediction. Using the proposed expression, the predicted deflections before the cracking moment are satisfactory compared to the observed behavior. More research needs to be conducted on precast

concrete panels with initial cracks reinforced with GFRP bars, in terms of the effects of reinforcement ratio and concrete strength on the moment of inertia.

5. All panels tested satisfied the service moment deflection requirements of the AASHTO LRFD Bridge Design Specifications, even though some of them had longer spans than typical GFRP reinforced precast bridge deck panels, or normal weight concrete panels with reduced reinforcement ratio. However, lightweight concrete panels with reduced reinforcement ratio did not satisfy the service moment deflection requirements of AASHTO.
6. Lifting of precast concrete panels reinforced with GFRP bars requires extra care. Embedded lifting hoops should not be used for lifting these panels. It is recommended that such panels be lifted with straps placed underneath the panels at multiple points in the long dimension of the panel.

4.8 Acknowledgments

The research reported in this paper was supported by the Utah DOT and the Expanded Shale Clay and Slate Institute. The authors acknowledge the contribution of Hughes Bros Inc., Utelite Corporation, and Hanson Structural Precast. The authors acknowledge the assistance of Professor L. D. Reaveley, M. Bryant, B. T. Besser, and C. A. Burningham of the University of Utah in the experimental portion of the research.

4.9 Notation

B = steel bearing plate length;

DL = dead load per foot width of slab;

E_c = modulus elasticity of concrete;

E_f = design or guaranteed modulus of elasticity of GFRP bars;

E_s = modulus of elasticity of steel reinforcement;

I_{ave} = average moment of inertia for the panel span;

I_{cr} = moment of inertia of transformed cracked section;

I_e = effective moment of inertia;

I_g = gross moment of inertia;

L = span length;

$m(x)$ = moment due to unit load;

$M(x)$ = bending moment due to applied load from the left side support;

M_a = maximum moment in the member at stage at which deflection is computed;

M_{cr} = cracking moment;

M_{DL} = dead load moment per foot-width of slab;

M_{LL} = live load moment per foot-width of slab;

P = load from actuator;

P_L = live load;

S = effective span length;

α_b = bond dependent coefficient taken as 0.5;

β_d = reduction coefficient used in calculating deflection;

Δ = measured deflection at midspan;

Δ_a = allowable deflection;

ρ_f = GFRP reinforcement ratio;

ρ_{fb} = GFRP reinforcement ratio producing balanced strain conditions.

4. 10 References

American Association of State Highway and Transportation Officials, (AASHTO). (2007). "LRFD Bridge Design Specifications." 4th Edition, AASHTO, Washington, D.C. 1526 pp.

American Association of State Highway and Transportation Officials, (AASHTO). (2009). "AASHTO LRFD Bridge Design Guide Specifications for GFRP Reinforced Concrete Decks and Traffic Railings." 1st edition, AASHTO, Washington, D.C., 68 pp.

American Concrete Institute, (ACI 440.1R-03). (2003). "Guide for the Design and Construction of Structural Concrete Reinforced with FRP Bars". American Concrete Institute, Farmington Hills, Mich., 42 pp.

American Concrete Institute, (ACI 440.1R-06). (2006). "Guide for the Design and Construction of Structural Concrete Reinforced with FRP Bars". American Concrete Institute, Farmington Hills, Mich., 44 pp.

Bischoff, P. H. (2005). "Reevaluation of Deflection Prediction for Concrete Beams Reinforced with Steel and Fiber Reinforced Polymer Bars," Journal of Structural Engineering, 131(5), 752-767.

Bischoff, P. H. (2007). "Deflection Calculation of FRP Reinforced Concrete Beams Based on Modifications to the Existing Branson Equation," Journal of Composites for Construction, ASCE, 11(1).

Bischoff, P. H., and Gross, S. P. (2011). "Design Approach for Calculating Deflection of FRP Reinforced Concrete," Journal of Composites for Construction, 15(4), 490-499.

Bischoff, P. H., and Paixao, R. (2004). "Tension stiffening and cracking of concrete reinforced with glass fiber reinforced polymer (GFRP) bars." Canadian Journal of Civil Engineering, 31, 579-588.

Bischoff, P.H., and Scanlon, A. (2007). "Effective moment of inertia for calculating deflections of concrete members containing steel reinforcement and fiber-reinforced polymer reinforcement", ACI Structural Journal, 104(1), 68-75.

Branson, D.E. (1965). "Instantaneous and time-dependent deflections of simple and continuous reinforced concrete beams." HPR Report No. 7, Part 1, Alabama Highway Department, Bureau of Public Roads, Montgomery, AL, pp. 78.

El-Salakawy, E., and Benmokrane, B. (2004). "Serviceability of Concrete Bridge Deck Slabs Reinforced with Fiber-Reinforced Polymer composite Bars," ACI Structural Journal, 101(5), 727-736.

Said, H. (2010). "Deflection Prediction for FRP-Strengthened Concrete Beams," Journal of Composites for Construction, ASCE, 14(2), 244-248.

Kassem, C, Farghaly, A. S. and Benmokrane, B. (2011). "Evaluation of Flexural Behavior and Serviceability Performance of Concrete Beams Reinforced with GFRP Bars," Journal of Composites for Construction, ASCE, accepted.

Theriault, M. and Benmokrane, B. (1998). "Effects of FRP Reinforcement Ratio and Concrete Strength on Flexural Behavior of Concrete Beams." Journal of Composites for Construction, 2(1), 7-16.

Toutanji, H., and Saafi, M. (2000). "Flexural Behavior of Concrete Beams Reinforced with Glass Fiber-Reinforced Polymer (GFRP) Bars," ACI Structural Journal, 97(5), 712-719.

Yost, J., Gross, S., and Dinehart, D. (2003). "Effective Moment of Inertia for GFRP Reinforced Concrete Beams," ACI Structural Journal, 100(6), 732-739.

Table 4.1 Series A panels: 0.61 m wide x 235 mm thick with 2.44 m span

Specimen number	f_c' (MPa)	ρ_f %	ρ_{fb} %	Cracking moment (kN*m)	Service moment (kN*m)
#1 B1NW	71.50	0.94	0.95	31.7	18.1
#2 B2NW	87.22	0.94	1.16	25.0	18.1
#3 B2NW	60.40	0.94	0.80	23.3	18.1
#5 B1LW	75.36	0.94	1.00	20.5	17.8

NW=normal weight, LW=lightweight

Table 4.2 Series B panels: 0.61 m wide x 273 mm thick with 2.90 m span

Specimen number	f_c' (MPa)	ρ_f %	ρ_{fb} %	Cracking moment (kN*m)	Service moment (kN*m)
#8 B1NW	78.74	0.79	1.05	11.7	21.5
#9 B2NW	60.95	0.79	0.81	24.1	21.5
#10 B1LW	62.60	0.79	0.83	26.8	21.0
#11 B2LW	59.98	0.79	0.80	18.5	21.0

NW=normal weight, LW=lightweight

Table 4.3 Series C panels: 1.83 m wide x 235 mm thick with 2.44 m span

Specimen number	f_c' (MPa)	ρ_f %	ρ_{fb} %	Cracking moment (kN*m)	Service moment (kN*m)
#12 B1NW	83.63	0.96	1.11	93.9	52.8
#13 B2NW	58.67	0.96	0.78	63.8	52.8
#14 B1LW	62.60	0.96	0.83	66.1	51.9
#15 B1LW	62.60	0.96	0.83	50.8	51.9
#16 B2LW	56.88	0.96	0.76	32.8	51.9
#17 B2LW	55.57	0.96	0.74	69.9	51.9

NW=normal weight, LW=lightweight

Table 4.4 Series D panels: 1.83 m wide x 235 mm thick with 2.44 m span

Specimen Number	f_c' (MPa)	ρ_f %	ρ_{fb} %	Cracking moment (kN*m)	Service moment (kN*m)
#18 B1NWE	83.63	0.54	1.11	68.0	52.8
#19 B1LWE	62.60	0.54	0.83	41.9	51.9
#20 B2LWE	55.57	0.54	0.74	45.5	51.9

NW=normal weight, LW=lightweight;
E = panels with reduced reinforcement ratio

Table 4.5 Midspan deflection of panels at service and ultimate moment

Series	Specimen	Initial crack width (mm)	Service moment			Ultimate moment		
			$\Delta_{experiment}$ (mm)	$\Delta_{prediction}$ (mm)	$\Delta_{exp}/\Delta_{pre}$	$\Delta_{experiment}$ (mm)	$\Delta_{prediction}$ (mm)	$\Delta_{exp}/\Delta_{pre}$
A	#1 B1NW	0.051	2.01	0.41	4.9	37.7	46.7	0.8
	#2 B2NW	0.051	1.02	0.38	2.7	43.7	45.8	1.0
	#3 B2NW	0.051	1.22	0.43	2.8	41.3	42.2	1.0
	#5 B1LW	0.051	1.68	0.51	3.3	73.0	35.3	2.1
B	#8 B1NW	0.406	3.05	0.41	7.5	41.5	41.8	1.0
	#9 B2NW	0.051	1.45	0.46	3.2	51.6	54.4	1.0
	#10 B1LW	0.102	1.88	0.56	3.4	38.7	40.3	1.0
	#11 B2LW	0.076	1.73	0.58	3.0	41.3	42.9	1.0
C	#12 B1NW	0.178	1.80	0.38	4.7	52.2	44.3	1.2
	#13 B2NW	0.051	1.88	0.43	4.4	51.0	36.4	1.4
	#14 B1LW	0.076	1.75	0.53	3.3	34.7	31.5	1.1
	#15 B1LW	0.178	2.74	0.53	5.1	39.0	33.5	1.2
	#16 B2LW	0.051	2.79	0.56	5.0	66.8	27.7	2.4
	#17 B2LW	0.127	1.83	0.56	3.3	31.0	35.4	0.9
D	#18 B1NWE	0.127	1.60	0.38	4.2	61.7	51.4	1.2
	#19 B1LWE	0.229	3.63	0.53	6.8	53.0	47.9	1.1
	#20 B2LWE	0.127	3.71	0.56	6.6	48.8	41.6	1.2

NW=normal weight, LW=lightweight, E = panels with reduced reinforcement ratio

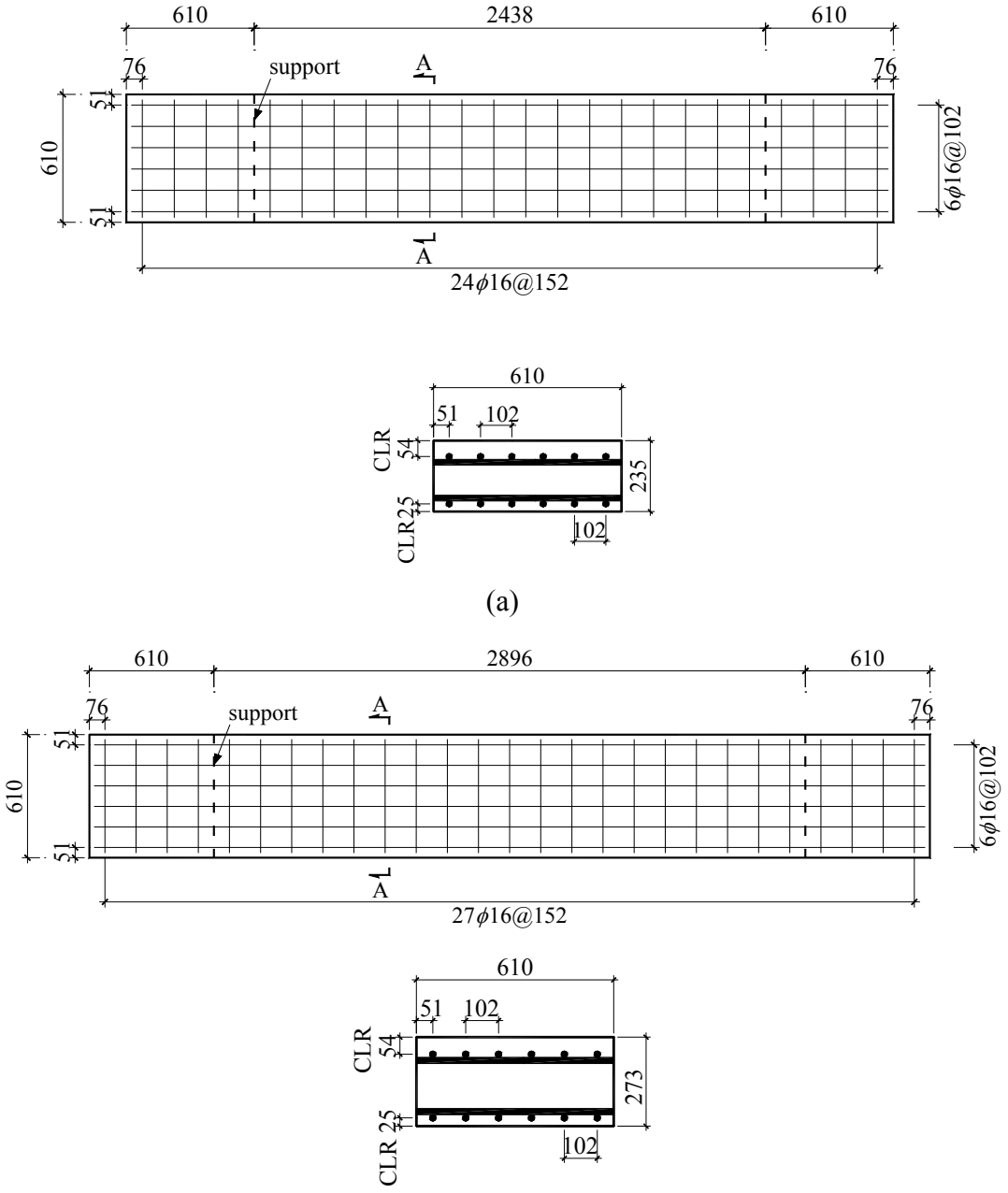

Fig. 4.1 Dimensions, top and bottom GFRP reinforcement mat for slabs: (a) Series A; (b) Series B; (c) Series C; (d) Series D; Test setup: (e) elevation; (f) plan (mm)

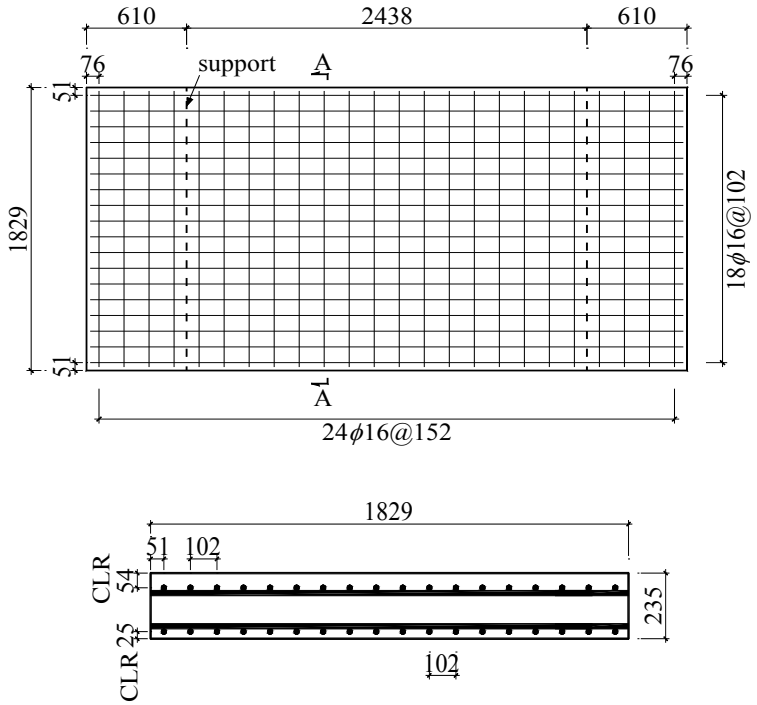

Section A-A

(c)

Fig. 4.1 (continued)

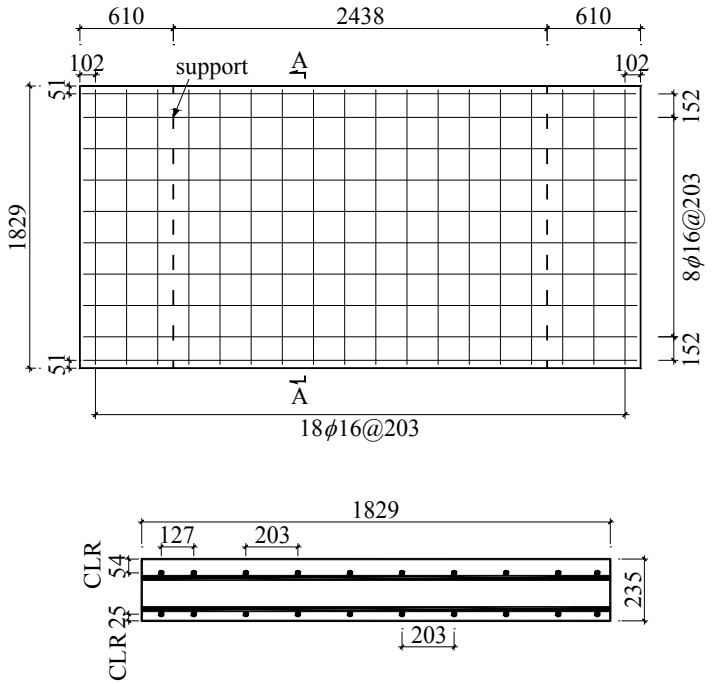

Section A-A

(d)

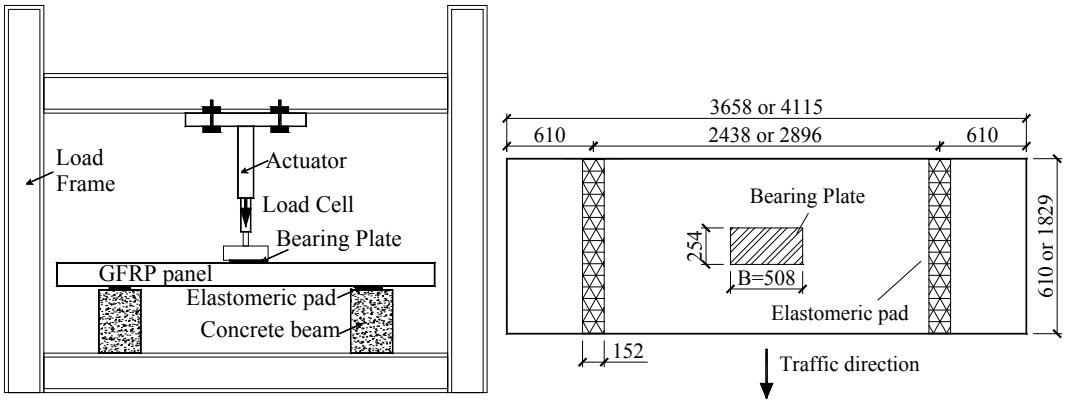

(e) (f)

Fig. 4.1 (continued)

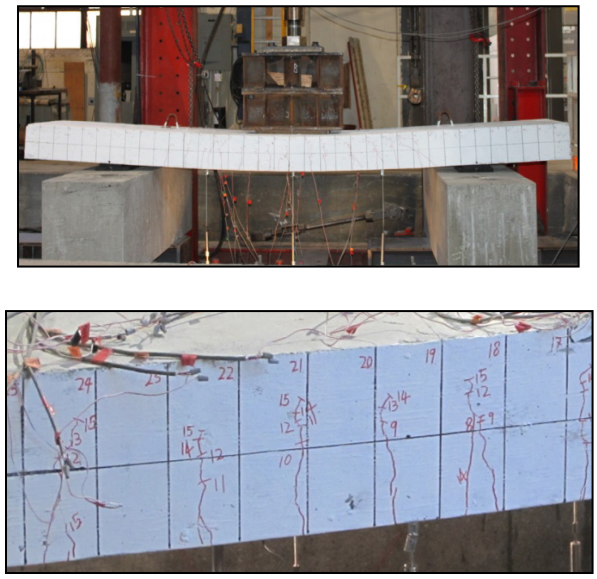

(a) (b)

Fig. 4.2 Panel performance: (a) deflection, and (b) cracks on one side of panel

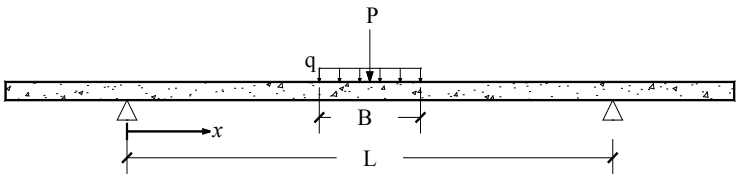

Fig. 4.3 Deflection prediction

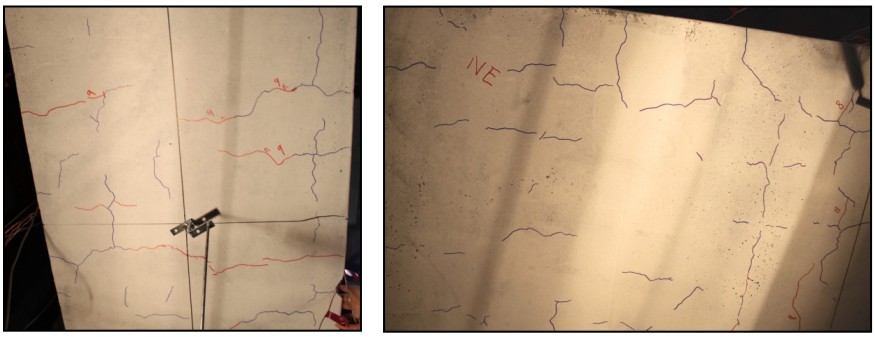

(a) (b)

Fig. 4.4 Initial cracks caused by shrinkage, handling, lifting, and transportation at the underside of the panel: (a) 0.61 m wide panel; (b) 1.83 m wide panel

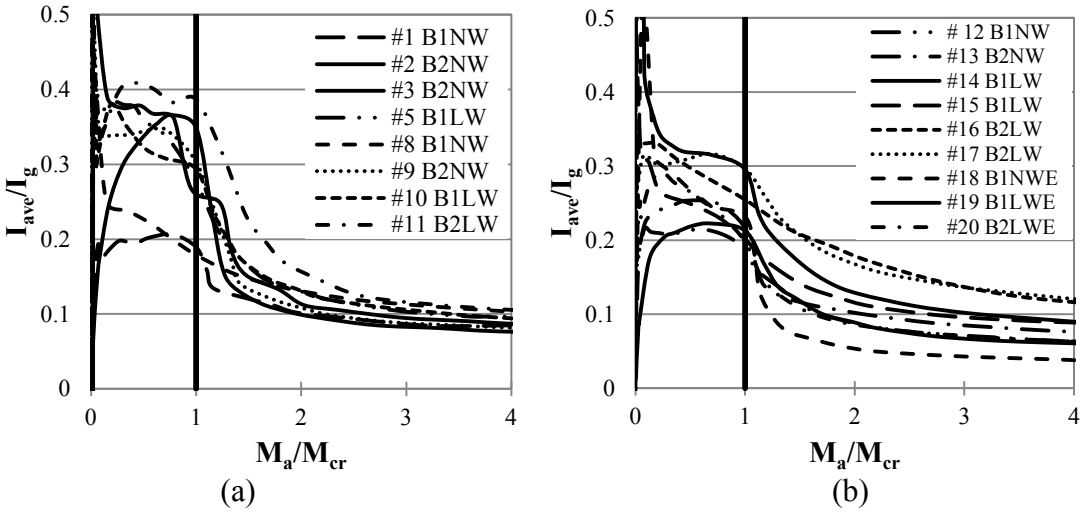

Fig. 4.5 Normalized moment of inertia: (a) 0.61 m wide panel; (b) 1.83 m wide panel

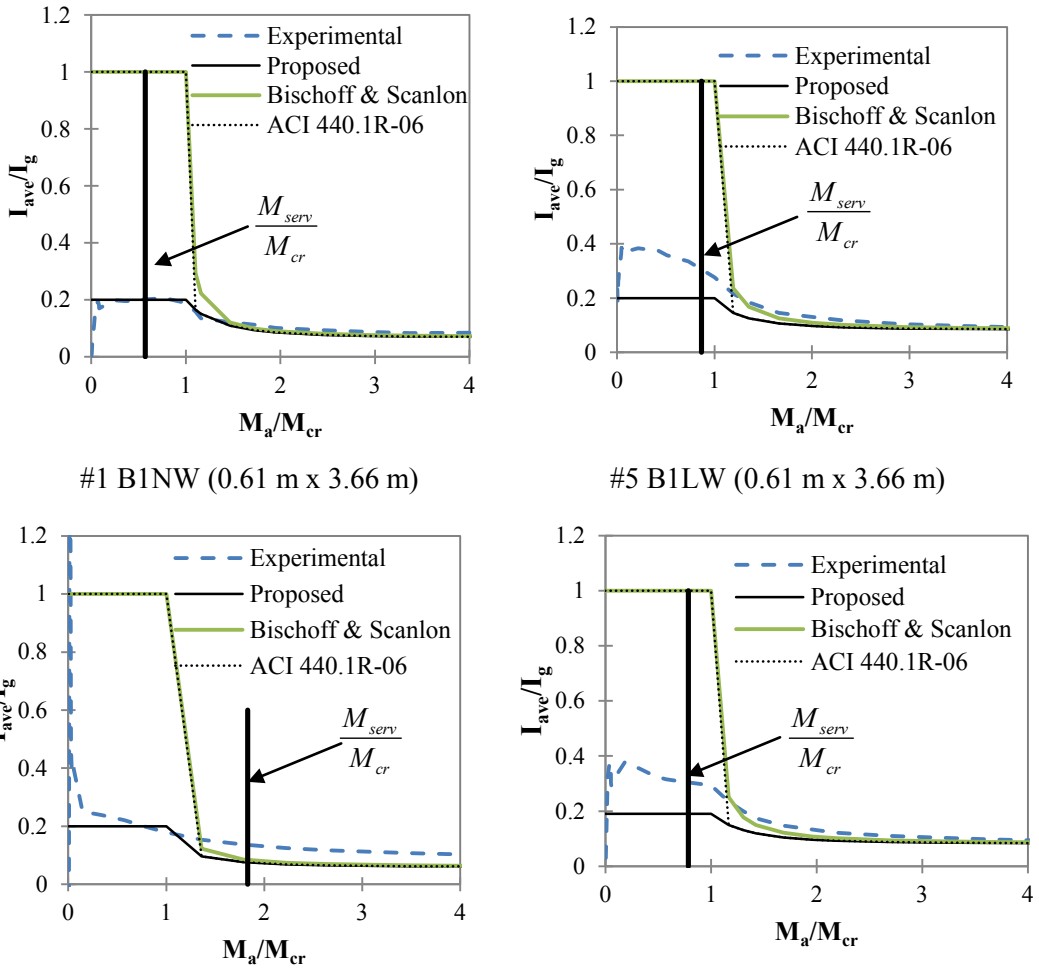

Fig. 4.6 Comparison of normalized moment of inertia for 0.61 m wide panels

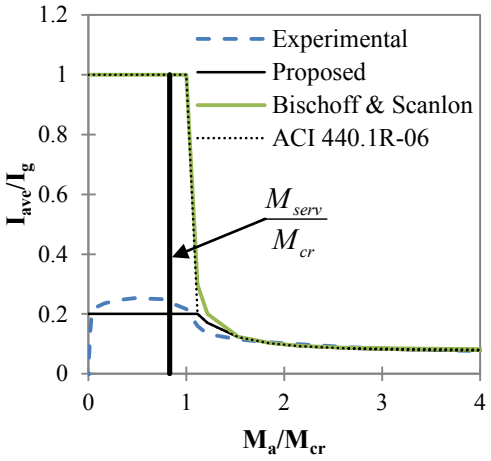

#13 B2NW (1.83 m x 3.66 m)

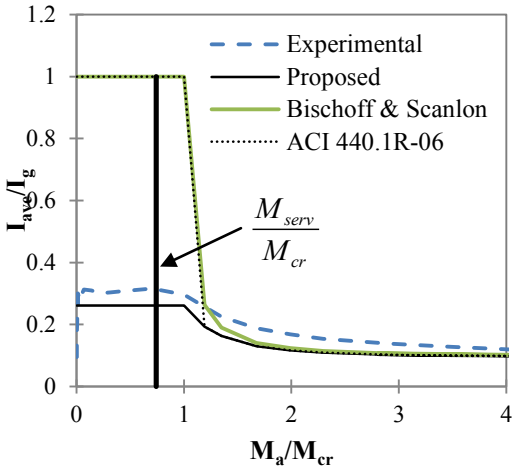

#17 B2LW (1.83 m x 3.66 m)

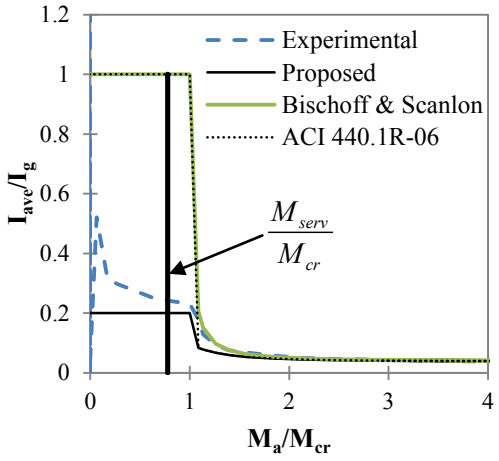

#18 B1NWE (1.83 m x 3.66 m)

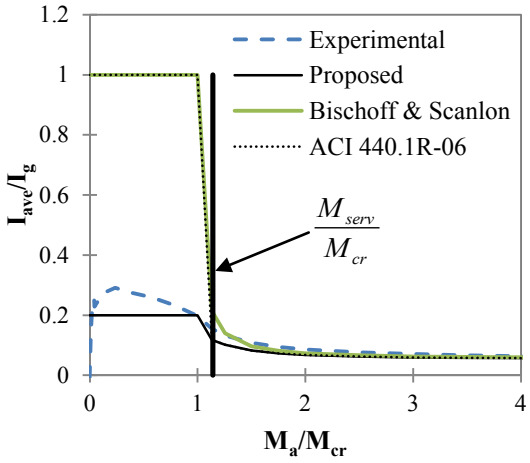

#20 B2LWE (1.83 m x 3.66 m)

Fig. 4.7 Comparison of normalized moment of inertia for 1.83 m wide panels

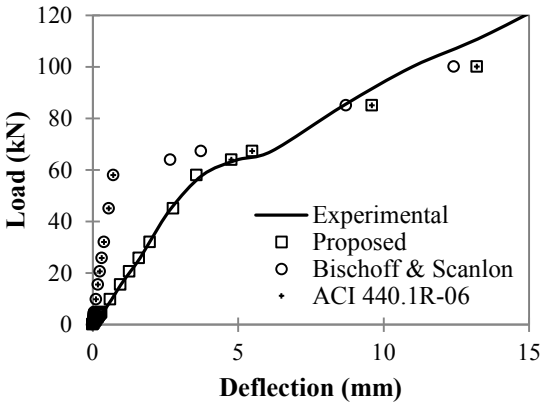

#1 B1NW (0.61 m x 3.66 m)

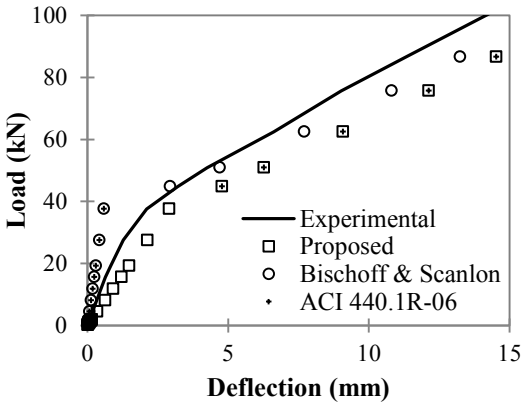

#5 B1LW (0.61 m x 3.66 m)

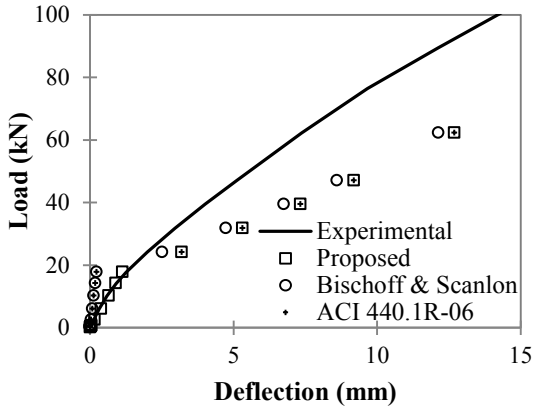

#8 B1NW (0.61 m x 4.12 m)

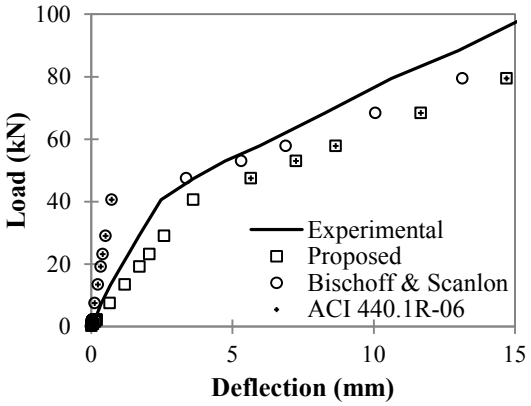

#10 B1LW (0.61 m x 4.12 m)

Fig. 4.8 Comparison of load deflection curve for 0.61 m wide panels

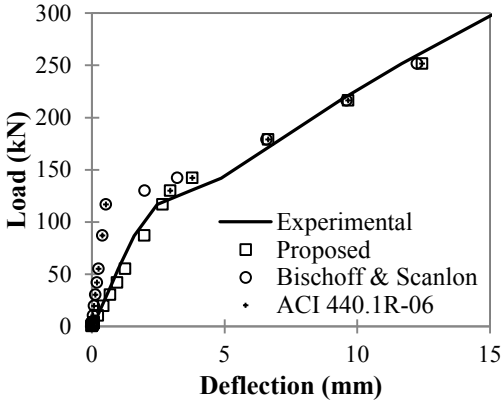

#13 B2NW (1.83 m x 3.66 m)

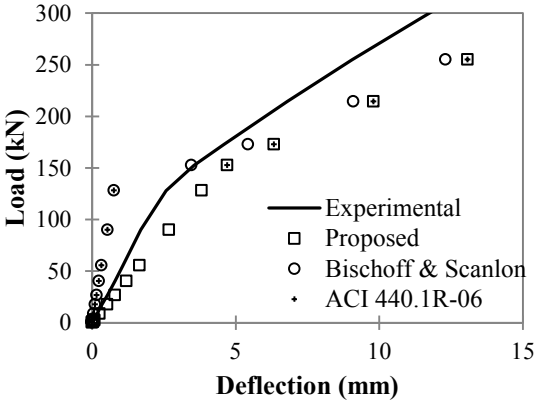

#17 B2LW (1.83 m x 3.66 m)

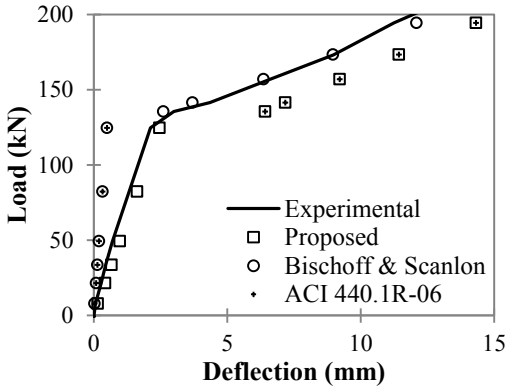

#18 B1NWE (1.83 m x 3.66 m)

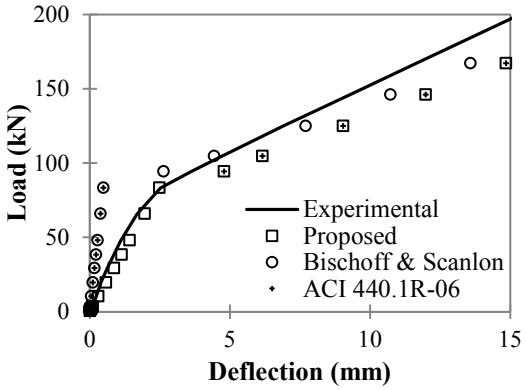

#20 B2LWE (1.83 m x 3.66 m)

Fig. 4.9 Comparison of load deflection curve for 1.83 m wide panels

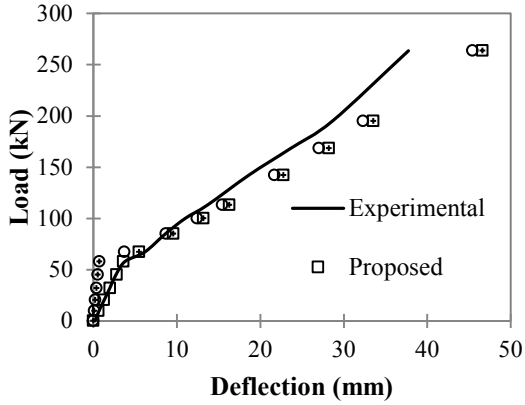

#1 B1NW (0.61 m x 3.66 m)

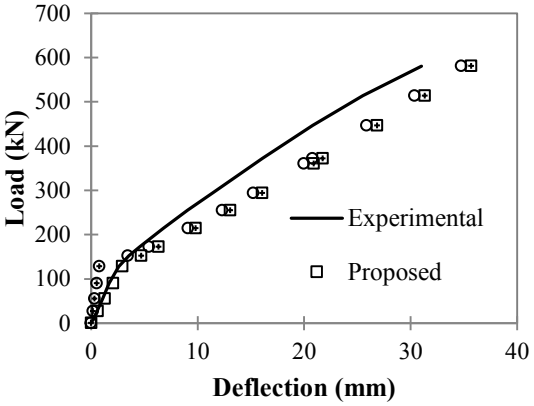

#17 B2LW (1.83 m x 3.66 m)

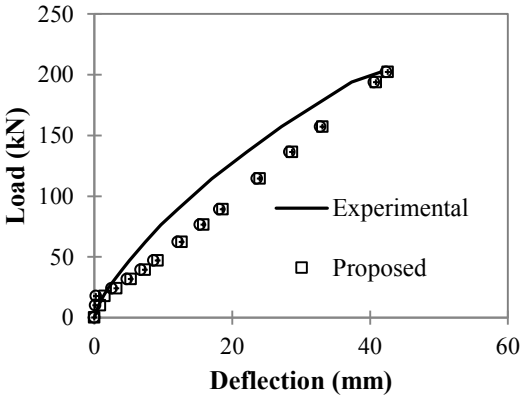

#8 B1NW (0.61 m x 4.12 m)

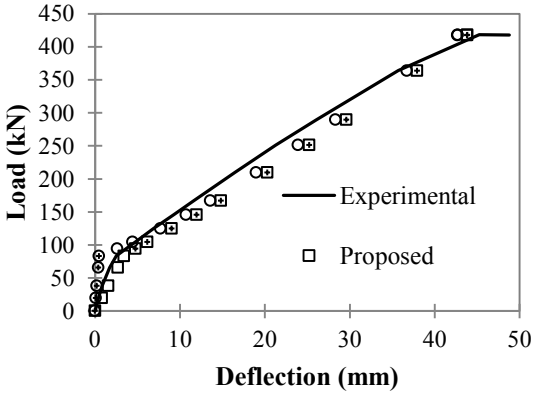

#20 B2LWE (1.83 m x 3.66 m)

Fig. 4.10 Comparison of load deflection curve up to ultimate for four panels

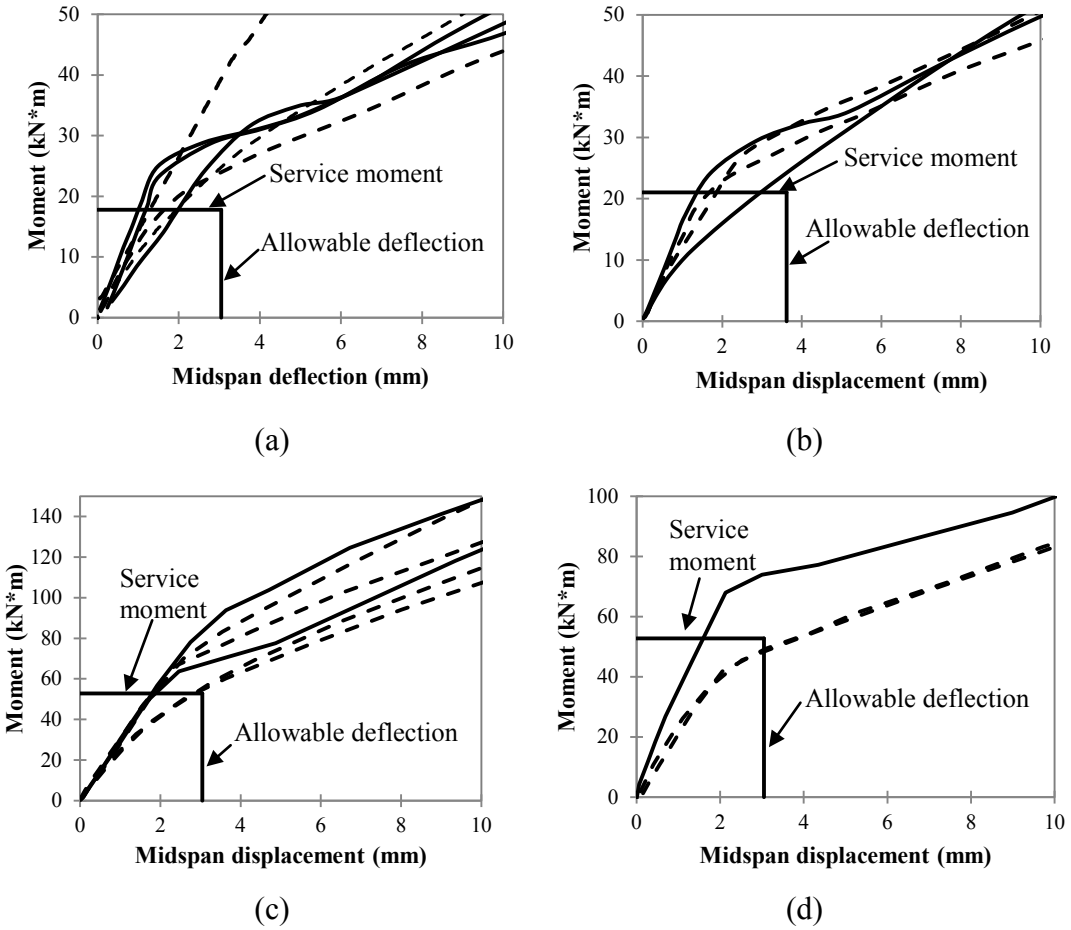

Fig. 4.11 Deflection requirement under service moment for: (a) Series A panels; (b) Series B panels; (c) Series C panels; (d) Series D panels; ── =NW; - - - =LW

5 SHEAR CAPACITY OF HIGH STRENGTH CONCRETE SLABS REINFORCED WITH GFRP BARS USING THE MODIFIED COMPRESSION FIELD THEORY

Ruifen Liu, and Chris P. Pantelides

5.1 Abstract

The ultimate shear capacity of slabs reinforced with GFRP bars is compared to the shear strength predicted using the Modified Compression Field Theory (MCFT). This paper utilizes the results of twenty tests of GFRP reinforced slabs with either lightweight or normal weight high-strength concrete. Several parameters were examined including slab width, span, thickness, and reinforcement ratio of GFRP bars. It is shown that the MCFT can predict accurately the shear strength for both high-strength normal weight and lightweight concrete slabs reinforced with GFRP bars.

5.2 Introduction

Corrosion of steel in reinforced concrete structures is one of the main factors that reduces durability and service life of bridge decks and parking garages. The use of deicing salts or the presence of a marine environment can accelerate the corrosion of steel in concrete structures; corrosion mitigation requires expensive maintenance or slab replacement. The use of Glass Fiber Reinforced Polymer (GFRP) bars as internal reinforcement is a possible solution to corrosion of steel bars. In addition to their

noncorrosive properties, GFRP bars have a higher strength, they are light and easy to handle, which makes them attractive as reinforcement for certain concrete elements, such as slabs. However, GFRP bars have different mechanical properties compared to steel; GFRP bars behave in a linear elastic manner until failure which makes concrete members reinforced with GFRP bars vulnerable to brittle failure.

Considerable research has been undertaken for both flexural and shear performance of GFRP reinforced concrete structures. Even though GFRP bars have different material properties compared to steel bars, the prediction of flexural capacity using the strain compatibility approach is still effective. However, the behavior of lightweight concrete slabs reinforced with GFRP bars without any shear reinforcement is still a topic of active research. The shear capacity prediction is essential in the design of GFRP reinforced concrete members as the ACI 440 Committee recommends such members be designed as over-reinforced, which makes them a candidate for shear-type failure[1]. There is not a substantial amount of research available for GFRP reinforced slabs constructed with high strength normal weight or lightweight concrete.

The Modified Compression Field Theory (MCFT) is an analytical model with fifteen equations which produce accurate estimates of shear strength for steel reinforced concrete members[2]. Bentz and Collins[3] reduced the MCFT equations to two, and these equations still provide accurate estimates of the shear strength of steel reinforced concrete members[4]. Hoult et al.[5] found that crack widths are affected by both a size effect and a strain effect regardless of the type of reinforcement used; they also showed that the two MCFT equations proposed by Bentz and Collins[3] work equally well in predicting the shear capacity of normal weight concrete slabs

reinforced with steel or FRP reinforcement. Sherwood et al.[6] demonstrated that the width of a member does not have a significant influence on the shear stress at failure for steel reinforced concrete members, which indicates that the MCFT could be used for both beams and slabs. Bentz et al.[7] found that despite the brittle nature of the reinforcement, FRP reinforced large concrete beams have a similar shear behavior as steel reinforced concrete beams. In this paper, a series of twenty tests are presented to investigate the influence of the slab width and depth, the slab span, the concrete compressive strength, and the type of concrete (lightweight concrete versus normal weight concrete) on the shear strength of GFRP reinforced slabs. The maximum deflection of the slabs under service loads satisfied the AASHTO Specifications in the tests for the slabs designed for flexure according to ACI 440.1R[1] guidelines, as reported elsewhere (Pantelides et al.[8]).

5.3 Experimental Program

A total of twenty slabs were tested to investigate the behavior of GFRP reinforced concrete slabs constructed with high strength normal or lightweight concrete. The construction variables included type and compressive strength of concrete, slab span and depth, slab width, and reinforcement ratio. Four series of slabs were built with different dimensions or reinforcement ratios. Figure 5.1 shows the top and bottom reinforcement for Series A and B slabs; Series A and B slabs have the same width (2 ft (610 mm)) but have different span and slab depth; Series C slabs have the same reinforcement, thickness, and span as Series A, but their width is 6 ft (1829 mm); Series D slabs have the same dimensions as Series C slabs, but a reduced GRRP reinforcement ratio which is approximately one-half that of Series C slabs.

5.4 Material Properties

The normal weight concrete used in this study was ready-mix concrete. Hard rock aggregate was used for normal weight concrete which had a size of ¾ in. (19 mm). The compressive strength of normal weight and lightweight concrete was designed as 6,000 psi (41 MPa); however, several batches were cast at different times and consequently, the concrete compressive strength for normal weight concrete at the time of testing ranged from 8,500 psi (59 MPa) to 12,600 psi (87 MPa) and for lightweight concrete from 8,100 psi (56 MPa) to 10,900 psi (75 MPa). The lightweight concrete used was sand-lightweight concrete, which had a coarse aggregate size of ½ in. (12.7 mm). The unit weight of the sand-lightweight concrete used was 123 lb/ft3 (1970 kg/m3).

The Glass Fiber Reinforced Polymer bars used for construction were #5 (ϕ16) diameter Aslan 100 bars. The tensile strength of the specific lot of GFRP bars used in these tests was 103,700 psi (715 MPa), and the modulus of elasticity 6,280,000 psi (43 GPa) as determined from tensile tests of the bars according to ACI 440.3R[9].

5.5 Test Setup and Procedure

All slabs were tested as simply supported members on two reinforced concrete beams, as shown in Fig 5.2. Elastomeric pads 6 in. (152 mm) wide and 2 in. (51 mm) thick were placed on the two supporting beams so the slabs could rotate freely near the support without coming into contract with the beams.

The load was applied using a hydraulic actuator through a 10 in. x 20 in. x 1 in. (254 mm x 508 mm x 25 mm) steel bearing plate for all slabs, which simulates the area of a double tire truck load on a bridge deck[10]. The load was applied as a series of

half-sine downward cycles of increasing amplitude without stress reversals. The load application was displacement controlled, with a slow constant loading rate of 0.2 in./min (5 mm/min). The loading scheme was intended to simulate the repeated truck loading applied to the slab of a precast concrete bridge deck.

5.6 Test Results

During testing, all slabs developed flexural cracks at lower load levels and additional diagonal cracks at higher loads. Ultimately the slabs failed in a diagonal tension failure mode, as shown in Fig 5.3. After formation of the critical diagonal crack near one of the two supports, the concrete crushed on the compression face of the slabs. All slabs failed with the same failure mode regardless of concrete type (normal weight concrete or lightweight concrete), slab dimensions, or amount of reinforcement. In a small number of tests, a few GFRP bars in the top mat near the outer edges of the slab snapped and sheared off after the ultimate load was reached, shortly before the ultimate deflection, as shown in Fig 5.3; this occurred after the concrete cover had spalled off and the bars were exposed, and was the result of the GFRP bars trying to carry the compression forces arising from the applied load. The GFRP bars in the bottom mat did not fracture in any of the tests even though they experienced significant tensile strain and deformation. The concrete compressive strength at the time of testing, the actual reinforcement ratio, the balanced reinforcement ratio, and the experimental shear capacity are shown in Tables 5.1-5.4.

5.7 Shear Strength Prediction using the Modified Compression Field Theory

To predict the shear strength of the slabs, the Modified Compression Field Theory (MCFT) is used. The MCFT assumes that the ultimate shear strength of concrete members is related to the crack width at shear failure, which is controlled by the strain effect and the size effect. The strain effect indicates that the larger the longitudinal strain, the wider the cracks, and the lower the aggregate interlock and ultimate shear strength. The size effect means that if two geometrically similar beams or slabs with different depths are subjected to the same shear stresses, the deeper the beam, the wider the crack width, and the lower the ultimate shear strength; the size effect is influenced by the aggregate size. Two simplified equations were used for shear capacity predictions. The first equation is a first-order linear approximation, which was initially developed for steel reinforced concrete sections with the value of strain at failure (ε_x) being less than 0.1%, as shown below (Houlet et al[5]):

$$V_c = \left[\frac{0.40}{(1+1500\varepsilon_x)}\right]\left[\frac{1300}{(1000+s_{xe})}\right]\sqrt{f_c'}\, b_w d_v \tag{5.1}$$

where ε_x = longitudinal strain at mid-depth of the section at predicted shear failure (mm/mm); s_{xe} = effective crack spacing (mm); f_c' = concrete compressive strength (MPa); b_w = web width (mm); d_v = effective shear depth to be taken as 0.9 d (mm), where d = distance from extreme compression fiber to the middle of the bottom FRP bar.

The size effect term for members without stirrups is given by Hoult et al.[5] as:

$$s_{xe} = \frac{31.5d}{16 + a_g} \geq 0.77d \tag{5.2}$$

where a_g = maximum aggregate size (mm). For high strength normal weight concrete (compressive strength above 10,000 psi (70 MPa)) or for lightweight concrete, the aggregate size should be taken as zero because the cracks tend to pass through the aggregate particles; this was confirmed in the present tests in which both the normal weight and lightweight concrete were high strength. To avoid a discontinuity in strength predictions, for normal weight concrete, it is suggested that the aggregate size be linearly reduced from the specified size to zero as the concrete strength increases from 8,700 psi (60 MPa) to 10,000 psi (70 MPa) (Hoult et al.[5]).

The strain effect is included via the strain term ε_x; for members not subjected to axial load that are not prestressed, the strain term is given by Hoult et al.[5] as:

$$\varepsilon_x = \frac{M_f / d_v + V_f}{2E_r A_r} \tag{5.3}$$

where E_r = elastic modulus of the reinforcement (GPa); A_r = area of the longitudinal reinforcement (mm^2); M_r and V_r are the bending moment and shear force at the critical section for shear, respectively, which is evaluated at a distance d away from the maximum moment location.

When FRP reinforcement is used, typically higher longitudinal strains will be developed compared to steel reinforcement. A second-order approximation to the MCFT theoretical diagonal crack width calculation leads to the shear capacity prediction equation as (Hoult et al.[5]):

$$V_c = \left[\frac{0.30}{0.5 + (1000\varepsilon_x + 0.15)^{0.7}}\right]\left[\frac{1300}{(1000 + s_{ze})}\right]\sqrt{f_c'}\,b_w d_v \qquad (5.4)$$

The experimental shear strength of the specimens was compared to Eq. (5.1) and Eq. (5.4). As shown in Fig 5.4, the shear cracks pass through the coarse aggregate even though some of the normal weight concrete compressive strength was slightly less than 10,000 psi (70 MPa); thus, the aggregate size was considered to be zero in the shear prediction equations for all specimens. The predicted shear capacity of the slabs using the first-order Eq. (5.1) (V_{pred1}) and the second-order Eq. 5.14 (V_{pred2}) are shown in Tables 5.1-5.4. A comparison of the ratios of tested to predicted shear strength versus concrete compressive strength is shown in Figs 5.5 and 5.6 for the first-order and second-order MCFT predictions, respectively.

Considering Fig 5.5, the average ratio of experimental shear strength to predicted shear strength is 1.97, with a coefficient of variation (COV) of 10.6%; in Fig 5.6, the average ratio of experimental shear strength to predicted shear strength is 1.46, with a coefficient of variation of 10.7%. The results show that both equations predict conservative estimates of the shear strength; the second-order equation predicts results that are closer to the experimentally obtained shear capacity. This is expected because of the higher longitudinal strain in the GFRP bars. However, the ratio of experimental shear strength to predicted shear strength for both the first-order

Eq. (5.1) and the second-order Eq. (5.4) is 43% and 27% higher, respectively, than the beams or slabs in the study by Hoult et al.[5]. This may be caused by the high compressive strength of the concrete and the fact that only GFRP reinforced concrete specimens were included in this research, whereas the study by Hoult et al.[5] considered steel, GFRP, CFRP, and AFRP reinforced specimens.

Comparing the experimental to predicted shear strength ratios in Figs 5.5 and 5.6, respectively, it is shown that normal weight concrete slabs generally have higher ratios of experimental shear strength to predicted shear strength than lightweight concrete slabs. In Fig 5.5 for the first-order expression, the average ratio of experimental to predicted shear strength for normal weight concrete slabs is 2.14, with a COV of 9.2%; the average ratio for lightweight concrete slabs is 1.86, with a COV of 6.1%; in Fig 5.6 for the second-order expression, the average ratio for normal weight concrete slabs is 1.58 with a COV of 9.9%; the average ratio for lightweight concrete slabs is 1.38 with a COV of 8.1%. In both the first-order and second-order MCFT predictions, the lightweight concrete slabs have an experimental to predicted shear strength ratio equal to 87% of the normal weight concrete slabs. This shows that even though the predictions are conservative for lightweight concrete, they are less conservative than the predictions for normal weight concrete. Thus, the density of the concrete needs to be considered in predictions for shear strength.

Figures 5.7 and 5.8 show the experimental shear strength normalized by the shear predictions Eq. (5.1) and Eq. (5.4), respectively, using the actual strain in the GFRP bars measured during the tests. In Fig 5.7 for the first-order MCFT expression, the average ratio for normal weight concrete slabs is 3.05, with a COV of 17.3%; the average ratio for lightweight concrete slabs is 2.54, with a COV of 12.0%. In Fig 5.8,

for the second-order MCFT expression, the average ratio for normal weight concrete slabs is 1.62 with a COV of 15.7%; the average ratio for lightweight concrete slabs is 1.37 with a COV of 9.7%. In both the first-order and second-order MCFT predictions, the lightweight concrete slabs have a shear ratio of 83% to 85% of the normal weight concrete slabs, respectively. Comparing the results of Fig 5.5 to Fig 5.7, and Fig. 5.6 to Fig 5.8, the different ratios of experimental shear strength to predicted shear strength demonstrate that Eq. (5.3) slightly under-predicts the actual strain of the tested concrete slabs in this research.

Tables 5.5 to 5.8 show the measured and predicted strain using the first-order (ε_{pred1}) and second-order (ε_{pred2}) approximations at the mid-depth of the slabs. The measured mid-depth strain is defined as the maximum strain measured at the bottom longitudinal GFRP bars divided by two. The overall average ratio of the first-order MCFT expression predicted to measured strain is 60.5% for normal weight concrete slabs, and 61.6% for lightweight concrete slabs. In addition, the measured to predicted strain ratio is higher for slabs with a longer span (Series B) and slabs with a smaller reinforcement ratio (Series D) for both the first-order and second-order equations. The overall average ratio of the second-order MCFT expression predicted to measured strain is 82.0% for normal weight concrete slabs, and 83.1% for lightweight concrete slabs. It is shown that the second-order equation predicts more accurately the mid-depth strain than the first-order equation; both the first-order and second-order equations predict similar strains for normal weight and lightweight concrete.

5.8 Shear Design using the MCFT

It is interesting to examine the conservatism of the two MCFT equations from the designer's perspective. The assumptions used in the design of normal weight and lightweight concrete slabs are as follows: the design concrete compressive strength is 60,000 psi (41 MPa); the GFRP bar modulus of elasticity is 5,920,000 psi (40.8 GPa), and the ultimate tensile strength is 95,000 psi (655 MPa). Using the design approach recommended by Hoult et al.[5] with strain compatibility analysis, the predicted shear strength of the concrete slabs is found to be conservative. The resulting average experimental to predicted shear strength ratio is 3.57 and 3.54 for normal weight and lightweight concrete slabs, respectively, when using the first-order MCFT prediction; the COV is 10% and 7.4% for normal weight and lightweight concrete slabs, respectively. Using the second-order MCFT prediction, the ratio of experimental to predicted shear strength is 1.86 and 1.85 for normal weight and lightweight concrete slabs, respectively; the COV is 11.3% and 8.1%, respectively. The conservatism of the second-order MCFT in the design process is found to be slightly higher than the experimental predicted ratios observed in the tests. However, this is desirable in actual design and thus the design approach recommended by Hoult et al.[5] produces acceptable results.

To compare the results of the GFRP reinforced slabs tested in the present study, in particular those cast with lightweight concrete, to existing data for normal weight concrete slabs reinforced with GFRP bars, a comparison is made of the present test results to the database provided in Hoult et al.[5], which includes references[11-20]. Additional studies of normal weight concrete specimens reinforced with GFRP bars (references[7, 21-23]) were included in the present study to create an updated database.

All specimens in the updated database are normal weight concrete beams or slabs reinforced with GFRP bars without any transverse reinforcement, which failed in one-way shear. Figures 5.9 and 5.10 show the strain effect using the first-order and second-order MCFT equations for the GFRP reinforced members using the updated database, respectively. The longitudinal strain at mid-depth is the strain predicted using the MCFT, and the shear strength is normalized, so only the strain effect is shown. Figures 5.9 and 5.10 show that lightweight concrete slabs follow the same trend as normal weight concrete beams or slabs, which indicates that the strain effect is unchanged and could be predicted using the MCFT for lightweight concrete slabs.

Figure 5.11 shows the size effect for normal weight and lightweight concrete members reinforced with GFRP bars. The size effect is derived using the tested shear strength normalized by the strain effect and the quantity $\sqrt{f_c'}b_w d_v$. Figure 5.11 shows that lightweight concrete slabs follow the same trend as normal weight concrete beams or slabs, which indicates that the size effect is unchanged and could be predicted using the MCFT for lightweight concrete slabs.

The size effect and the strain effect do not exhibit significant differences between normal weight concrete and lightweight concrete beams or slabs. This is also verified by comparing the predicted and experimental shear strength results of all beams or slabs in the updated experimental database. For the first-order MCFT equation, the average ratio of experimental to predicted shear strength is 1.59 and 1.84 for normal weight concrete and lightweight concrete members, respectively; the COV is 35.0% and 5.9% for normal weight and lightweight concrete members, respectively. The normalized shear strength versus concrete compressive strength using the second-order MCFT is shown in Fig 5.12. For the second-order MCFT

equation, the average ratio of experimental shear strength to predicted shear strength is 1.27 and 1.37, and the COV is 27.2% and 5.8% for normal weight and lightweight concrete members, respectively. It is noted that the ratio of experimental to predicted shear strength is lower for normal weight concrete beams or slabs than the ratio for lightweight concrete slabs when the ratios are compared with the updated database; these results are the opposite of what was found for the specimens tested in the present study. However, this is caused by the member depth effect. The yellow diamond in Fig. 5.12 represent slab specimens collected from other research. Comparing the experimental to predicted shear strength ratio, it is noted that slab specimens have a higher ratio than the beam specimens. Considering only the slabs collected from other research and specimens from the current research, the average experimental ratio for normal weight concrete slabs is 1.56 and 1.37 for lightweight concrete slabs using the second-order equation. Lightweight concrete specimens have a ratio 88% of normal weight concrete slabs, which follows the same trend as the specimens tested in the current research. The comparison for tested slab specimens indicates that a reduction factor is needed for the use of lightweight concrete members. The reduction factor generally used for sand lightweight concrete reinforced with steel 0.85 seems appropriate for GFRP reinforced sand-lightweight concrete members.

The size effect factor used in Eq. (5.1) and Eq. (5.4) was developed based on steel reinforced concrete members, which has a maximum strain at mid-depth of the member of 0.001 in./in. (0.001 mm/mm) (Bentz and Collins[3]). The measured average strain in the bottom GFRP bars in the present research at midspan is 0.012 in./in. (0.012 mm/mm), thus the mid-depth strain is 0.006 in./in. (0.006 mm/mm). The

measured strain in the tested slabs is six times the maximum strain used to develop the size effect factor. Figure 5.9 in Bentz and Collins[3] was re-developed and higher strain data curves were added, as shown in Fig 5.13. In Fig 5.13, six of the curves represent the assumed mid-depth strain from 0.001 in./in. (0.001 mm/mm) to 0.006 in./in. (0.006 mm/mm). A new curve shown in Fig 5.13 was chosen to compare with the one in the MCFT; this curve lies close to the middle of the data from the MCFT analyses across the size range and is similar to the size factor used in Eq. (5.1) and Eq. (5.4). The size effect factor intended to compare with the MCFT is obtained as:

$$\frac{1450}{1000+1.5s_{ze}} \tag{5.5}$$

Using Eq. (5.5) to replace the size effect factor in Eq. (5.1) and Eq. (5.4), the prediction results are shown in Table 5.9. Table 5.9 shows that using Eq. (5.5), the ratio both for first-order and second-order experimental to predicted shear strength improved slightly; predictions were closer to the experimental results. However, note that the size effect factor in Eq. (5.1) and Eq. (5.4) could be used for both steel and FRP reinforcement, and the ratio of experimental to predicted shear strength improved only slightly using Eq. (5.5). This indicates that even if the strain achieved in GFRP reinforced concrete members is higher than that in steel reinforced concrete members, the size effect factor in Eq. (5.1) and Eq. (5.4) is sufficiently accurate for the shear capacity prediction of GFRP reinforced concrete members.

5.9 Conclusions

This paper presents experimental results for twenty Glass Fiber Reinforced Polymer (GFRP) reinforced concrete slabs, cast with either normal or lightweight concrete, and compares the shear strength obtained in the tests to the Modified Compression Field Theory (MCFT). The following conclusions can be made:

1. The second-order MCFT equation predicts the shear strength of normal weight and lightweight concrete slabs reinforced with GFRP bars accurately. The first-order MCFT equation is more conservative compared to the second-order equation. Lightweight concrete slabs, which failed in one-way shear, show the same size and strain effects as normal weight concrete slabs or beams reinforced with GFRP bars.
2. The average ratio of predicted to measured mid-depth strain was 60% for both normal weight and lightweight concrete slabs using the first-order MCFT equation; the average ratio was 82% for both normal weight and lightweight concrete slabs using the second-order MCFT equation.
3. Using the strains from flexural design for the first-order and second-order MCFT equations results in conservative designs since the actual concrete compressive strength and guaranteed GFRP properties are generally higher than the design values.
4. A reduction factor is needed for the use of lightweight concrete when GFRP is used as reinforcement. The ratio of 0.85 which is used for steel reinforced concrete members seems appropriate for GFRP reinforced concrete members.
5. Even though the size effect factor in the original MCFT was developed based on strains in steel reinforced concrete members, it is still accurate for the shear

prediction of GFRP reinforced concrete members which achieve much higher strains.

6. Both normal weight and lightweight concrete slabs tested in this study were constructed with high strength concrete. Additional results for normal strength lightweight concrete slabs are required to validate the findings of the present study.

5.10 Acknowledgments

The research reported in this paper was supported by the Utah DOT and the Expanded Shale Clay and Slate Institute. The authors acknowledge the contribution of Hughes Bros Inc., Utelite Corporation, and Hanson Structural Precast. The authors acknowledge the assistance of Professor L. D. Reaveley, M. Bryant, B. T. Besser, and C. A. Burningham of the University of Utah in the experimental portion of the research. The authors are grateful to Professor N. A. Hoult of Queen's University and Professor E. C. Bentz of the University of Toronto for making their database available to the authors.

5.11 Notation

a_g = maximum aggregate size in *mm*;

A_r = area of the longitudinal reinforcement;

b_w = web width;

COV_1 = coefficient of variation for first-order MCFT;

COV_2 = coefficient of variation for second-order MCFT;

d = distance from extreme compression fiber to the middle of the bottom FRP bar;

d_v = effective shear depth to be taken as 0.9 d ;

E_r = elastic modulus of the reinforcement;

$f_c^{'}$ = concrete compressive strength;

M_f = bending moment at the critical section for shear, a distance d away from the maximum moment location;

s_{xe} = effective crack spacing;

V_c = predicted shear strength;

$V_{\exp}$ = experimental shear strength;

V_f = shear force at the critical section for shear, a distance d away from the maximum moment location;

V_{pred1} = predicted shear capacity using first-order MCFT;

V_{pred2} = predicted shear capacity using second-order MCFT;

ε_x = longitudinal strain at mid-depth at predicted shear failure;

ε_{m_ave} = average longitudinal strain at mid-depth at shear failure;

ε_{pred1} = predicted longitudinal strain at mid-depth at shear failure using first-order MCFT;

ε_{pred2} = predicted longitudinal strain at mid-depth at shear failure using second-order MCFT;

ρ_b = FRP reinforcement ratio producing balanced strain conditions;

ρ_f = FRP reinforcement ratio;

5.12 References

1. American Concrete Institute, (ACI 440.1R-06). 2006. Guide for the Design and Construction of Structural concrete Reinforced with FRP Bars. American Concrete Institute, Farmington Hills, Mich., 44 pp.

2. Vecchio, F. J., and Collins, M. P. 1986. The Modified Compression Field Theory for Reinforced Concrete Elements Subjected to Shear. ACI Structural Journal, Proceedings, V. 83, No. 2, pp. 219-231.

3. Bentz, E. C., and Collins, M. P. 2006. Development of the 2004 CSA A23.3 shear provisions for reinforced concrete. Canadian Journal of Civil Engineering, V. 33, No. 5, pp. 521-534.

4. Sherwood, E. G., Bentz, E. C., and Collins, M.P. 2007. The effect of aggregate size on the beam-shear strength of thick slabs. ACI Structural Journal, V. 104, No. 2, pp. 180-190.

5. Hoult, N. A., Sherwood, E. G., Bentz, E. C. and Collins, M. P. 2008. Does the Use of FRP Reinforcement Change the One-Way Shear Behavior of Reinforced Concrete Slabs? Journal of Composites for Construction, V. 12, No. 2, pp. 125-133.

6. Sherwood, E. G., Lubell, A. S., Bentz, E. C., and Collins, M. P. 2006. One-way shear strength of thick slabs and wide beams. ACI Structural Journal, V. 103, No. 6, pp. 794-802.

7. Bentz, E. C., Massam, L., and Collins, M. P. 2010. Shear strength of large concrete members with FRP reinforcement. Journal of Composites for Construction, V. 14, No. 6, pp. 637-646.

8. Pantelides, C. P., Liu, R. and Reaveley, L. D. 2011. Lightweight Concrete Precast Bridge Deck Panels Reinforced with GFRP Bars. ACI Structural Journal, submitted.

9. American Concrete Institute (ACI 440.3R). 2004. Guide Test Methods for Fiber-Reinforced Polymers (FRPs) for Reinforcing or Strengthening Concrete Structures. American Concrete Institute, Farmington Hills, Mich., 40 pp.

10. American Association of State Highway and Transportation Officials (AASHTO). 2007. AASHTO LRFD Bridge Design Specifications, 4th Edition, AASHTO, Washington, D.C., 1526 pp.

11. Alkhrdaji, T., Wideman, M., Belarbi, A., and Nanni, A. 2001. Shear strength of RC beams and slabs. Proceedings, Composites in Construction, pp. 409-414.
12. Ashour, A. F. 2006. Flexural and shear capacities of concrete beams reinforced with GFRP bars. Construction and Building Materials, V. 20, No. 10, pp. 1005-1015.

13. Deitz, D. H., Harik, I. E., and Gersund, H. 1999. One-way slabs reinforced with glass fiber reinforced polymer reinforcing bars. Proceedings, 4th Int. Symp. FRPRCS4, Baltimore, Marryland, pp. 279-286.

14. El-Sayed, A. K., El-Salakawy, E., and Benmokrane, B. 2005. Shear strength of one-way concrete slabs reinforced with fiber-reinforced polymer composite bars. Journal of Composites for Constructions, V. 9, No. 2, pp. 147-157.

15. El-Sayed, A. K., El-Salakawy, E., and Benmokrane, B. 2006. Shear strength of FRP-reinforced concrete beams without transverse reinforcement. ACI Structural Journal, V. 103, No. 2, pp. 235-243.

16. El-Sayed, A. K., El-Salakawy, E., and Benmokrane, B. 2006. Shear capacity of high-strength concrete beams reinforced with FRP bars. ACI Structural Journal, V. 103, No. 3, pp. 383-389.

17. Gross, S. P., Yost, J. R., Dinehart, D. W., Svensen, E., and Liu, N. 2003. Shear strength of normal and high strength concrete beams reinforced with GFRP reinforcing bars. Proceedings, International Conference on High Performance Materials in Bridges, ASCE, pp. 426-437.

18. Tariq, M., and Newhook, J. P. 2003. Shear testing of FRP reinforced concrete without transverse reinforcement. Proceedings, Annual Conference of the Canadian Society for Civil Engineering, Moncton, Canada, Paper No. GCF-340-1-GCF340-10.

19. Tureyen, A., and Frosch, R. J. 2002. Shear tests of FRP-reinforced beams without stirrups. ACI Structural Journal, V. 99, No. 4, pp. 427-434.

20. Yost, J., R., Gross, S. P., and Dinehart, D. W. 2001. Shear strength of normal strength concrete beams reinforced with deformed GFRP bars. Journal of Composites for Construction, V. 5, No. 4, pp. 268-275.

21. Alam, M. S., and Hussein, A. 2009. Shear strength of concrete beams reinforced with Glass Fibre Reinforced Polymer (GFRP) bars. Proceedings of 9th International Symposium, FRPRCS-9, Sydney, Australia.

22. Jang, H., Kim, M., Cho, J., and Kim, C. 2009. “Concrete shear strength of beams reinforced with FRP bars according to flexural reinforcement ratio and

shear span to depth ratio." Proceedings of 9th International Symposium, FRPRCS-9, Sydney, Australia.
23. Swamy, N. and Aburawi, M. 1997. Structural implications of using GFRP bars as concrete reinforcement. Proceedings of 3rd International Symposium, FRPRCS-3, Hokaido, Jampan,Vol. 2, pp. 503-510.

Table 5.1 Series A slabs: 2 ft wide x 9 ¼ in. thick with 8 ft span

Specimen Number	f_c', psi	ρ_f, %	ρ_b, %	V_{exp}, kip	V_{pred1}, kip	V_{pred2}, kip
#1 B1NW	10,370	0.94	0.95	30.6	12.7	17.1
#2 B2NW	12,650	0.94	1.16	30.2	13.4	18.2
#3 B2NW	8,760	0.94	0.80	27.6	12.2	16.2
#4 B1LW	9,090	0.94	0.83	25.1	12.3	16.4
#5 B1LW	10,930	0.94	1.00	22.9	12.9	17.4
#6 B2LW	8,700	0.94	0.80	23.0	12.1	12.2
#7 B1LW*	9,900	0.94	0.91	27.4	15.1	19.9

*For this specimen the span was 6.7 ft; 1 ft = 304.8 mm; 1 psi = 6.895 kPa; 1 kip = 4.448 kN

Table 5.2 Series B slabs: 2 ft wide x 10 ¾ in. thick with 9 ft-6 in. span

Specimen Number	f_c', psi	ρ_f, %	ρ_b, %	V_{exp}, kip	V_{pred1}, kip	V_{pred2}, kip
#8 B1NW	11,420	0.79	1.05	23.8	13.0	19.0
#9 B2NW	8,840	0.79	0.81	27.7	13.0	17.5
#10 B1LW	9,080	0.79	0.83	22.0	13.1	17.7
#11 B2LW	8,700	0.79	0.80	23.3	13.0	17.5

1 psi = 6.895 kPa; 1 kip = 4.448 kN

Table 5.3 Series C slabs: 6 ft wide x 9 ¼ in. thick with 8 ft span

Specimen Number	f_c', psi	ρ_f, %	ρ_b, %	V_{exp}, kip	V_{pred1}, kip	V_{pred2}, kip
#12 B1NW	12,130	0.96	1.11	87.6	39.3	52.9
#13 B2NW	8,510	0.96	0.78	72.7	35.7	47.3
#14 B1LW	9,080	0.96	0.83	61.3	36.3	48.3
#15 B1LW	9,080	0.96	0.83	64.8	36.3	48.3
#16 B2LW	8,250	0.96	0.76	66.8	35.4	46.9
#17 B2LW	8,060	0.96	0.74	67.6	35.1	46.5

1 psi = 6.895 kPa; 1 kip = 4.448 kN

Table 5.4 Series D slabs: 6 ft wide x 9 ¼ in. thick with 8 ft span

Specimen Number	f_c', psi	ρ_f, %	ρ_b, %	V_{exp}, kip	V_{pred1}, kip	V_{pred2}, kip
#18 B1NWE	12,130	0.54	1.11	62.1	29.9	42.5
#19 B1LWE	9,080	0.54	0.83	55.6	27.7	38.8
#20 B2LWE	8,060	0.54	0.74	49.3	26.8	37.4

1 psi = 6.895 kPa; 1 kip = 4.448 kN

Table 5.5 Series A slabs mid-depth strain

Specimen Number	Measured average strain ε_{m_ave}, %	1st order predicted strain ε_{pred1}, %	$\varepsilon_{pred1}/\varepsilon_{m\_ave}$	2nd order predicted strain ε_{pred2}, %	$\varepsilon_{pred2}/\varepsilon_{m\_ave}$
#1 B1NW	0.61	0.36	0.59	0.48	0.79
#2 B2NW	0.60	0.38	0.63	0.51	0.85
#3 B2NW	0.59	0.34	0.59	0.46	0.78
#4 B1LW	n.d.	0.35	n.d.	0.46	n.d.
#5 B1LW	0.59	0.37	0.62	0.49	0.84
#6 B2LW	0.60	0.34	0.57	0.46	0.76
#7 B1LW*	n.d.	0.31	n.d.	0.41	n.d.

*For this specimen the span was 6.7 ft; 1 ft = 304.8 mm; n.d. = no data

Table 5.6 Series B slabs mid-depth strain

Specimen Number	Measured average strain ε_{m_ave}, %	1st order predicted strain ε_{pred1}, %	$\varepsilon_{pred1}/\varepsilon_{m\_ave}$	2nd order predicted strain ε_{pred2}, %	$\varepsilon_{pred2}/\varepsilon_{m\_ave}$
#8 B1NW	0.55	0.39	0.72	0.54	0.98
#9 B2NW	0.66	0.37	0.56	0.50	0.75
#10 B1LW	0.56	0.37	0.66	0.50	0.89
#11 B2LW	0.55	0.37	0.66	0.39	0.89

Table 5.7 Series C slabs mid-depth strain

Specimen Number	Measured average strain ε_{m_ave}, %	1st order predicted strain ε_{pred1}, %	$\varepsilon_{pred1}/\varepsilon_{m\_ave}$	2nd order predicted strain ε_{pred2}, %	$\varepsilon_{pred2}/\varepsilon_{m\_ave}$
#12 B1NW	0.79	0.37	0.47	0.50	0.63
#13 B2NW	0.58	0.34	0.58	0.45	0.78
#14 B1LW	0.70	0.34	0.49	0.46	0.65
#15 B1LW	0.60	0.34	0.57	0.46	0.76
#16 B2LW	0.45	0.33	0.74	0.44	0.98
#17 B2LW	0.63	0.33	0.53	0.44	0.70

Table 5.8 Series D slabs mid-depth strain

Specimen Number	Measured average strain ε_{m_ave}, %	1st order predicted strain ε_{pred1}, %	$\varepsilon_{pred1}/\varepsilon_{m\_ave}$	2nd order predicted strain ε_{pred2}, %	$\varepsilon_{pred2}/\varepsilon_{m\_ave}$
#18 B1NWE	0.72	0.51	0.70	0.72	1.00
#19 B1LWE	0.79	0.47	0.60	0.65	0.84
#20 B2LWE	0.64	0.46	0.72	0.64	1.00

Table 5.9 Comparison results for different size effect factor

Size effect factor	Concrete type	V_{exp}/V_{pre1}	COV_1	V_{exp}/V_{pre2}	COV_2
$\frac{1300}{1000+s_{ze}}$ Eq. (5.1)	NW	1.59	0.35	1.27	0.27
	LW	1.84	0.06	1.37	0.06
$\frac{1450}{1000+1.5s_{ze}}$ Eq. (5.5)	NW	1.52	0.20	1.22	0.20
	LW	1.70	0.06	1.29	0.06
	$NW_{(5)}/NW_{(1)}$	0.95	0.57	0.96	0.62
	$LW_{(5)}/LW_{(1)}$	0.92	0.97	0.94	1.01

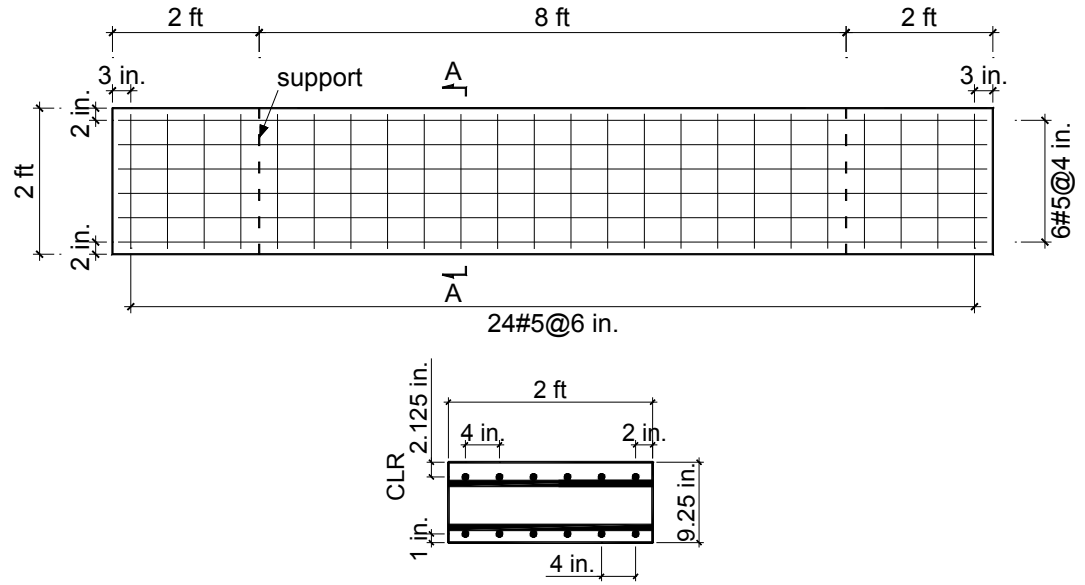

Series A slabs

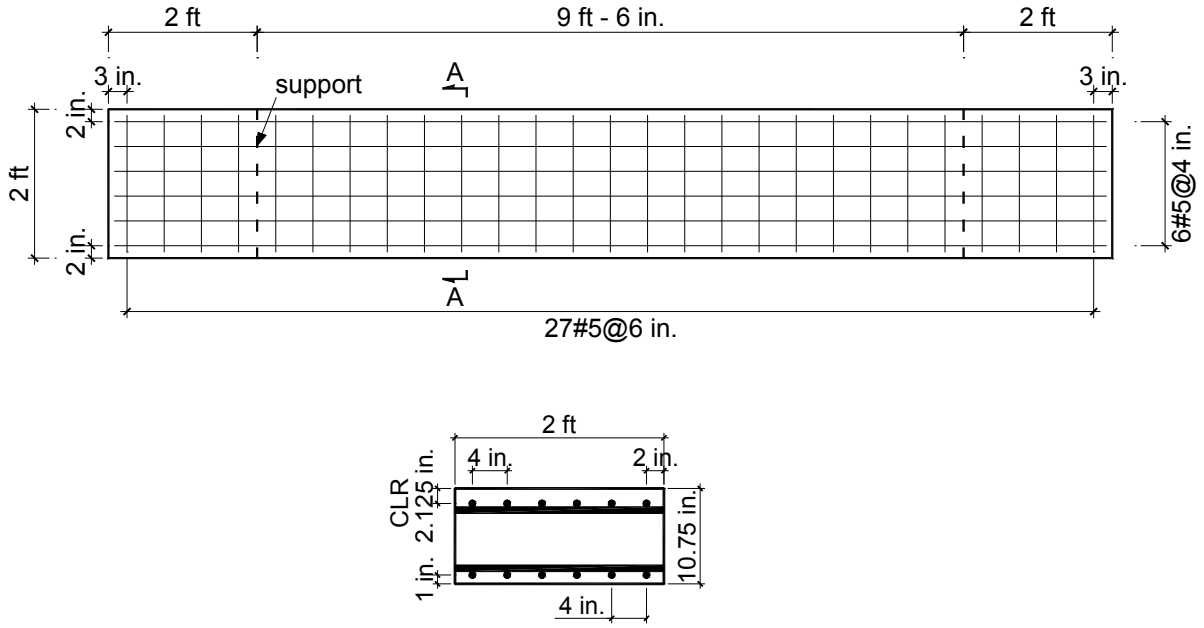

Series B slabs

Fig 5.1 Dimensions, top and bottom GFRP reinforcement mat for slabs

(1 in. = 25.4 mm; 1 ft = 304.8 mm)

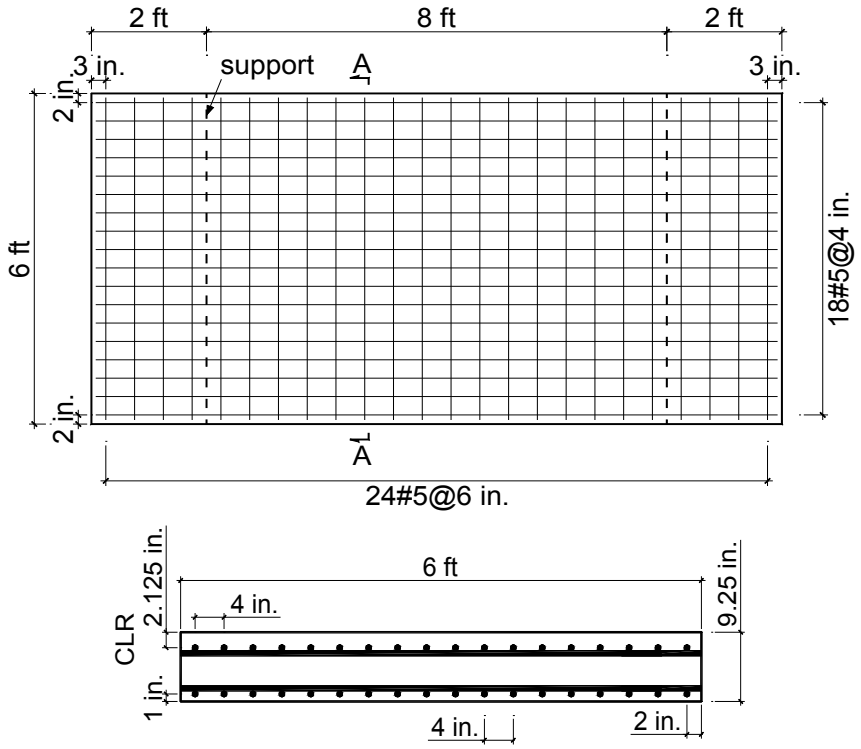

Section A-A

Series C slabs

Fig 5.1 (continued)

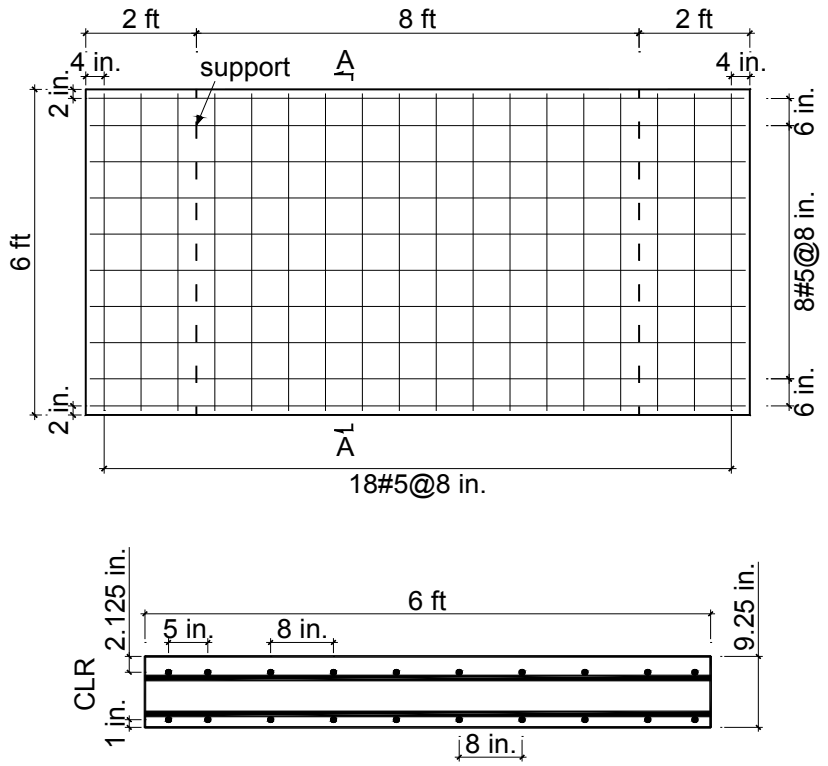

Section A-A

Series D slabs

Fig 5.1 (continued)

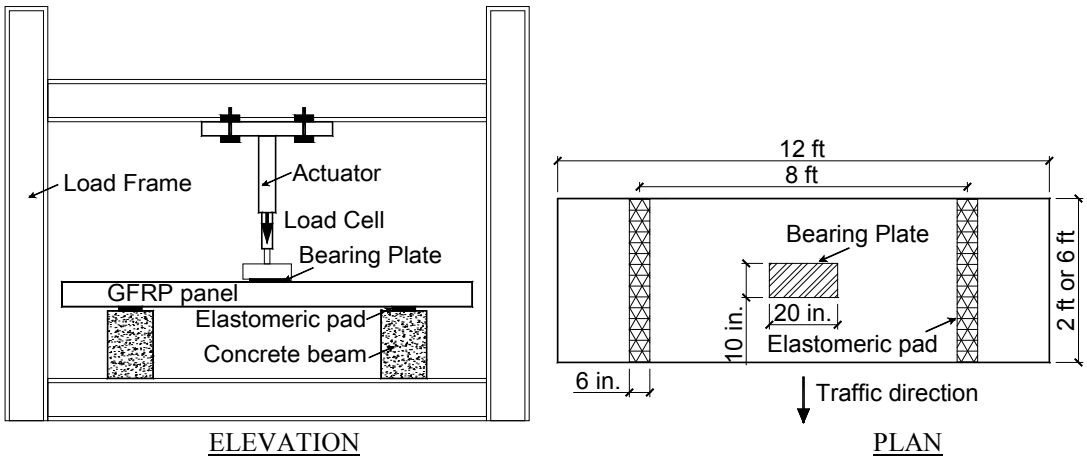

Fig 5.2 Test setup (1 in. = 25.4 mm; 1 ft = 304.8 mm)

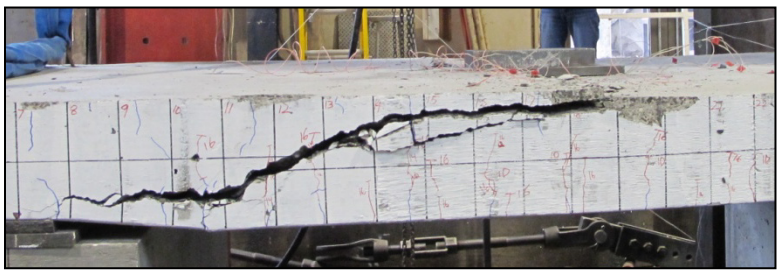

Shear failure mode

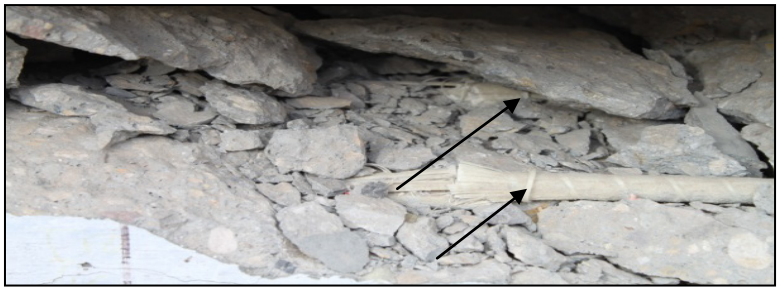

Snapping and Shearing off of top GFRP bars

Fig 5.3 Slab performance

Normal weight concrete slab Lightweight concrete slab

Fig 5.4 Shear cracks pass through the aggregate

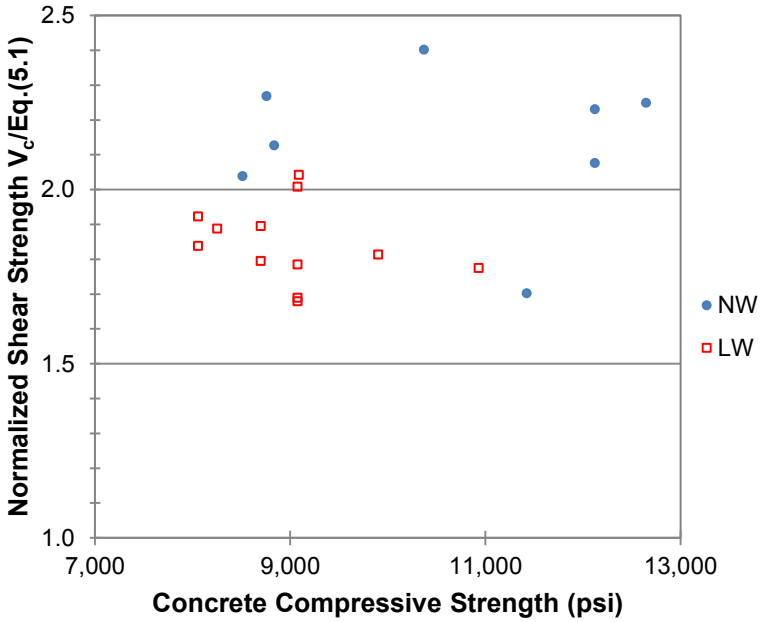

Fig 5.5 Normalized shear strength versus concrete compressive strength using the first-order MCFT Eq. (5.1) (1 psi = 6.895 kPa)

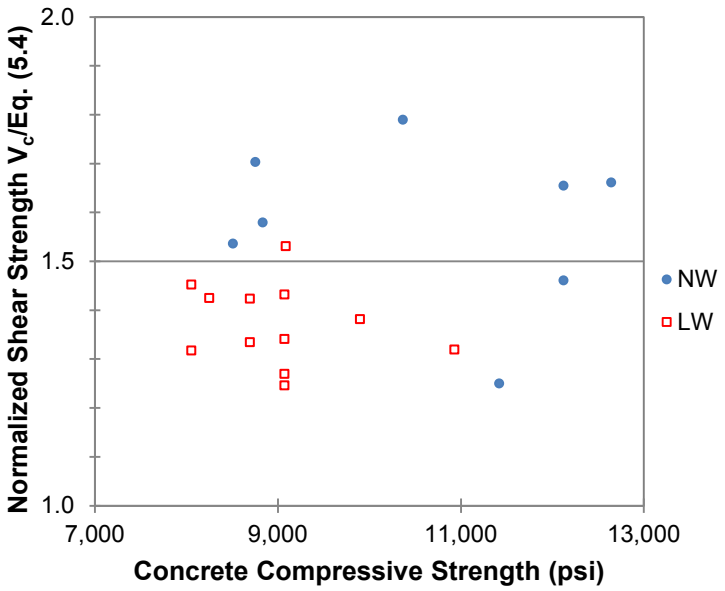

Fig 5.6 Normalized shear strength versus concrete compressive strength using the second-order MCFT Eq. (5.4) (1 psi = 6.895 kPa)

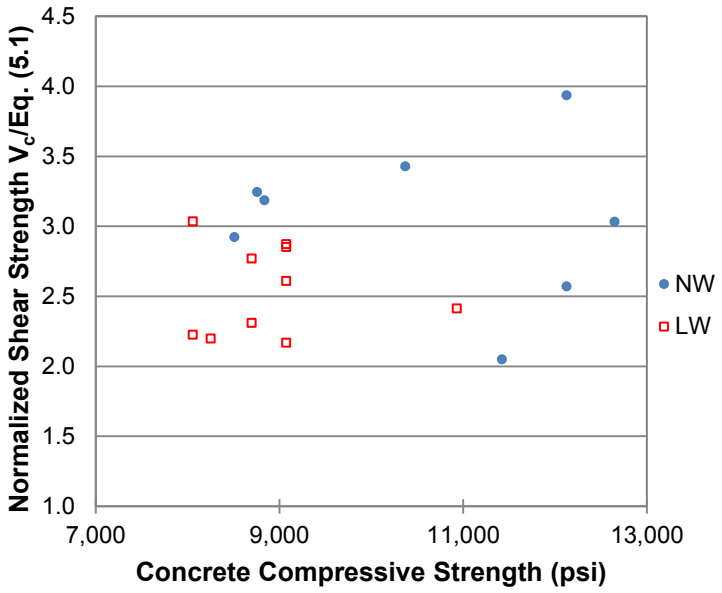

Fig 5.7 Normalized shear strength versus concrete compressive strength using actual strain and the first-order MCFT Eq. (5.1) (1 psi = 6.895 kPa)

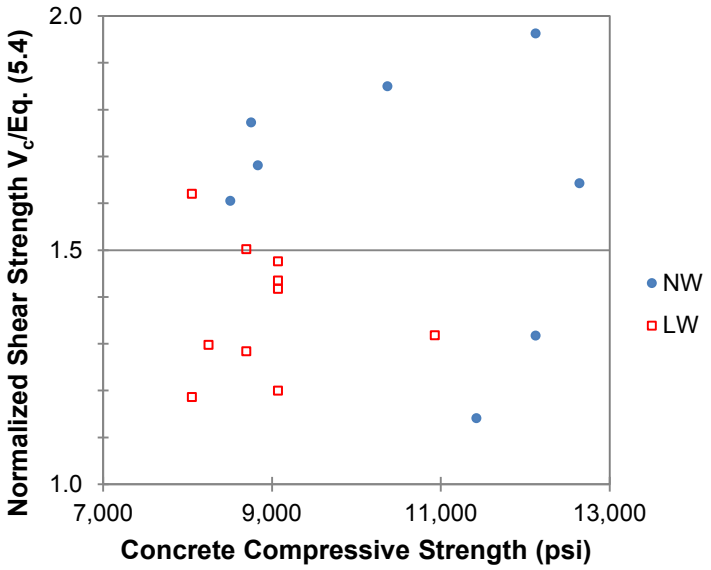

Fig 5.8 Normalized shear strength versus concrete compressive strength using actual strain and the second-order MCFT Eq. (5.4) (1 psi = 6.895 kPa)

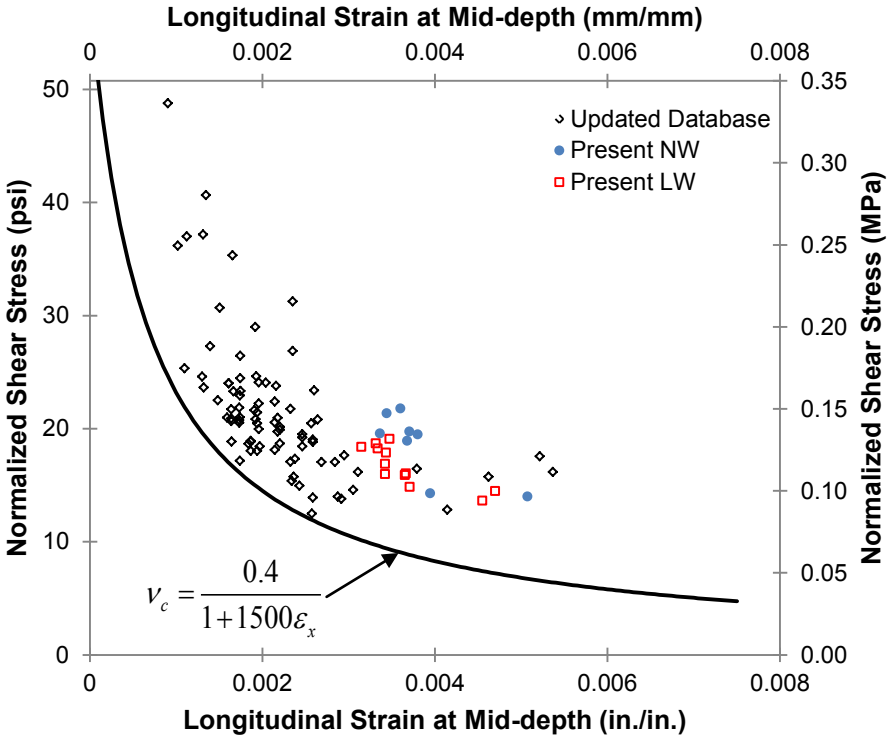

Fig 5.9 Strain effect: normal weight concrete versus lightweight concrete slabs for first-order MCFT Eq. (5.1) (1 MPa = 145 psi)

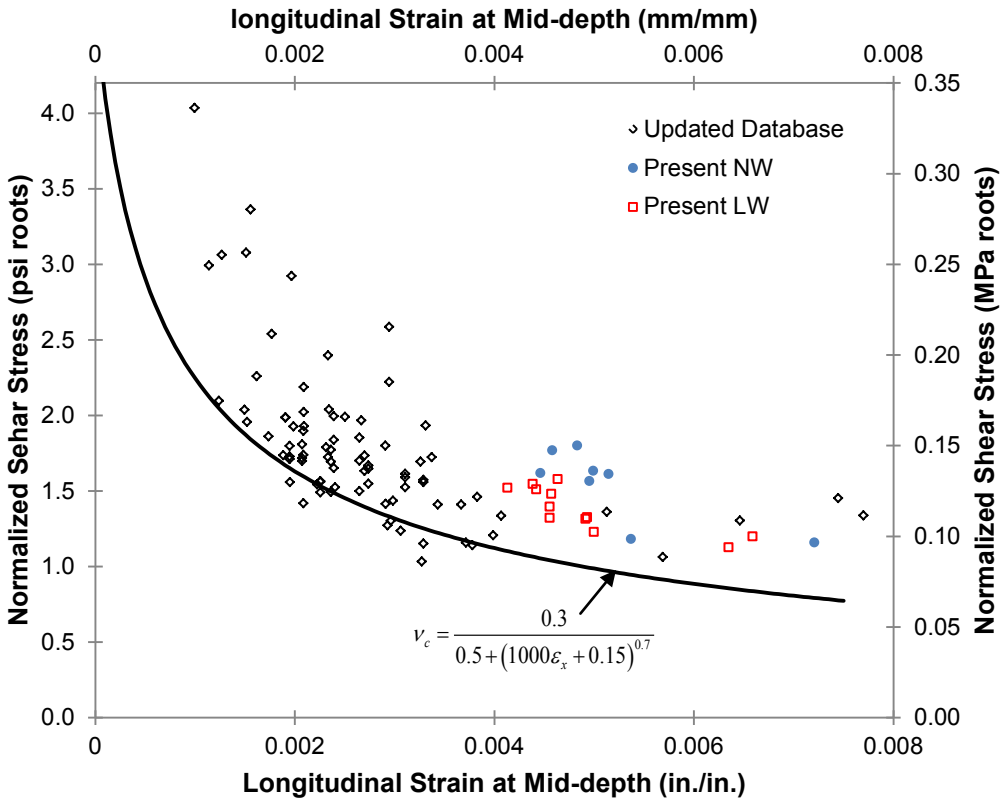

Fig 5.10 Strain effect: normal weight concrete versus lightweight concrete slabs for second-order MCFT Eq. (5.4) (1 MPa = 145 psi)

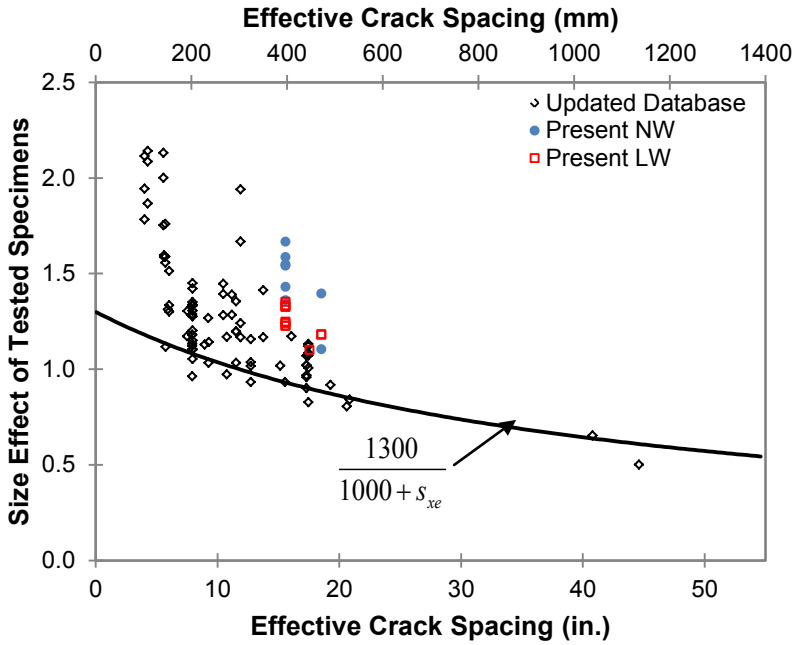

Fig 5.11 Size effect: normal weight concrete versus lightweight concrete slabs for second-order MCFT Eq. (5.4) (1 in. = 25.4 mm)

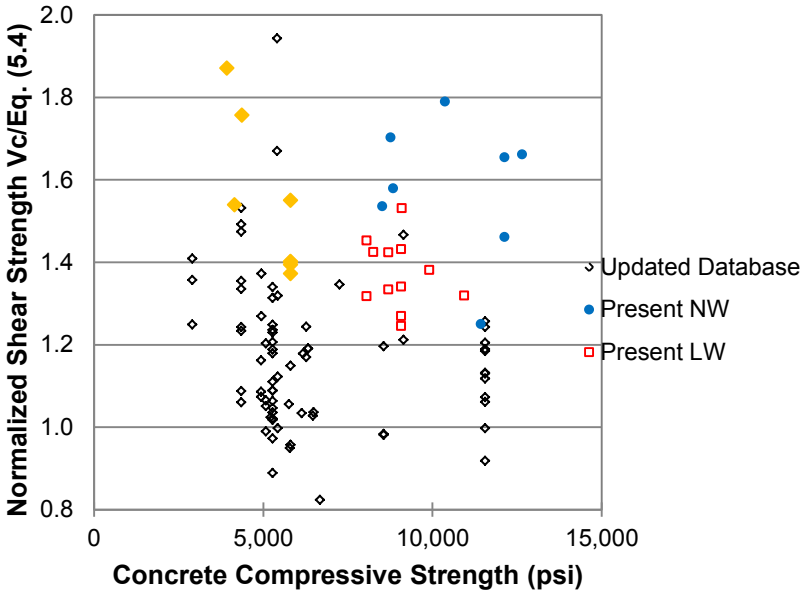

Fig 5.12 Normalized shear strength versus concrete compressive strength using the second-order MCFT Eq. (5.4) for the updated database (1 psi = 6.895 kPa)

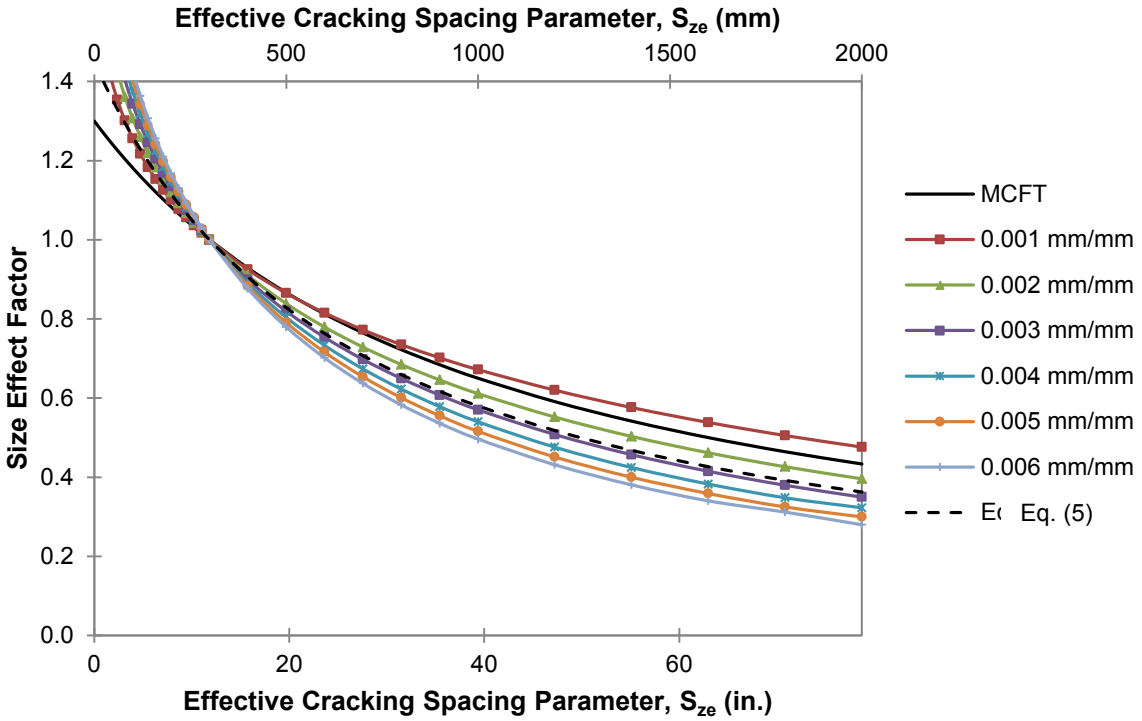

Fig 5.13 Size effect factor for mid-depth strain

6 CONCLUSIONS

The performance of precast lightweight concrete panels reinforced with Glass Fiber Reinforced Polymer (GFRP) bars was investigated and compared to that of normal weight concrete panels reinforced in an identical manner. The results for the lightweight concrete panels reinforced with GFRP bars are the only ones available in the literature to the knowledge of the author. Four sets of specimens were built and tested. The first set of specimens and the third set of specimens had the same span (8 ft) which is smaller than the typical prestressed concrete girder spacing for steel reinforced concrete panels, with a slab thickness of 9 ¼ in. The second set of specimens had a typical prestressed concrete girder spacing (9 ½ ft) with an increased slab thickness of 10 ¾ in. The first and second set of specimens had the same width (2 ft) which simulates the behavior of a strip from the deck panel; the third set of specimens had a larger width (6 ft), which is typical of actual bridge precast deck panels similar to the ones used at a recently constructed bridge near Price on US 6 in Utah (6 ft-10 in. x 41 ft-5 in. x 9 ¼ in.). The fourth set of specimens had a dimension exactly the same as the third set of specimens but with a reinforcement ratio approximately one-half that of the third set. All panels tested were simply supported which is a much more severe condition than the detail used in actual precast bridge deck panels; the latter method attaches the precast panels to the girders using blockouts by anchoring the panels through grout and steel studs in the blockouts to the top face of the girder flanges; in addition, actual bridge decks are continuous over several spans. The main findings of this research are summarized as follows:

1. Satisfactory performance of panels with different spans was achieved following the ACI 440.1R guidelines. Panels were tested for two different deck spans, 8 ft and 9 ½ ft, with the same reinforcement spacing. By increasing the thickness of the panels to 10 ¾ in., panels with a 9 ½ ft span achieved a similar performance in terms of stiffness, service load deflection, and ultimate load compared to 8 ft span panels with a 9 ¼ in. thickness.
2. The shear strength of lightweight concrete panels reinforced with GFRP bars was on average 81% that of normal weight concrete panels reinforced with GFRP bars. This is due to the lower tensile strength of lightweight concrete compared to normal weight concrete, and the resulting reduction of the splitting resistance.
3. The ultimate shear strength of panels with a reduced reinforcement ratio (56% of flexurally designed panels) was 77% and 80% of the panels designed according to ACI 440.1R for normal weight and lightweight concrete, respectively. The reason for this is that GFRP bars in panels with the reduced amount of reinforcement developed higher strains (10%-16%) than the flexurally designed panels; however, this increase in strain was limited due to the shear failure mode of the panels.
4. The ultimate load performance of both normal weight and lightweight concrete panels is acceptable when compared to the standard design truck load. The 2 ft wide panels with the load configuration tested in this research achieved a capacity of 1.3 to 1.7 times the load, and 4.4 to 6.1 times the moment requirement of the AASHTO LRFD Specifications. The 6 ft wide

panels achieved a capacity of 1.8 to 2.7 times the load, and 3.1 to 5.5 times the moment requirement of the AASHTO LRFD Specifications.

5. The predictions using the Canadian CAN/CSA guidelines, the Japanese JSCE guidelines, and an equation proposed by El-Sayed et al. had a smaller conservatism compared to the ACI 440.1R guidelines for both normal weight and lightweight concrete panels reinforced with GFRP bars. However, in a few cases the last three predictions (CAN/CSA, JSCE, El-Sayed et al.) were slightly unconservative.
6. This research has shown that precast concrete panels can be designed using either normal weight or lightweight concrete provided that an appropriate reduction factor is used for lightweight concrete using ACI 440.1R guidelines. The Canadian CAN/CSA and Japanese JSCE guidelines predict the shear strength of lightweight concrete panels reinforced with GFRP bars for flexure, without any shear reinforcement, with the same degree of conservatism as normal weight concrete panels.
7. The current ACI 440.1R design guidelines provide a lower bound for the shear capacity of panels reinforced with GFRP bars for flexure without any shear reinforcement, for both lightweight concrete and normal weight concrete panels; moreover, all panels in the database achieved 1.3 times the ACI 440.1R predicted shear capacity.
8. A reduction factor is introduced to modify the shear prediction equation in ACI 440.1R for lightweight concrete members reinforced with GFRP bars for flexure without any shear reinforcement. A value of the reduction factor of $\lambda_f = 0.80$ was determined comparing a database of 97 members reinforced

with GFRP bars without stirrups, 85 of which were normal weight concrete beams or panels and 12 were lightweight concrete panels. Using the modified equation proposed herein and a reduction factor λ_f = 0.80, the lightweight concrete panels achieved a similar conservatism as the normal weight concrete panels in the database.

9. The fact that the reduction factor for sand-lightweight concrete reinforced with GFRP bars (λ_f =0.80) is lower than the corresponding factor for steel bars (λ =0.85) is justified because of the different failure mode, bond mechanism, modulus of elasticity, maximum stress, and stress distribution for the two reinforcing bar types.
10. All panels designed and reinforced according to ACI 440.1R satisfied the service load deflection limit of the AASHTO LRFD Specifications. Lightweight concrete panels with only 56% the reinforcement ratio of the panels designed according to ACI 440.1R did not satisfy the service load deflection limit of the AASHTO LRFD Specifications, even though normal weight concrete panels with reduced reinforcement ratio satisfied the deflection requirement. On average, the service load deflection of lightweight concrete panels was 1.4 times that of normal weight concrete panels.
11. The number and width of initial cracks controlled panel stiffness before the section reached the cracking moment. Initial crack widths resulting from handling of the specimens had no effect on the ultimate load capacity provided they were smaller than 0.01 in. wide. After the panels reached the cracking moment, both normal weight and lightweight concrete panels had a reduced stiffness ranging from 13% to 35% of the initial stiffness.

12. The second-order MCFT equation predicts the shear strength of normal weight and lightweight concrete slabs reinforced with GFRP bars accurately. The first-order MCFT equation is more conservative compared to the second-order equation. Lightweight concrete slabs, which failed in one-way shear, show the same size and strain effects as normal weight concrete slabs or beams reinforced with GFRP bars.
13. The average ratio of predicted to measured mid-depth strain was 60% for both normal weight and lightweight concrete slabs using the first-order MCFT equation; the average ratio was 82% for both normal weight and lightweight concrete slabs using the second-order MCFT equation.
14. Using the strains from flexural design for the first-order and second-order MCFT equations results in conservative designs since the actual concrete compressive strength and guaranteed GFRP properties are generally higher than the design values.
15. The ratio of experimental to predicted shear strength from MCFT is lower for lightweight compared to normal weight concrete if one considers only the specimens in this research. However, when the ratio of experimental to predicted shear strength is compared with an updated database of GFRP reinforced slabs and beams, the ratio for normal weight is less than lightweight concrete. This is caused by the relatively smaller number of data samples for lightweight (12) compared to normal weight concrete members (92), and the higher concrete compressive strength of the slabs in this research (both normal weight and lightweight).

16. Even though the size effect factor in the original MCFT was developed based on strains in steel reinforced concrete members, it is still accurate for the shear prediction of GFRP reinforced concrete members which achieve much higher strains.
17. For precast concrete panels with initial cracks, the experimental moment of inertia is much smaller than the ACI 440.1R guidelines when the applied bending moment is less than the cracking moment. The effective moment of inertia predicted by the ACI 440.1R guidelines from the cracking moment to ultimate moment is close to that observed in this research.
18. For precast concrete panels reinforced with GFRP bars with initial cracks, the moment of inertia should not be taken as the gross moment of inertia when the service moment is less than the cracking moment. The present tests show that before reaching the cracking moment, the moment of inertia was 20% to 40% of the gross moment of inertia for 0.61 m wide panels. The moment of inertia was 20% to 32% of the gross moment of inertia for 6 ft wide panels.
19. High strength concrete increases the design cracking moment; in this case, the service moment can be smaller than the cracking moment. Since precast concrete panels reinforced with GFRP bars can develop initial cracks due to shrinkage, handling, lifting, and transportation-induced stresses, use of the gross moment of inertia is unconservative. The type of concrete, i.e. normal weight concrete or lightweight concrete, does not affect the moment of inertia significantly before the cracking moment is reached.
20. For initially cracked precast concrete panels reinforced with GFRP bars, an expression is proposed to evaluate the moment of inertia when the design

service moment is less than the cracking moment; in the range of applied bending moments, the equation predicts deflections more accurately compared to the ACI 440.1R prediction. Using the proposed expression, the predicted deflections before the cracking moment are satisfactory compared to the observed behavior.

21. All panels tested satisfied the service moment deflection requirements of the AASHTO LRFD Bridge Design Specifications, even though some of them had longer spans than typical GFRP reinforced precast bridge deck panels, or normal weight concrete panels with reduced reinforcement ratio. However, lightweight concrete panels with reduced reinforcement ratio did not satisfy the service moment deflection requirements of AASHTO specifications.
22. Lifting of precast concrete panels reinforced with GFRP bars requires extra care. Embedded lifting hoops should not be used for lifting these panels. It is recommended that such panels be lifted with straps placed underneath the panels at multiple points in the long dimension of the panel.

7 RECOMMENDATIONS FOR FURTHER RESEARCH

The results of the tests carried out in this research are sufficient to recommend the use of lightweight concrete reinforced with GFRP bars for construction of precast concrete bridge decks. Both normal weight and lightweight concrete panels had a residual capacity after failure which was approximately equal to one-half the ultimate load capacity. The research has also shown that there is a choice for the designer when it comes to meeting the AASHTO LRFD Bridge Design Specifications deflection requirement. The first option is to keep the slab thickness at 9 ¼ in. and reduce the deck span from 9 ½ ft to 8 ft; this option involves the addition of new girder lines. The second option is to keep the deck span at 9 ½ ft and increase the slab thickness to 10 ¾ in. Bridge decks using the Accelerated Bridge Construction method could benefit from the use of GFRP reinforced lightweight concrete precast panels. In addition, deflections measured at service loads were less than the allowable deflections permitted by the AASHTO LRFD Bridge Design Specifications. Implementation with a smaller GFRP reinforcement ratio would be more economical and should include the use of lightweight concrete with the appropriate modification factor for shear strength capacity found in this research. The Beaver Creek Bridge on US 6 near Price, Utah, has used GFRP reinforcement in normal weight concrete deck panels and was constructed in September 2009. The deck span used was 7 ft-7 in.; the bridge deck with a 9 ¼ in. thickness slab has performed very well to date. Further implementation of lightweight concrete or normal weight precast concrete panels for

bridge decks reinforced with GFRP bars is recommended based on the results of this research project.

More research needs to be conducted on precast concrete panels with initial cracks reinforced with GFRP bars, in terms of the effects of reinforcement ratio and concrete strength on the moment of inertia. Both normal weight and lightweight concrete slabs tested in this research were constructed with high strength concrete. Additional results for normal strength lightweight concrete slabs are required to validate the findings of the present research.